THE DEVELOPMENT, ELECTROCHEMICAL CHARACTERIZATION AND APPLICATIONS OF SULPHONATED SILICA SOL-GELS

WANDA MARIE AYLWARD

The Development, Electrochemical Characterization and Applications of Sulphonated Silica Sol-Gels

By

Wanda Marie Aylward

BSc (Hons), St. Francis Xavier University
Antigonish, Nova Scotia 1999
MSc, Memorial University of Newfoundland
St. John's, Newfoundland 2002

A thesis submitted to the School of Graduate Studies in partial fulfillment of the requirements for the degree of Doctor of Philosophy

Department of Chemistry
Memorial University of Newfoundland
St. John's, Newfoundland
December 2006

Your file Votre référence
ISBN: 978-0-494-31310-7
Our file Notre référence
ISBN: 978-0-494-31310-7

Abstract

The major goals of this research were to prepare novel proton conducting materials and to investigate their ion exchange and ion transport properties.

The sol-gel process was used to synthesize silica ORMOSIL hydrogels with sulphonate functionality by incorporating 2(4-chlorosulfonylphenyl) ethyl-trichlorosilane into a tetramethyl orthosilicate sol-gel network. Gel modified carbon fiber paper working electrodes were prepared by suspending strips of carbon fiber paper into a sol solution.

Cyclic voltammetry, chronoamperometry and chronocoulometry using $Ru(NH_3)_6^{2+/3+}$ redox probes were used to investigate the ion exchange and ion transport properties within the hydrogels. It was found that the hydrogels studied in this work exhibited excellent ion exchange and ion transport properties and were very stable in electrochemical studies.

The effects of electrolyte concentration and pH on these properties were studied. As well, sol-gel synthetic conditions such as sol-gel aging, sulphonate concentration, solvent and catalyst effects were also studied. The degree of interaction between the redox probes and sol-gel network was investigated by studying the ion exchange and transport properties of probes having different size and charge than $Ru(NH_3)_6^{2+/3+}$. The sulphonated silica hydrogels were found to exhibit excellent permselectivity, allowing the positively charged redox probes to diffuse into their porous network but not a negatively charge probe.

Electrochemical impedance spectroscopy was used to study the ionic conductivity of the hydrogels. It was found that incorporating the sulphonate functionality into the silica sol-gel greatly increased the ionic conductivity when compared to a tetramethyl

orthosilicate sol-gel. The sulphonated silica sol-gels displayed rather large ionic conductivities, larger in fact than most reports in the literature for various other ormosil materials.

Composites of a sulphonated silica sol-gel and polypyrrole (PPY/gel) were prepared to incorporate the electronic conductivity of the conducting polymer into the ionic conducting network of the sol-gel. Ion transport in these composites was investigated using cyclic voltammetry, impedance spectroscopy and X-Ray emission analysis. It was found in this work that reduction and reoxidation of the PPY/gel involved the uptake and expulsion of cations and anions.

Another goal of this work was to modify a proton exchange membrane fuel cell catalyst with a sulphonated silica sol-gel. Composites consisting of a sulphonated silica sol-gel and Pt/C were prepared and preliminary investigations using these catalysts in hydrogen and direct methanol fuel cells are discussed.

Acknowledgements

First off I would like to express my deepest gratitude to Dr. Peter Pickup for all of his guidance and support throughout this project. I would also like to thank my supervisory committee, Dr. Dave Thompson and Dr. Chris Flinn for all of their helpful comments and suggestions throughout my degree.

I would also like to thank the Pickup research group for all of their help and friendly chatter over the past few years. In particular, I would like to thank Guangchun Li for his help with the fuel cells and Omar Yepez for his input and optimistic view of things. I would also like to thank Aaron Rowe for all the good conversations.

I would also like to express my gratitude to Lisa Lee for all of her help with the scanning electron microprobe.

Financial support from the School of Graduate Studies, the Chemistry Department and NSERC are gratefully acknowledged.

I would like to thank my parents for their encouragement and support (emotional and financial) throughout my entire university career. I would like to thank my sisters for always being on the other end of the phone whenever I needed to talk. Thanks to all of my friends who have made my time at MUN and in St. John's a very memorable and fun time. And lastly I would like to thank my husband, Jon, for always being there and for being able to make me laugh through the stressful times.

Table of Contents

List of Abbreviations and Symbols

A – total electrode area

AC – alternating current

APTES - aminopropyltriethoxysilane

C – calibration constant for 2-electrode cell

C – concentration of redox probe

C_{dl} – double layer capacitance

C_F – capacitance

CA - chronoamperometry

CC – chronocoulometry

CFP – carbon fiber paper

ch – chemically bonded

CV – cyclic voltammetry

d – film thickness

D_{app} – apparent diffusion coefficient

DC – direct current

DMFC – direct methanol fuel cell

E - potential

EDX – energy dispersive X-ray

EIS – electrochemical impedance spectroscopy

EW – equivalent mass

F – Faraday's constant

$Fe(CN)_6^{3-/4-}$ - hexacyanoferrate (III/IV), or ferricyanide as referred to in thesis

GDE – gas diffusion electrode

HOA – complexing ligand, e.g. OA = acetylacetonate

I – current

I_{pa} – anodic peak current

ITO – indium tin oxide

j - $\sqrt{-1}$

K_p – partition coefficient

MEA – membrane electrode assembly

MeOH - methanol

MgO – magnesium oxide

MnO_2 – manganese oxide

MoO_3 – molybdic oxide or molybdenum oxide

$M(OR)_n$ – metal alkoxide

MPTMS - mercaptopropyltrimethoxysilane

MTMOS – methyltrimethoxysilane

MW – molecular weight

n – number of electrons in a redox reaction

N – coordination number

NMR – nuclear magnetic resonance

ORMOSIL – ORganically MOdified SILicate

PEMFC – proton exchange membrane fuel cell

PEFC – polymer electrolyte fuel cell

ph – physically bonded

PPY - polypyrrole

Pt/C – platinum supported on carbon

PTFE – polytetrafluoroethylene

PVDFHFP – poly(vinylidene fluoride)-cohexafluoropropylene

r – electrode radius

R – resistance

$R_{electronic}$ – electronic resistance

R_{high} – high frequency resistance

R_{ionic} – ionic resistance

R_{low} – low frequency resistance

R_s – solution resistance

R_u – uncompensated solution resistance

$Ru(bpy)_3^{2+/3+}$ - ruthenium (III/IV) tris(bipyridine)

$Ru(NH_3)_6^{2+/3+}$ - ruthenium(III/IV) hexamine

RuO_2 – ruthenium dioxide

S - Siemens

SEM – scanning electron microscope

Silane-$(COOH)_3$ – trimethoxysilylpropyl ethylenediamine triacetic acid

Silane-NH_2 – 3-aminopropyl-methyl-diethoxysilane

SiO_2 – silicon dioxide

SiO^- - siloxide

SiOH - silanol

$Si(OR)_4$ – silicon alkoxide

SiOSi - siloxane

SO_3^- - sulphonate

t - time

TEOS – tetraethyl orthosilicate

TiO_2 – titanium dioxide

TMOS – tetramethyl orthosilicate

V_2O_5 – vanadium oxide

WO_3 – tungsten oxide

Z - impedance

$\Delta E_{p/2}$ – peak width at half height

δ - diffusion layer

Ω - Ohms

ε - dielectric constant

κ - conductivity

σ - ionic conductivity

ω - frequency

List of Tables

List of Figures

List of Schemes

Chapter 1

General Introduction to Sol-Gels and Electrochemical Techniques

1.1 Introduction

Aerogels are nanoscale, mesoporous (pore size > 2 nm) materials in which nanometer-sized solid domains are networked through a continuous, highly porous volume of free space.[1] Because of this unique structure, aerogels display a number of important physical properties, including high surface area, low (and controllable) densities and accessibility of molecular reactants in the nanoscale size domains throughout the aerogel via rapid mass transport through the continuous volume of mesopores.[1] Sol-gel chemistry is being widely used in today's labs as a means of preparing inorganic and organic-inorganic composite materials because of the ease with which these materials can be made, modified, and processed.[2] Such hybrid materials are of interest to researchers because they show controllable optical, electrical and mechanical properties by combining the properties of both organic and inorganic components.[3]

Sol-gel chemistry has a long history; beginning in the 1840's when Ebelman[4] synthesized glass-like SiO_2 by hydrolyzing tetraethylorthosilicate (TEOS) under acidic conditions. Studies performed on the structure of inorganic gels in 1864 supported a theory that these gels consisted of a solid network with continuous porosity.[4] This theory remained until the 1930's, when Hurd[5] proved that silica gels actually consisted of a polymeric backbone of silicic acid surrounding a liquid phase. Another event in the 1930's, the discovery of the first aerogels,[1] increased the interest of sol-gels. Kistler used supercritical drying to replace the liquid phase in a wet gel with air.[1] In doing so, he was able to avoid the subsequent collapse of the drying gel's porous network. Removing the

pore liquid without collapsing the microstructure is important in preserving both the solid and porous networks so that the resulting solid retains all of the desirable attributes of the starting gel.[1] By the 1950's and 1960's the preparation of homogeneous powders by sol-gel chemistry was extended to Al, Si, Ti and Zr oxides.[4]

However, it wasn't until the 1960's that Teichner and Nicolaon prepared the first aerogels using the technique that we refer to today as the "sol-gel process".[1] The development of the sol-gel process brought new interest to the investigation of aerogels because it eliminated the time-consuming salt removal and solvent-exchange steps inherent to the Kistler method.[1] The sol-gel process also has several other advantages: it is a liquid-phase synthesis performed at moderate temperature,[1] thereby allowing mixing on the molecular scale to give rise to homogeneous products.[6] It also enabled aerogels to be made in much shorter time, for example, hours instead of days.[1] In addition, the sol-gel method extended the aerogel chemistry to include transition metal oxides, binary and ternary oxide compositions, metal/metal oxide systems and organic/inorganic hybrid materials.[1] The ambient conditions associated with the sol-gel processing also allow for the preparation of hybrid materials that contain a wide variety of dopants that would not survive the high-temperature conditions for traditional "melt" chemistry glass preparations.[2,4] Such temperature-sensitive dopants include organic dyes, metal complexes, enzymes, antibodies, whole cells and even higher biological structures.[2,6,7,14]

Sol-gels have gradually attracted the attention of the electrochemical community since the 1980's.[4,8] Initially, electrochemists were interested in using the sol-gel process as a convenient means of mixing different metal oxides for the preparation of crystalline

materials.[8] However, during the past decade amorphous sol-gel materials have become more appealing to electrochemists because they function better than their crystalline counterparts in applications such as lithium intercalation batteries, supercapacitors, and solid electrolytes due to their enlarged ionic conductivity.[8] Because aerogels offer more active sites per gram for gas/solid interactions than do most solid, dense materials,[1] they have been investigated as heterogeneous catalysts.[1,9,10] Since the sol-gel chemistry and processing enables specific compositions to be developed with a highly porous morphology, the tailoring of the sol-gels to specific catalytic reactions while maintaining rapid molecular transport through the mesoporous network is possible.[1]

The high surface area and mesoporous volume of aerogels also offer opportunities for chemical reactivity other than in catalysis. For example, MgO and CaO sol-gels have been used as stoichiometric chemical reactants for the base-catalyzed decomposition of organic molecules that are environmental hazards.[1] Measurement of surface area and porosity is usually accomplished by measurement of gas adsorption isotherms, typically for N_2, Ar or Kr.[6] The surface area of accessible pores largely defines the measured surface area and the actual external surface area contributes very little to the total.[1] For measurements made by N_2 adsorption, surface areas typically range from 5 $m^2 \cdot g^{-1}$ to over 1000 $m^2 \cdot g^{-1}$ in aerogels.[6]

Materials that have oxidation states with markedly different absorbance spectra in the visible region can serve as electrochromic devices and the sol-gel process serves as a convenient means of depositing the electrochromic layer onto a supporting material.[4]

The synthesis of organic-inorganic hybrid materials to develop materials with unique microstructures and properties has received much attention in the past few years.[15,16] For example, the combination of conducting polymers with transition metal oxides is of interest because these "nanocomposites" would be able to incorporate the electronically conductive properties of the polymer within the spaces of the inorganic sol-gel.[1,2,3] This would circumvent the need to add carbon to electrode structures.[1]

There exist many other examples of applications of sol-gels based on their unique physical properties. Due to their extremely low thermal conductivities, aerogels are among the best thermal insulators available.[1] This can further be exploited by using the ability of the sol-gel to effectively transmit solar light but strongly block thermal radiation to make transparent thermal insulators.[1] Since sol-gels can be prepared in an optically transparent form, they are suitable for the development of optical sensing devices for a range of species.[6,8,13] Sol-gel based pH sensors have been fabricated by incorporating various chemicals, such as bromophenol blue which responds rapidly to changes in pH, into the transparent sol-gel matrix.[3] It has also been reported that incorporating pyoverdin, a natural fluorescent pigment, into a silica-based sol-gel can act as a sensor for detecting Fe(III).[11] Lanthanide ions entrapped within sol-gel matrices allow for the development of optical or solar devices that take advantage of the fluorescent characteristics of the dopants.[12] In terms of bioanalytical applications, amperometric biosensors have been prepared by entrapping proteins and enzymes within sol-gel matrices.[2,4,7,17] This is possible because the proteins and enzymes entrapped

within a sol-gel matrix have been shown to maintain their individual properties and reactivities.[2]

1.2 The Sol-Gel Process

A general definition of a sol-gel procedure is any process that involves the "polymerization of soluble precursor molecules to afford a polymeric material via the intermediate formation of a colloidal sol phase".[6] Although several routes are currently used to prepare sol-gels, the use of network-forming species in an organic or aqueous solution has emerged as the most widely used method because network-formers can be modified to control the resulting chemistry and processing of the gel.[1,4,6] Aqueous-based methods originate with a solution of a metal salt while alcohol-based methods employ an organometallic precursor that is dissolved in an appropriate alcohol.[6] The most important of these network-forming precursors are metal alkoxides ($M(OR)_n$)[1] and the sol-gel route may be thought of as a two-step inorganic polymerization.[1,2,3,4,6] The first step is the hydrolysis of the alkoxy ligands, as shown below[1]:

$$M(OR)_n + H_2O \rightarrow [M(OR)_{n-1}(OH)] + ROH \qquad \text{Eq. 1.1}$$

The starting mixture usually consists of a metal alkoxide, e.g. tetramethyl orthosilicate or tetraethyl orthosilicate, water, acid or base catalyst, and often a cosolvent such as methanol or ethanol.[6]

Polycondensation then occurs, involving an oxylation reaction that creates oxygen bridges and expels XOH species as follows[1]:

$$M\text{-}OH + M\text{-}OX \rightarrow M\text{-}O\text{-}M + XOH \qquad \text{Eq. 1.2}$$

(X = H or R)

Condensation takes place by either nucleophilic substitution or nucleophilic addition.[4]

Hydrolysis and polycondensation of the alkoxide occur in a complicated sequence of nonconsecutive pathways that consume water, release alcohol, and then produce water again.[6]

The sol-gel process can be broken down into four stages: sol formation, gelation, aging and drying.[4,6] The sol, or dispersion of colloidal particles in a liquid,[4] forms as a result of the hydrolysis and condensation reactions that initially occur.[4,6] At this point, the sol is a very fluid solution comprised of subnanometer sized oxide particles in liquid solvent.[2,4] The sol is easy to handle and can be cast into molds, coated onto the surfaces of substrates or drawn into fibers.[6] As cross-linking and aggregation of the colloidal particles occur, the viscosity of the fluid sol increases sharply and gelation occurs.[1,2,6] The "gel point" is the time at which this visually observable phase transition occurs.[6] The materials obtained at this point are porous, solvent-filled gels[6] consisting of an interconnected, rigid network of submicron pores and polymeric chains.[4] The gelation process takes place on a timescale ranging from seconds to months.[2] The sol-gel structure continues to evolve after gelation in a process known as aging. During the aging period, condensation continues and the gel structure begins to stabilize.[6] Aging takes place in four steps: polymerization, synerisis, coarsening and phase transformations.[4] Polymerization is simply the continuation of condensation reactions during which the number of linkages increases while synerisis is the spontaneous

shrinkage of the gel.[4] Coarsening is the dissolution of smaller particles of the gel followed by their reprecipitation onto larger particles and in phase transformations the solid phase separates from the liquid on a local scale.[4] Following aging is a process called drying where the solvent is removed to form a condensed solid.[4,6] As molecules evaporate from the exterior of the gel, molecules from the interior will migrate to the surface thus depleting the interior of solvent.[6] This solvent depletion generates further rearrangement of the gel structure as pores collapse considerably and the gel monolith shrinks.[2,13] When essentially all of the solvent is released a xerogel is obtained.[2,6] Drying of a gel too vigorously will often lead to substantial cracks and fissures appearing in the gel.[6]

The manner in which the liquid phase is removed from a gel determines whether the dried solid is a highly porous aerogel, a more dense xerogel, or a "wet" hydrogel.[2] When supercritical drying techniques are used to remove the solvent at a temperature and pressure above the critical point, the liquid-vapor interface and hence surface tension effects are eliminated.[6] This allows the removal of the solvent without pore collapse, resulting in very low-density solids with very high surface areas called "aerogels". [1,6] Ambient-pressure methods for preparing aerogels have emerged and include surface modification and network strengthening procedures,[1] the addition of surfactants or "drying control chemical additives" (such as glycerol, formamide, oxalic acid and tetramethylammonium hydroxide) to the liquid[60] and freeze drying.[60] Drying of the gel by simple evaporation of the solvent is characterized by a collapse of the gel's structure as the pore liquid evaporates and the resulting dense solid is termed a "xerogel".[1]

Xerogels do not provide stable microenvironments but instead continue to shrink as they age.[4] Aging of the gel in its mother liquor[1] produces a gel with high solvent, usually water, content termed a "hydrogel".[1,6] The various sol-gel network structures are shown in Figure 1.1. The extent and manner of aging and drying of the sol material depends on the purpose for which the material is to be used or studied.

The relative rates of the overlapping hydrolysis and condensation processes are dependent on the starting solution and are also important factors in determining the final structure of the material.[1,6] Under acid-catalyzed conditions, condensation reactions are rate limiting and small hydroxylated oligomers predominate yielding polymer-like gels with relatively small pores.[1,6,18,19] However, under basic catalysis, hydrolysis and particle nucleation steps are rate limiting so the sol contains fewer, larger particles and the resulting gel network consists of interconnected colloidal particles and large pores.[1,6,18,19]

1.3 Silica Sol-Gels

Silica chemistry has been extensively explored, as silica materials have a vast range of applications.[20] The sol-gel process allows for new modifications of silica. These modifications include composite materials, such as hybrid organic-inorganic materials also known as ORganically MOdified SILicates, or ORMOSILs. These new materials have blurred the traditional boundaries between inorganic silicate polymers, such as clays and quartz, and their organic counterparts, such as the silicones.[6]

Silica aerogels constitute a model aerogel system because detailed investigations have been conducted to establish the relationships between sol-gel chemistry, the

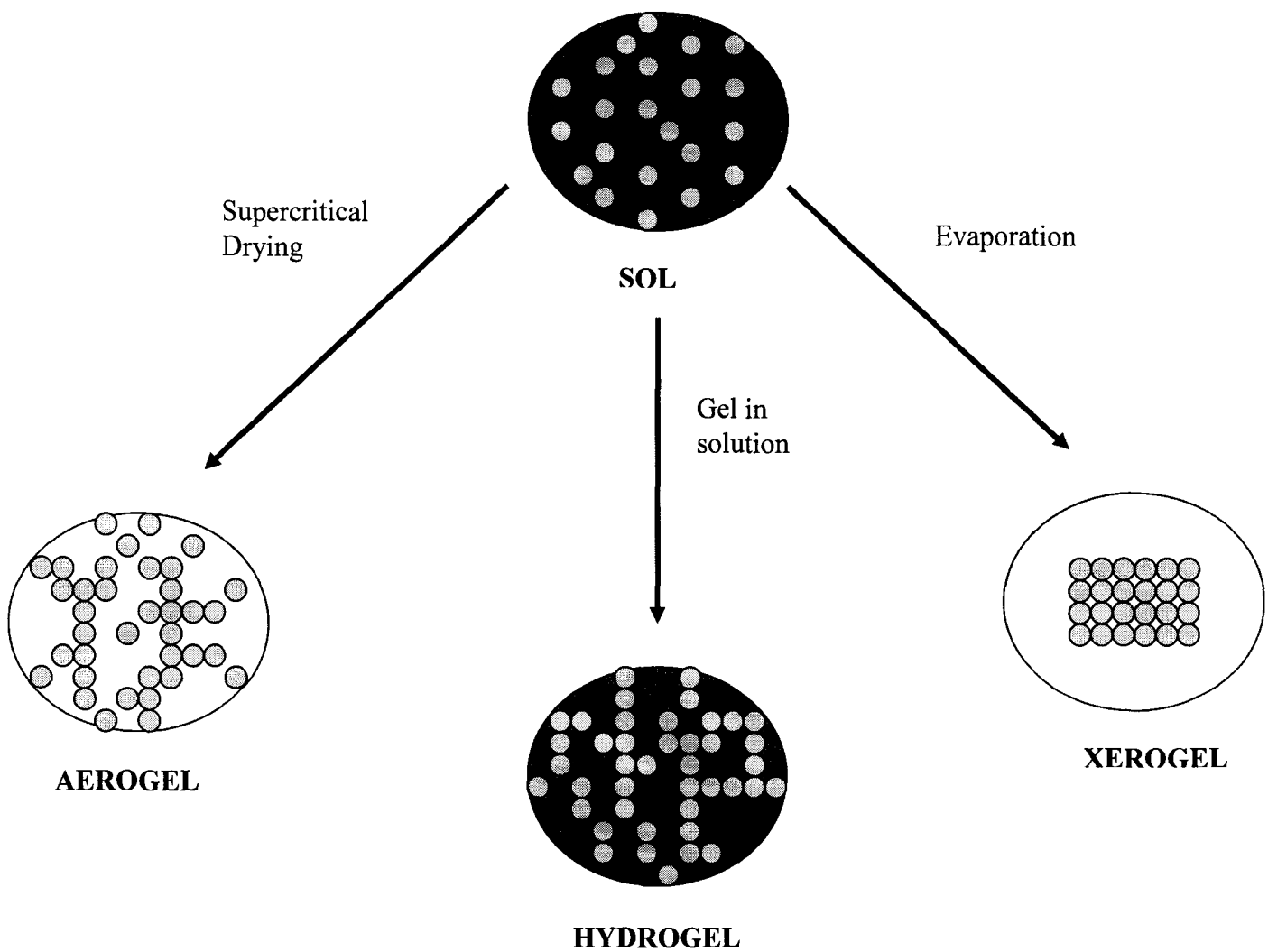

Figure 1.1 The different sol-gel network structures

resulting aerogel microstructure and the effect on physical properties.[21] Silica atoms have only one relevant stable oxidation state and materials made with silica metal centers do not undergo redox reactions in aqueous solutions.[8] Silica gels have large surface areas and large ion-exchange capacity, contributed by surface hydroxyls, and they also show good adhesion to metal oxides and ceramic supports.[8] This makes them attractive for electrochemical applications. The properties of silica sol-gels are readily manipulated by changes in the synthetic parameters. Adjustable parameters include the monomer composition (including the nature and number of types of precursors, as well as their absolute and relative concentrations), solvents used to homogenize the reaction mixtures, the amount of water available relative to the number of silicon alkoxide groups available for hydrolysis and condensation reactions (R_r = [Si-OR]/[H_2O]), pH, temperature, the nature of the active catalysts, and many other factors.[6] Even conditions used to treat the gel after initial formation (postprocessing) can have a profound impact on the structure and behavior of the silica sol-gel.[6]

Amorphous silicas are built up from aggregates of small colloidal particles of silica having dimensions of 1 – 100 nm and many important parameters that determine the properties of a silica gel are determined by the size of these particles and the degree to which they are packed together.[6] When initially formed, silica sols have very open silica structures with large solvent-filled pores and channels pervading the material.[6] The open and porous network of the original gel is retained in aerogels. However, normal processing conditions usually result in a considerable collapse of this open structure,

resulting in gels with much less porous structures.[1] Denser gels resulting from this collapse of pore structure are termed xerogels.

Silicon centers are capable of making up to four siloxane linkages, although complete condensation happens for only a limited population of these centers.[6] The more common situation in amorphous silica is for the silica sites to make two or three linkages.[6] The degree of condensation is readily measured by solid-state nuclear magnetic resonance (NMR) spectroscopy.[6] This is an important parameter affecting porosity and surface structure. The silicon sites that do not undergo complete condensation afford one or more active hydroxyl groups that have a strong influence on the nature of the solvent-surface interface and are capable of reacting with external reagents, such as metal complexes or tethering side chains.[6,21] Silicon alkoxide $Si(OR)_4$ precursors have a low electrophilicity and stable coordination number (because the silicon precursor and product oxide have the same coordination number, N = 4).[1,27] Therefore, hydrolysis of $Si(OR)_4$ is slow and the rates of the polymerization reactions of these alkoxides are mainly controlled by acid or base catalysis.[1]

The development of sol-gel chemistry allowed for an increase in the number of accessible surface sites relative to pre-formed silica gel.[6] Thus, sol-gel processing allows for higher loadings of metal complexes per unit mass of the support.[28] For example, it has been reported that loadings of [metal]/[Si] can be increased using the sol-gel method by at least 30 times over that achieved by adsorption.[6]

Silica aerogels exhibit extremely low thermal conductivities making them among the best thermal insulators available.[1] There is great interest in exploiting the fact that

silica aerogels are non-flammable, inert and optically transparent.[1] Because of the low sound velocity in SiO_2 aerogels, these materials are useful in acoustics for impedance-matching applications in ultrasonic sensor systems.[23] Cerenkov detectors widely use silica aerogels because they offer a range of low refractive index values, 1.007 to 1.024, otherwise difficult to achieve except with compressed gases.[21,24] Physicists have used silica aerogels as matrices to hold supercooled helium when studying phase transitions.[25] Silica aerogels are used in space exploration for the intact capture of cosmic dust particles traveling at hypervelocities as they provide a thermally stable, inert medium to dissipate the kinetic energy of the speeding particle while their transparency enables the captured particle's final location to be observed.[1] And lastly, silica aerogels represent one of the most promising of all materials in microelectronics[26] because of their low static dielectric constant ($\varepsilon < 2$), thermal and dimensional stability, and compatibility with semiconductor processing.[1,26]

1.4 Functionalization of Sol-Gel Silicas

One of the key advantages of the sol-gel process is the variety of means available to modify the gels chemically.[1] This allows tailoring of the final properties of the modified aerogels for specific chemical applications. There are several means of chemically modifying sol-gel materials, such as modifying the sol-gel precursor, adding a particulate phase during sol-gel formation, liquid-phase modification of the wet gel or gas-phase modification of the aerogel.[1]

Noncovalent inclusion of dopants within the silica matrix (i.e. untethered) is accomplished simply by mixing a solution of the dopant with the sol prior to gelation.[6,8] In these cases, association of the dopant with the sol is achieved through physical entrapment of the dopant molecules, by entanglement within the pore structures of the silicate network, and/or by specific association with the silicate matrix through hydrogen bonding, ion pairing with ionized $Si\text{-}O^-$ residues, and coordination at the material-solvent interface.[6] Sol-gel doping is not confined to the molecular level and dopants ranging in size from nanometer to the submillimeter level can also be encapsulated in sol-gel matrices using the same methodology.[29]

While noncovalently doped materials are readily prepared and sufficiently stable for many purposes, the absence of covalent attachment means that the dopants can be relatively mobile within the sol-gel matrix and may be prone to migration out of the gel matrix when exposed to an external solution.[6,8]

To overcome this problem, covalent attachments to the silica matrix (i.e. tethers) are prepared. This is achieved by adding molecules with pendant $-Si(OR)_3$ to the silicate sol.[6] In this manner, the silylated side chains copolymerize with the silica sol to afford stable linkages.[6] The Si-C bond does not participate in the sol-gel hydrolysis and condensation reactions and the organo-functional groups remain exposed on the surface.[8] A second means for providing covalent bonding to a sol-gel is to derivatize the surface of preprepared gels by organic compounds containing reactive functional groups such as chloro- or alkoxysilanes.[8] It is also possible to combine the two methods. Covalently-bonded organic-inorganic hybrids benefit from the high stability of the carbon-silicon

bond.[8] Covalent inclusion is particularly advantageous in the preparation of catalytic materials where the leaching of a dopant can represent a serious limitation.[6,8]

Lastly, sol-gels can also be impregnated by adsorption or precipitation of organic compounds onto preprepared gels.[8] This is especially useful when modifying inert supports.

Many examples of aerogel design flexibility have been reported in the literature. For example, catalysts based on the dispersion of metals on aerogel supports,[30] the addition of opacifiers (chemical agents added to a material to make it opaque, e.g. tin oxide and zircon compounds) to aerogels to reduce thermal transport[31], partially densified aerogels prepared by heating at elevated temperatures[32] and doping of aerogels[33] have all been discussed in the literature. Oxide aerogels are even being made electrically conductive and explored as new materials in electrochemisty, batteries, ultracapacitors and fuel cells.[1,4,8,9,10,34,35] Selected aspects of these areas of research are reviewed in the introductions to the relevant chapters of this thesis.

1.5 Silica-Based Ion-Exchanger Gels

The development of ion-exchanger and permselective coatings on electrode surfaces has received considerable attention. This is due in part to the need for improving the sensitivity and selectivity of voltammetric sensors.[36] Sol-gel films or membranes are well-suited for sensor applications and electrochemical studies because of their excellent physical and chemical stability and the ease with which they can be prepared. The

chemical and physical properties of these materials can be selectively tailored and controlled by the judicious choice of the functional group in the organosilane precursors.

There are several examples of silica-based ion-exchanger gels reported in the literature. Hsueh et al.[36] have prepared both anion and cation exchangers from methyltrimethoxysilane (MTMOS) sol-gels by modifying the films with 3-aminopropyl-methyl-diethoxysilane (silane-NH_2) or trimethoxysilylpropyl ethylenediamine triacetic acid (silane-$(COOH)_3$). Si clay electrodes have been modified by reaction with γ-aminopropyltriethoxysilane to prepare anion exchanger probes.[37,38] Walcarius et al.[15,16] describe the preparation of TEOS sol-gels modified with aminopropyltriethoxysilane (APTES) or mercaptopropyltrimethoxysilane (MPTMS) precursors. Wei and Collinson describe the modification of a TMOS sol-gel with APTES.[39]

Several other silica-based organic-inorganic ion-exchange materials have been reported in the literature.[40,-44] Silica-based ion-exchangers have been prepared with quartenary amines[41,42], N-octadecyldimethyl[3-(trimethoxysilyl)propyl]ammonium[43], 3-glycidoxypropyltrimethoxysilane[44] and 2-(3,4-epoxycyclohexyl)ethyltrimethoxysilane[44], are representative examples.

The film permselectivities and ion-exchange properties are attributed to the electrostatic interactions between the analyte and the acidic/basic functional group in the organosilane.[36]

1.6 Other Metal Oxide Sol-Gels

The sol-gel chemistry of non-silicates is not as easy to control. This is especially true for metal alkoxides in which the transition metal centers are highly electrophilic and exhibit several coordination states.[27] Because most transition metal alkoxides precipitate out of solution as soon as water is added, the sol-gel reaction needs to be modified.[1,27] This can be achieved by modifying the precursor by using a complexing ligand HOA (where OA = acetylacetonate, acetate) as shown below:[1]

$$M(OR)_n + mAOH \rightarrow [M(OR)_{n-m}(OA)_m] + mROH \qquad \text{Eq. 1.3}$$

From eq. 1.3 it is apparent that the alkoxy groups (OR) are replaced by new complexing ligand (OA). This makes the precursor more stable to hydrolysis.[1] During the hydrolysis step of the sol-gel process the alkoxy ligands are quickly removed.[1] The chelating ligands act as termination agents that limit the condensation reactions.[1]

Of the conductive oxides, V_2O_5 gels have received the most attention. These gels possess a variety of electrical, optical and electrochemical properties which make them attractive to researchers, particularly to lithium battery research. V_2O_5 has been shown to intercalate lithium reversibly with improved capacity for lithium over other metal oxides.[1,4] This high ionic capacity also extends to other cations.

Another transition metal oxide sol-gel that offers useful reversible lithium intercalation is MoO_3.[1] MnO_2 gels are being explored as lithium-ion insertion materials with lower cost and toxicity in lithium-ion batteries.[1]

TiO_2 is an important metal oxide sol-gel because of its low thermal conductivity.[1] These gels are often found in thermal insulation systems. RuO_2 and mixed RuO_2-TiO_2

are examples of sol-gels with good electrical conductivity. These gels are often used as electrocatalysts in various different systems.[1,4] WO_3 gels are very good electrochromic materials because they change from an initial light yellow-to-colorless state to a dark blue upon partial reduction.[4]

1.7 Introduction to Electrochemical Methods

1.7.1 Cyclic Voltammetry

Cyclic voltammetry is one of the most commonly used electrochemical methods for acquiring qualitative and quantitative information about electrochemical systems. This includes information on the thermodynamics of redox processes, on the kinetics of heterogeneous electron-transfer reactions and on coupled chemical reactions or adsorption processes.[61]

Cyclic voltammetry consists of linearly scanning the potential of a stationary working electrode using a triangular potential waveform, as illustrated in Figure 1.2. During this potential sweep, the potentiostat measures the current resulting from the applied potential and a plot of current versus potential, see Figure 1.3, is obtained. Initially, the experiment is started at a potential where only the oxidized form O is present and scanned towards a limiting negative potential. As the applied potential approaches the characteristic E^o for the redox process the cathodic current increases, until a peak is reached.[61] The direction of the potential sweep is reversed after the reduction process has been completed (at least 90 /n mV beyond the peak, where n is the number of electrons involved in the redox process).[61]

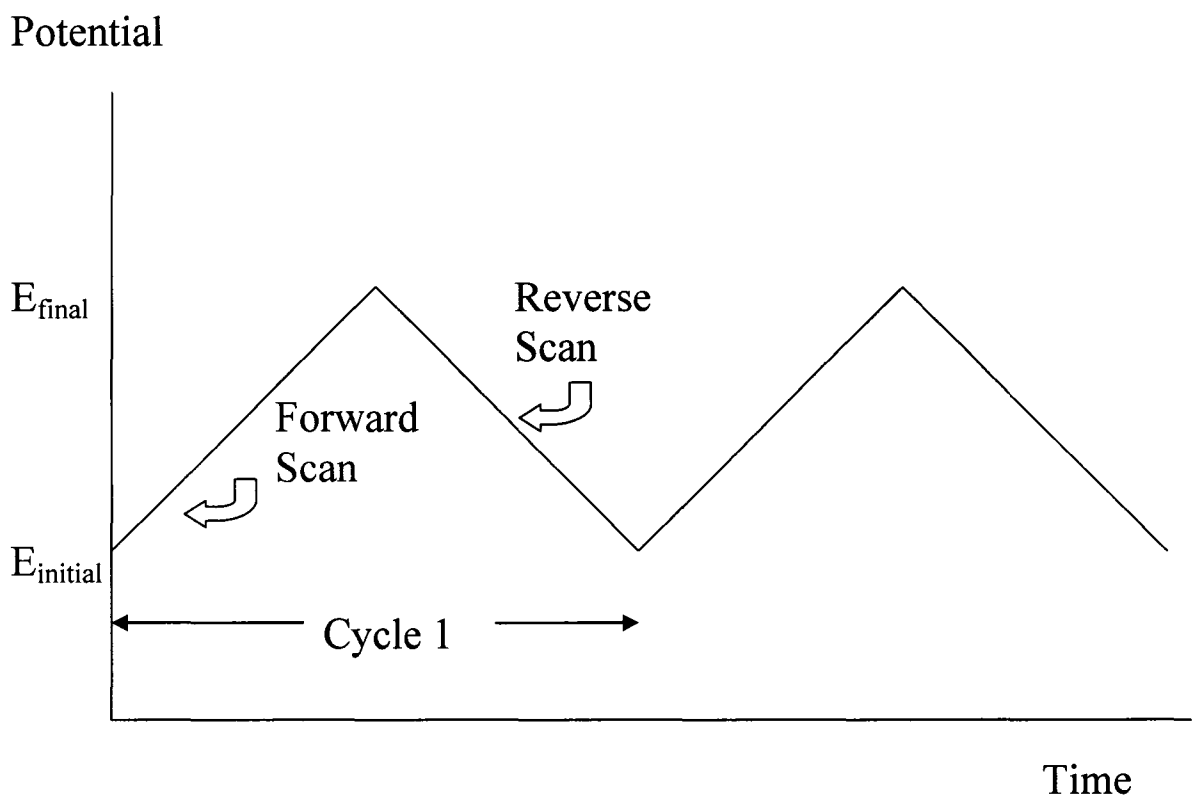

Figure 1.2 Potential-time waveform for a cyclic voltammetry experiment.

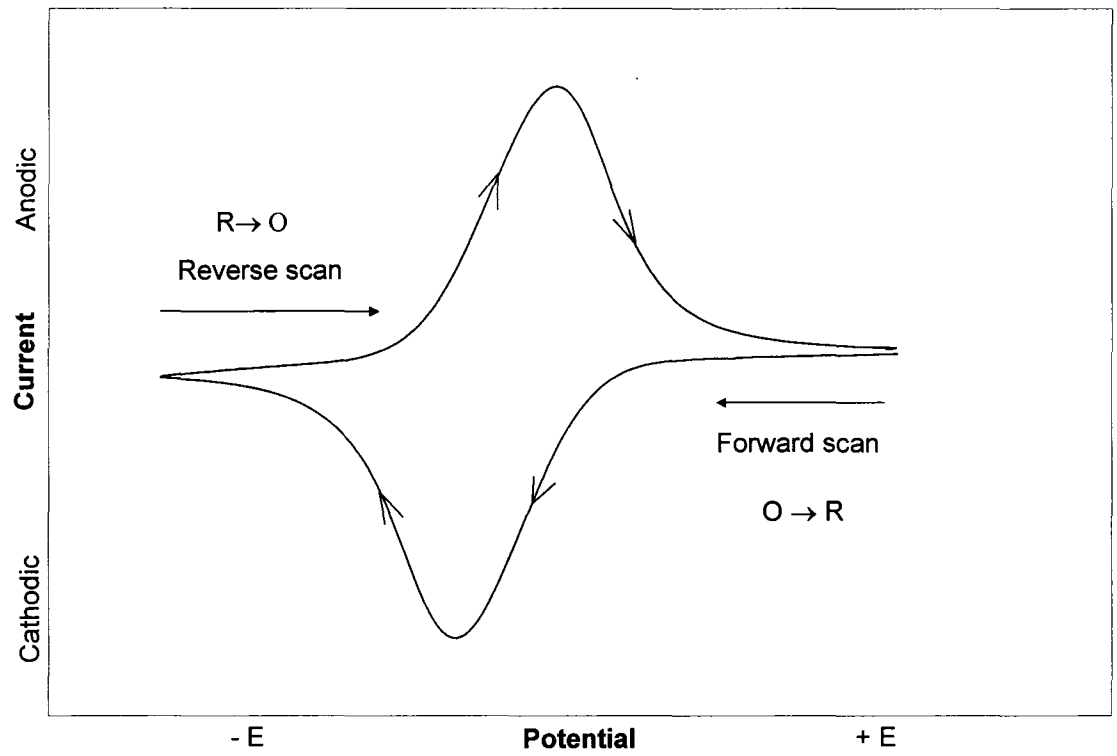

Figure 1.3 Typical cyclic voltammogram for a reversible O + ne- ℜ R redox process.

In the positive-going scan reduced molecules R are reoxidized back to O and an anodic current is observed. The two peak currents and two peak potentials are the basis for the experimental cyclic voltammogram or CV.

In a reversible system, the overall reaction is mass transport-limited.[61] This means that the reaction is controlled solely by the rate at which the electroactive species reach the surface of the electrode. This occurs when the system displays facile electron transport.[61] Because these systems obey thermodynamic relationships, they are sometimes called Nernstian systems.

In reversible systems, the peak currents are directly proportional to concentration and are scan rate dependant. The ratio of the reverse-to-forward currents is one for simple reversible couples. The formal potentials are centered between the two peak potentials with a peak separation of $\Delta E = 0.059 / n$ Volts.[61]

In the case where sluggish electron exchange occurs, the system is termed irreversible and the current is controlled by both charge transfer and mass transport.[61] Irreversible systems are characterized by displaying CVs with reduced peak currents and increased peak separation. Totally irreversible systems also show shifts in peak potential with scan rate.[61]

1.7.2 Chronoamperometry

Chronoamperometry is a controlled-potential technique that measures the current response to an applied potential. It is often used for measuring the diffusion coefficient of electroactive species or the surface area of the working electrode.[61]

In a chronoamperometric experiment, the potential of the working electrode is stepped from a value at which no faradaic reaction occurs (E_1) to a potential where the electroactive species transfers electrons to the electrode (E_2) and the resulting current-time dependence is measured.[61] The potential-time waveform and resulting current-time response are shown in Figures 1.4 and 1.5.

Chronoamperometric experiments are performed using stationary electrodes in unstirred solutions and mass transport is dictated by the diffusion coefficient of the electroactive species.[61] Therefore the current-time response reflects the change in the concentration gradient near the surface of the electrode, which involves a gradual depletion of the reactant as the diffusion layer expands.[61] The current decay with time is expressed by the Cottrell equation:[61]

$$i(t) = nFACD^{1/2} / \pi^{1/2}t^{1/2} \qquad \text{Eq. 1.4}$$

where n is the number of electrons involved in the redox reaction, F is Faraday's constant, A is electrode area, C is concentration, D is the diffusion coefficient and t is time.

Deviations from the Cottrell behavior occur at long times because of thermal convection effects.[61] At short times, a background contribution of the charging current is present.[61]

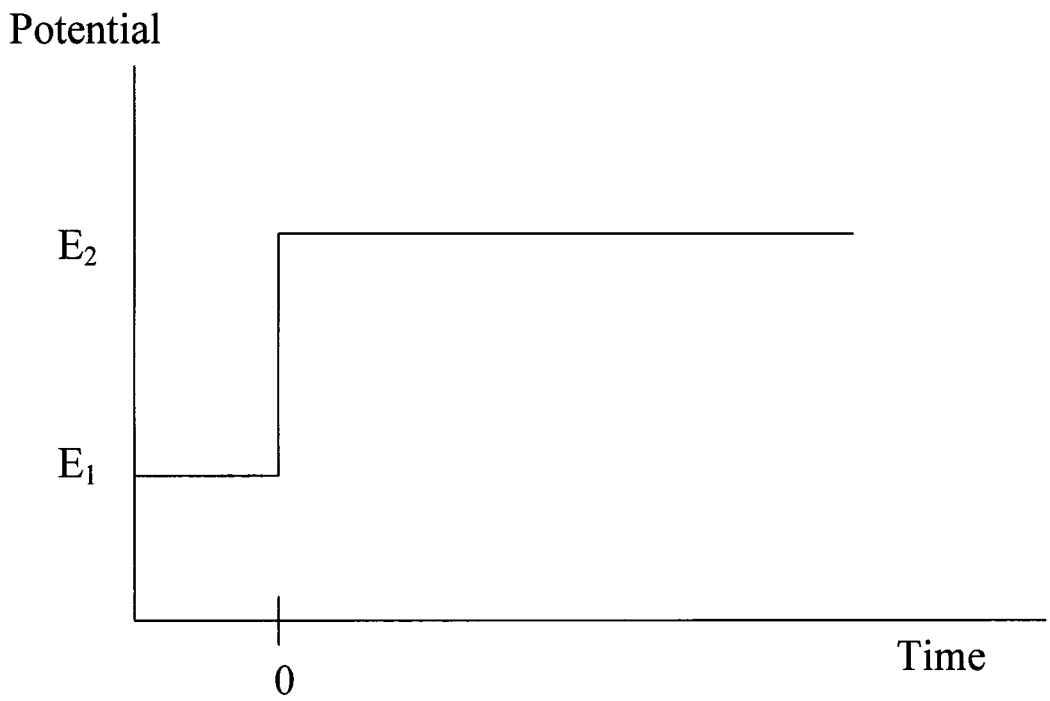

Figure 1.4 Potential-time waveform for a chronoamperometric experiment.

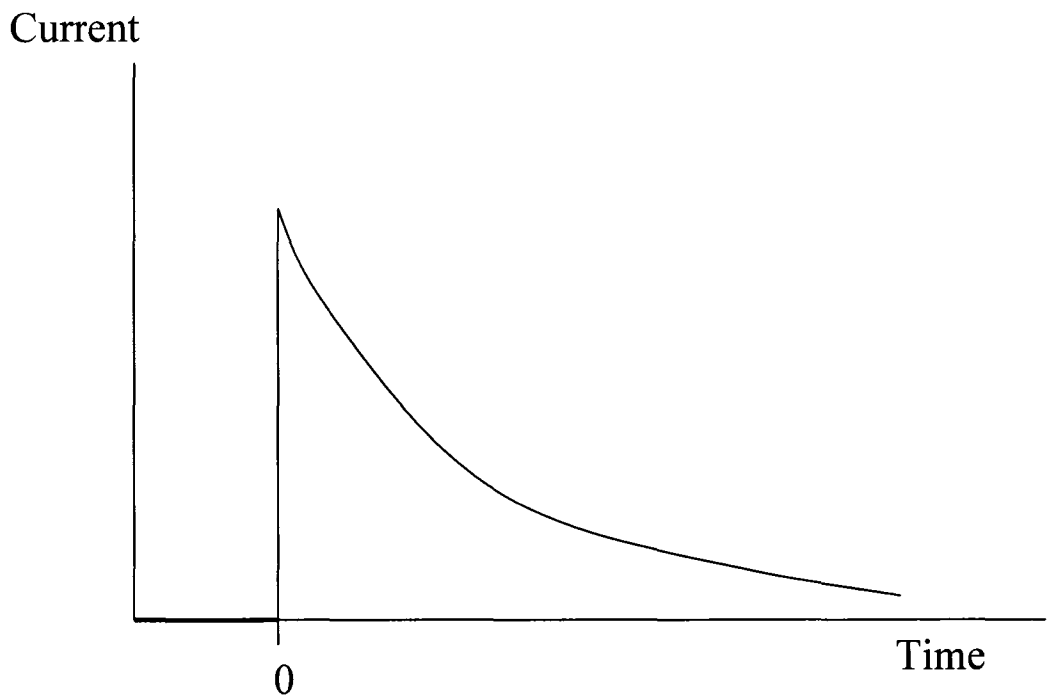

Figure 1.5 The resulting current-time response from a chronoamperometric experiment.

Charge versus time dependence can also be monitored using the potential-step experiment. This is done by integrating the current resulting from the potential step.[61] This is known as chronocoulometry and is useful for measuring the quantity of adsorbed reactants.[61] A chronocoulometric plot is one of charge versus the square root of time

1.7.3 Electrochemical Impedance Spectroscopy

Impedance, like resistance, is a measure of the ability of a circuit to resist the flow of electrical current and is used as a more general circuit parameter than resistance.[62] Electrochemical impedance is measured by applying an AC potential to an electrochemical cell and measuring the current through the cell.

Electrochemical Impedance Spectroscopy (EIS) is such a powerful tool that it is becoming the method of choice for characterizing systems whose electrical behaviour is determined by a number of strongly coupled processes, each of which is dictated by its own intrinsic rate constant.[53] These processes include electron transport through the electronic conductors, electron transfer at the electrode-electrolyte interfaces and flow of ions. The rate of flow of charged particles depends on the ohmic resistance of the electrodes and the electrolyte as well as on the reaction rates at the electrode-electrolyte interfaces.[52] Parameters derived from EIS include conductivity, dielectric constant, mobilities of charges, equilibrium concentrations of charged species, bulk generation-recombination rates, adsorption-reaction rate constants, capacitance of the interface region and diffusion coefficient of neutral species in the electrode.[52]

Electrochemical impedance spectroscopy is commonly used for determining ionic and electronic resistance in a porous electrode.[45]

1.7.3.1 AC Impedance

An electrochemical cell can be represented by a purely electronic model where the electrode interface during an electrochemical reaction is analogous to an electronic circuit consisting of resistors and capacitors.[45,53-55] AC impedance is a useful technique that allows one to characterize the electrochemical system in terms of its "equivalent circuit".[56,59] Figure 1.6 shows the equivalent circuit for a simple electrochemical cell.

AC impedance offers three distinct advantages over DC techniques. First, AC impedance techniques use very small excitation amplitudes which cause only minimal perturbation of the electrochemical system.[54] This helps to reduce errors caused by the technique itself. Second, AC impedance measurements can provide kinetic and mechanistic information when applied to the study of electrochemical systems because they can provide data on both electrode capacitance and charge-transfer reactions.[54] And finally, measurements can be made in low conductivity solutions because the method does not involve a potential scan.[54] In fact, AC impedance measurements are very useful in determining the uncompensated solution resistance of an electrochemical cell.[54]

The theory of AC impedance spectroscopy describes the response of a given circuit to an alternating current or voltage as a function of frequency. In DC methods, where the frequency is 0 Hz, the resistance is defined by Ohm's Law where $E = IR$.[54,57] The impedance of a resistor is independent of frequency and therefore has only a real

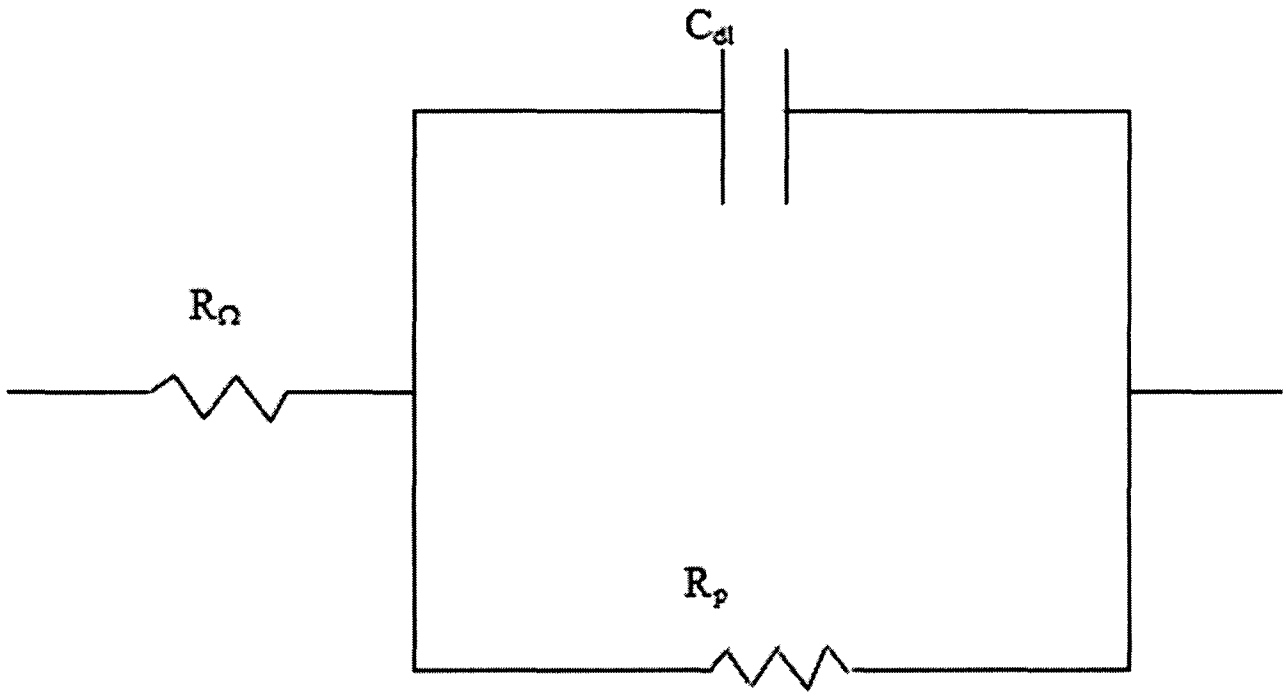

Figure 1.6 Equivalent circuit for a simple electrochemical cell. R_Ω is the uncompensated solution resistance, R_p is the polarization resistance and C_{dl} is the double layer capacitance.

component. The current through it is always in phase with the voltage.[62] For AC measurements, where the frequency is not zero, Ohm's Law is translated to E = IZ.[54,57] In this equation E and I are waveform amplitudes for potential and current respectively and Z is the impedance.[54,57] Impedance is defined as the AC equivalence of resistance and includes capacitors and inductors.[54] The impedance of an inductor increases as frequency increases and therefore is said to have only imaginary impedance components.[54,62] This results in the current generated at an inductor being phase shifted 90 degrees with respect to the voltage.[54,62] On the other hand, a capacitor's impedance decreases as the frequency increases and also contains only imaginary components.[54] Its current is phase shifted -90 degrees with respect to the voltage.[62] From the E-I relationship for a capacitor, an expression for impedance is obtained as follows:[57]

$$Z = 1/j\omega C \qquad \text{Eq. 1.5}$$

where $j = \sqrt{-1}$ and $\omega = 2\pi f$ (where f = frequency). From the E-I relationship for an inductor, the following expression for impedance is obtained:[57]

$$Z = j\omega C \qquad \text{Eq. 1.6}$$

A voltage sine wave applied across a given circuit results in an AC current waveform that differs in amplitude from and lags behind the voltage waveform which provides a measure of the phase shift.[54,57] The current waveform vector can be described graphically by defining the axes as real (I' and E') and imaginary (I" and E").[56] The imaginary axis is expressed by multiplying the I" by $\sqrt{-1}$, or j.[54] As such:

$$I_{total} = I' + I"j \text{ and } E_{total} = E' + E"j \qquad \text{Eq. 1.7}$$

The real and imaginary components of an AC waveform are defined with respect to a reference waveform. The real component is in phase with the reference waveform while the imaginary component is exactly 90° out of phase.[54]

The impedance is then simply calculated as

$$Z_{total} = (E' + E''j) / (I' + I''j) \qquad \text{Eq. 1.8}$$

and the resulting vector expression for the AC impedance is expressed as

$$Z_{total} = Z' + Z''j \qquad \text{Eq. 1.9}$$

1.7.3.2 Nyquist Plots

Nyquist plots, or complex impedance plane diagrams, are plots of the imaginary component of impedance versus the real component of impedance for each excitation frequency. Figure 1.7 shows an example of a theoretical Nyquist plot for an electrochemical system as described by Fig 1.6. At high frequencies only the uncompensated resistance contributes to the real impedance.[58] The polarization resistance contributes to the impedance measured at low frequencies due to mass transfer.[54] At high frequencies kinetic control is observed. θ is the phase angle.

1.7.3.3 Analysis of Electrochemical Impedance Spectroscopy

EIS may be performed using three different electrical stimuli:[52] (1) in the transient measurement, a step function of voltage is applied at t = 0 to the system and the resulting time-dependant current is measured. These time-dependant results are generally Fourier or Laplace-transformed into the frequency domain, resulting in a frequency-dependant

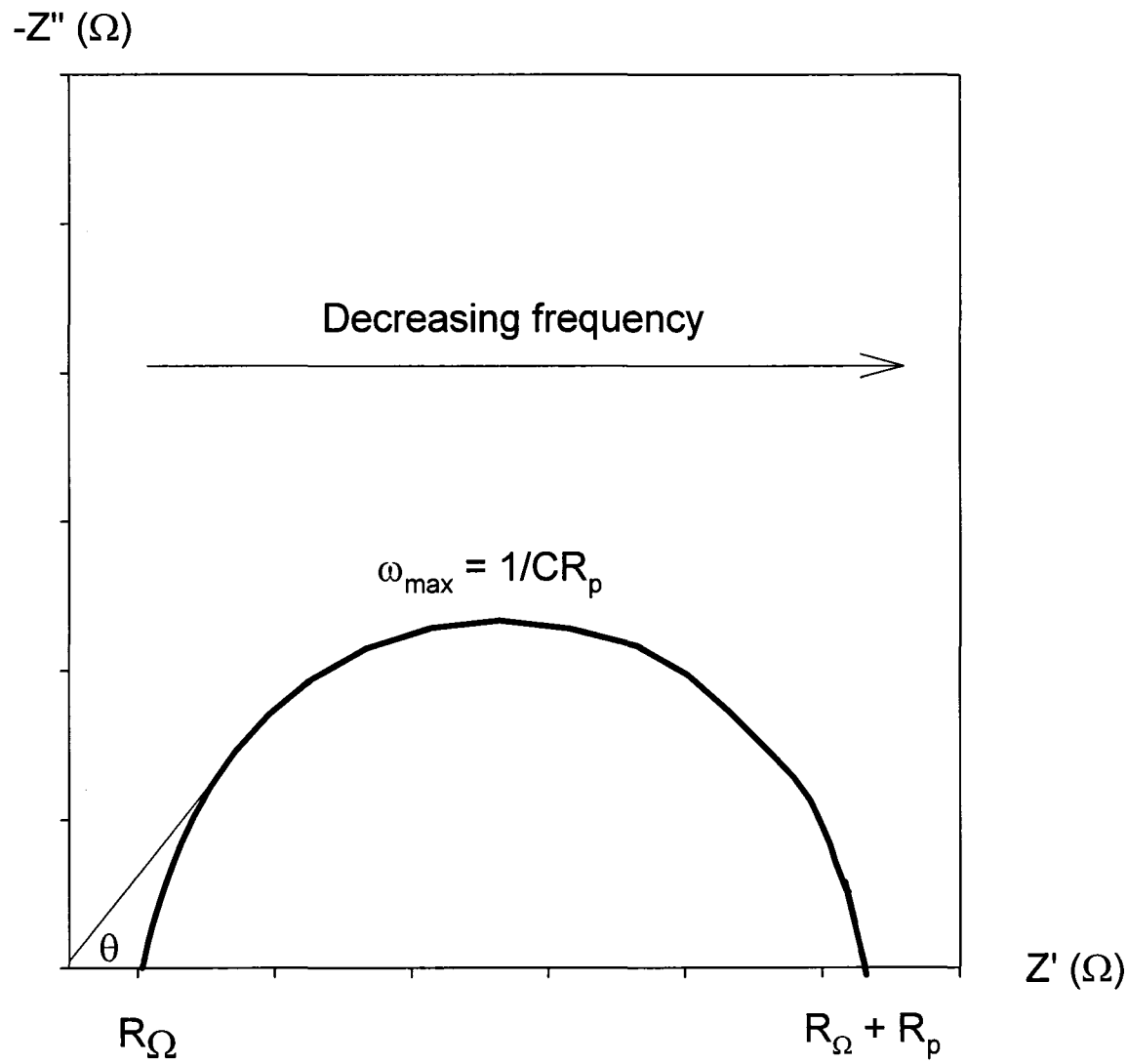

Figure 1.7 AC impedance profile for a simple electrochemical system. At high frequency, Z" → 0, Z'→ R_Ω. At low frequency, Z" → 0, Z'→ $R_\Omega + R_p$.

impedance. (2) In the fast data collection mode, a signal composed of random noise (or many discrete discrepancies) is applied to the interface and the resulting current is measured. Once again, this is generally converted to the frequency domain by Fourier transform. (3) The most common method of EIS is to apply a single-frequency voltage/current to the interface and measure the phase shift (real part) and amplitude (imaginary part) of the resulting current at that frequency.

The high frequency intercept with the real axis R_{high} is given as:[45]

$$R_{high} = 1 / (1/R_{electronic} + 1/R_{ionic}) \quad \text{Eq. 1.10}$$

Because R_{ionic} values are usually too high to significantly influence R_{high}, R_{high} is dominated by and approximately equal to $R_{electronic}$.[45]

The limiting low frequency resistance is[45]

$$R_{low} = (R_{electronic} + R_{ionic})/3 \quad \text{Eq. 1.11}$$

1.8 Thesis Objectives

The main objective of the work described in this thesis is to design and prepare sulphonated silica sol-gels as novel materials displaying good ion transport and exchange capabilities and high ionic conductivity. Chapter 3 describes the use of redox probes to explore the ion transport and ion exchange properties of these materials and how the different synthetic parameters affect these properties. Chapter 4 describes the interaction between the sol-gel matrix and different redox probes. Chapter 5 reports on the high ionic conductivity provided by the sulphonated silica sol-gels.

Chapters 6 and 7 describe the preparation of nanocomposites of a sulphonated sol-gel and a conducting polymer (Ch. 6) and of a sulphonated sol-gel and Pt/C (Ch. 7). These composites provide electronic conductivity to the materials made in this work, which make them useful as electrocatalysts. Chapter 7 reports on the use of a sulphonated sol-gel and Pt/C catalyst in hydrogen and direct methanol fuel cells.

References

[1]Rolison, D. R.; Dunn, B. *J. Mater. Chem.*, **2001**, 11, 963

[2]Collinson, M. M. *Anal. Chem.*, **2000**, 702A

[3]Kim, D. S.; Park, H. B.; Lee, Y. M.; Park, Y. H.; Rhim, J.-L. *J. Applied Polymer Science*, **2004**, 93, 209

[4]Alber, K. S.; Cox, J. A. *Mikrochim. Acta*, **1997**, 127, 131

[5]Hurd, C.B. *Chem. Rev.*, **1938**, 22, 403

[6]Watton, S. P.; Taylor, C. M.; Kloster, G. M.; Bowman, S. C. Coordination Complexes in Sol-Gel Silica Materials in *Progress in Inorganic Chemistry*, Vol. 51, ed. Kenneth D. Karlin. 2003, 333-420.

[7]Collinson, M. M.; Rausch, C. G.; Voigt, A. *Langmuir*, **1997**, 13, 7245

[8]Lev, O.; Bharathi, W. S.; Glezer, V.; Modestov, A.; Gun, J.; Rabinovich, L.; Sampath, S. *Chem. Mater.*, **1997**, 9, 2354

9Anderson, M. L.; Stroud, R. M.; Rolison, D. R. *Nano Letters*, **2002**, 2, 235

[10]Rolison, D. R. *Science*, **2003**, 299, 1698

[11]Barrero, J. M.; Camara, C.; Perez-Conde, M. C.; San Jose, C.; Fernandez, L. *Analyst*, **1995**, 120, 431

[12]Avnir, D.; Levy, D.; Reisfeld, R. *J. Phys. Chem.*, **1984**, 88, 5956

[13]Collinson, M. M.; Wang, H.; Makote, R.; Khramov, A. *J. Electroanal. Chem.*, **2002**, 519, 65

[14]Howells, A. R.; Zambrano, P. J.; Collinson, M. M., *Anal. Chem.*, **2000**, 72, 5265

[15]Walcarius, A.; Delacote, C.; Sayen, S. *Electrochimica Acta*, **2004**, 49, 3775

[16]Walcarius, A.; Delacote, C. *Chem. Mater.*, **2003**, 15, 4181

[17]Ellerby, L. M.; Nishida, C. R.; Nishida, F.; Yamanaka, S. A.; Dunn, D.; Valentine, J. S.; Zink, J. I., *Science*, **1992**, 255, 1113

[18]Kanungo, M.; Collinson, M. M., *Anal. Chem.*, **2003**, 75, 6555

[19]Hench, L. L.; West, J. K. *Chem. Rev.*, **1990**, 90, 33

[20]Iler, R. K. *The Chemistry of Silica*, John Wiley & Sons, Inc., New York, 1979

[21]Fricke, J.; Emmerling, A., *J. Am. Ceram. Soc.*, **1992,** 75, 2027

[22]Collinson, M. M.; Rausch, C. G.; Voigt, A., *Langmuir*, **1997**, 13, 7245

[23]Fricke, J.; Reichnauer, G., *Mater. Res. Soc. Symp. Proc.*, **1986**, 73, 775

[24]Bockhorst, M.; Heinloth, K.; Pajonk, G. M.; Begag, R.; Elaloui, E., *J. Non-Cryst. Solids*, **1995**, 186, 388

[25]Wong, G. K. S.; Crowell, P. A.; Cho, H. A.; Reppy, J. D., *Phys. Rev. B.*, **1993**, 48, 3558

[26]Smith, D. M.; Anderson, J.; Cho, C. C.; Johnston, G. P.; Jeng, S. P., *Mater. Res. Soc. Symp. Proc.*, **1995**, 381, 261

[27]Livage, J.; Henry, M.; Sanchez, C., *Prog. Solid State Chem.*, **1988**, 18, 259

[28]Schubert, U.; Huesing, N.; Lorenz, A., *Chem. Mater.*, **1995**, 7, 2010

[29]Avnir, D. *Acc. Chem. Res.*, **1995**, 28, 328

[30]Pajonk, G. M., *Appl. Catal.*, **1991**, 72, 217

[31]Cross, J.; Goswin, R.; Gerlach, R.; Fricke, J., *Rev. Phys. Appl.*, **1989**, 24, C4

[32]Woignier, T.; Phalippou, J.; Prassa, M., *J. Mater. Sci.*, **1990**, 25, 3118

[33]Merzbacher, C. I.; Barker, J. G.; Ryan, J. V.; Bernstein, R. A.; Long, J. W.; Rolison, D. R., *Nanostruct. Mater.*, **1990**, 12, 551

[34]Neves, S.; Fonseca, C. P., *J. Braz. Chem. Soc.*, **2004**, 15, 395

[35]Winter, M.; Brodd, R. J., *Chem. Rev.*, **2004**, 104, 4245

[36]Hsueh, C. C.; Collinson, M. M. *J. Electroanal. Chem.*, **1997**, 420, 243

[37]Tonle, I. K.; Ngameni, E.; Walcarius, A. *Electrochimica Acta*, **2004**, 49, 3435

[38]Shi, Y.; Seliskar, C. J.; Heineman, W. R. *Anal. Chem.*, **1997**, 69, 4819

[39]Wei, H., Collinson, M. M. *Anal. Chim. Acta.*, **1999**, 397, 113

[40]Wang, H.; Xu, G.; Dong, S. *Electroanalysis*, **2002**, 14, 853

[41]Lin, C.-L.; Tien, P.; Chau, L.-K. *Electrochim. Acta*, **2004**, 49, 573

[42]Kanungo, M.; Collinson, M. M. *Langmuir*, **2005**, 21, 827

[43]Liu, A.; Zhou, H.; Honma, I. *Electrochem. Communications*, **2005**, 7, 1

[44]Pandey, P. C.; Upadhyay, S.; Upadhyay, B. C.; Tripathi, V. S. *J. Sol-Gel Science and Technology*, **2005**, 33, 25

[45]Li, G.; Pickup, P.G. *Journal of the Electrochemical Society*, **2003**, 150. C745

[46]Pinol, S.; Najib, M.; Bastidas, D. M.; Calleja, A.; Capdevila, X. G.; Segarra, M.; Espiell, F.; Ruiz-Morales, J. C.; Marrero-Lopez, D.; Nunez, P. *J. Solid State Electrochem.*, **2004**, 8, 650

[47]Winter, M.; Brodd, R. J. *Chem. Rev.*, **2004**, 104, 4245

[48]Easton, E. B.; Astill, T. D.; Holdcroft, S. *J. Electrochem. Soc.*, **2005**, 152, A752

[49]Kreuer, K. D. *J. Membrane Sci.*, **2001**, 185, 29

[50]Li, G.; Pickup, P. G. *Electrochimica Acta*, **2004**, 49, 4119

[51]Mehta, V.; Cooper, J. S. *J. Power Sources*, **2003**, 114, 32

[52]Rolison, D. R.; Dunn, B. *J. Mater. Chem.*, **2001**, 11, 963

[53]Barsoukov, E.; MacDonald, J. R. Impedance Spectroscopy: Theory, Experiment, and Applications, 2nd ed. 2005

[54]EG&G Princeton Applied Research – Electrochemical Instruments Group. Princeton, NJ, 1984

[55]MacDonald, J. R.; Johnson, W. B. Impedance Spectroscopy: Emphasizing Solid Materials and Systems, ed. Mac Donald, J. R. John Wiley & Sons, Inc., New York, 1987

[56]de Levie, R. Advances in Electrochemistry and Electrochemical Engineering, ed. C. W. Tobais, NY, 1967

[57]Nilsson, J. W.; Riedel, S. A. Electric Circuits, 5th ed. Addison-Wesley Publishing Company, MA, 1996

[58]Raistrick, I. D. *Electrochimica Acta*, **1990**, 35, 1579

[59]Barcuam O. E.; D'Elia, E.; Frateur, I.; Mattos, O. R,.; Pebere, N.; Tribollet, B. *Electrochemica Acta*, **2002**, 47, 2109

[60]Pierre, A. C.; Pajonk, G. M. *Chem. Rev.*, **2002**, 102, 4243

[61]Wang, J. Analytical Electrochemistry, 2nd ed. Wiley-VCH Publishing, NY, 2000

[62]www.gamry.com/App_Notes/EIS_Primer/EIS_Primer.htm

Chapter 2:

Chemicals and Instrumentation

2.1 Materials

Tetramethyl orthosilicate (TMOS, 98%), ruthenium (III) hexamine chloride, ruthenium (II) tris(bipyridine), ferricyanide, trifluoroacetic acid (99+%), polytetrafluoroethylene (60 wt % in water) and Nafion 115 membranes were purchased from Sigma Aldrich. 2-(4-chlorosulfonylphenyl) ethyl-trichlorosilane (50% by volume in CH_2Cl_2) was purchased from United Chemical Technology Inc., Petrarch Silanes, Silicones and Bonded Silicas. ACS grade methanol and hydrochloric acid were purchased from Fisher Scientific. Sodium hydroxide pellets and potassium chloride were purchased from EM Science. Pyrrole and potassium nitrate (98%) were purchased from BDH Chemicals. Triton X-100 was purchased from Harleco. Carbon fiber paper and 20% Pt on Vulcan carbon were obtained from E-Tek. Nafion (5 wt % solution) was purchased from DuPont.

All commercial chemicals and solvents were used as received without further purification, except for pyrrole, which was distilled and kept refrigerated in a flask covered with foil to eliminate exposure to light. Triply deionized water was used in preparing all solutions. Experimental details relevant to a particular topic are located in each chapter.

2.2 Instrumentation

Electrochemical experiments were performed using one of the following sets of equipment:

Hokuto Denko HB-104 Function Generator and HA-301 Potentiostat/Galvanostat

A Hokuto Denko HA-301 Potentiostat/Galvanostat and HB-104 Function Generator were used to measure cyclic voltammetry, chronoamperometry and chronocoulometry using software written by Dr. P.G. Pickup and Dr. C.G. Cameron.

EG&G Par 273 A Potentiostat/Galvanostat/5210 Lock-in Amplifier

An EG&G Par 273A Potentiostat/Galvanostat with lock-in amplifier was used to collect iR compensated cyclic voltammograms, using EG&G/PAR M270 electrochemical software.

Solartron 1286/1250

Electrochemical Impedance Spectra (EIS) were collected from a Schlumberger Solartron 1286 electrochemical interface and 1250 frequency response analyzer using Z-Plot software (Scribner Associates, Inc.). CVs were obtained with this system by using software written by Dr. P.G. Pickup.

2.3 Hydrogel Modified Carbon Fiber Paper Electrodes

In preliminary experiments, films of the gel were prepared on polished glassy carbon disc electrodes by spin coating. However, in order to produce more stable gel modified electrodes, the wet gel was impregnated into porous carbon fiber paper (CFP) electrodes,[1] as described in Chapter 3. Although the use of three dimensional gel-impregnated CFP electrodes complicates the electrochemistry, makes quantitative

analysis more difficult, and introduces large experimental uncertainties, CFP electrodes are more relevant to many potential applications. These applications include sensors, fuel cells and batteries/supercapacitors, where large active electrode areas and mechanical stability are important. The use of planar glassy carbon electrodes are useful for fundamental experiments designed to understand the electrochemical dynamics for a given gel.

2.4 Stability of Gel Modified Electrodes

The (TMOS + sulphonated silane) gel modified electrodes showed no deterioration over several days of use and could by reloaded with redox probe following leaching and reused. This is further detailed in Chapter 3.

2.5 Hydrogel Physical Properties

Ion exchange and ion transport properties for hydrogels impregnated among the fibers of CFP electrodes were obtained from cyclic voltammetry (CV), chronoamperometry (CA) and chronocoulometry (CC). Ionic conductivities were obtained from EIS. Density and dry equivalent masses were estimated by mass and volume determinations.

2.6 Reproducibility of Electrochemical Results

CV, CA and CC measurements were performed in duplicate on different electrodes and yielded reproducible partition coefficients (within ca. 3 %) and diffusion

coefficients (within ca. 25 %) for most hydrogel compositions. Hydrogel compositions for which this was not the case are clearly labeled so. Ionic resistances obtained from EIS also showed good reproducibility (within ca. 20 %) from gel to gel.

2.7 Fuel Cell Testing

2.7.1 Fuel Cell Electrode Preparation

Fuel cell electrodes were prepared by thoroughly mixing the dry catalyst with the desired proportions of Nafion solution (5%, Dupont), "wet" sol or polytetrafluoroethylene (PTFE) to create "pastes". The pastes were then applied to the electrode backing (carbon fiber paper) by using a spatula to spread the paste evenly over the CFP.

For electrodes containing PTFE, a sintering step was used to bond the electrode as described in Chapter 7. Sintering enabled the PTFE to form an evenly distributed gas diffusion network.[2] After cooling to room temperature, wet sol was brush applied to the electrode as described in Chapter 7.

Catalyst, Nafion, hydrogel and PTFE loadings were determined gravimetrically using an analytical balance.

2.7.2 Membrane Electrode Assembly (MEA) Preparation

Nafion-based fuel cell MEAs were prepared by hot-pressing two electrodes across a Nafion 115 membrane at 130°C with a pressure of 140 $kg \cdot cm^{-2}$ for 90 seconds using a

Carver laboratory press equipped with temperature controlled heating blocks to maintain temperature with the applied pressure as described by Easton.[2] For hydrogel-based catalysts, no MEA pre-pressing was used and the MEA was assembled directly in the fuel cell.

2.7.3 Fuel Cell MEA Testing

Fuel cell membrane electrode assemblies were tested in 1 cm^2 or 5 cm^2 cells. The 1 cm^2 fuel cell was constructed in house from Plexiglass with an open current collector ring on each side which enabled gas to flow in each electrode. The 5 cm^2 cell, constructed from graphite blocks with serpentine flow-fields, was purchased from Fuel Cell Technologies. Both cells were sealed using silicone rubber gaskets. A schematic of the commercial cell is shown in Figure 2.1.

Gas flow was controlled by using rotameter flow meters. Hydrogen and oxygen gases were humidified by passing the gases through humidification chambers (bubbler) prior to entry into the cell. When using the Direct Methanol Fuel Cell (DMFC), the cell was run at 60°C and a pre-heater was used to maintain the methanol at the same temperature as the cell using a temperature controller. A one molar methanol solution was pumped into the cell using a Micropump 180 series magnetically driven suction shoe pump head equipped with a variable flow DC pump drive. The methanol solution was supplied at a flow rate of 25 mL/min. Air was not humidified when using the DMFC. A diagram of the DMFC test system is shown in Figure 2.2. Since a low percentage of the methanol is oxidized, the anode effluent was returned to the methanol tank and reused.

Fuel cells were tested by applying either a constant current or potential from a potentiostat and measuring the resulting potential or current. Measurements were recorded after sufficient time for the reading to stabilize. Further details are provided in Chapter 7.

2.8 Electron Microprobe Energy Dispersive X-Ray Analysis

Elemental compositions of sulfonated silica sol-gels + polypyrrole films grown under constant potential were obtained using energy dispersive X-ray (EDX) analysis with a Tracor Northern 5500 energy dispersive X-ray analyzer and a Hitachi S-570 scanning electron microscope. The relative elemental compositions were obtained using Tracor Northern's "SQ" (Standardless Quantitative Analysis) software. Calibration is described in Chapter 6.

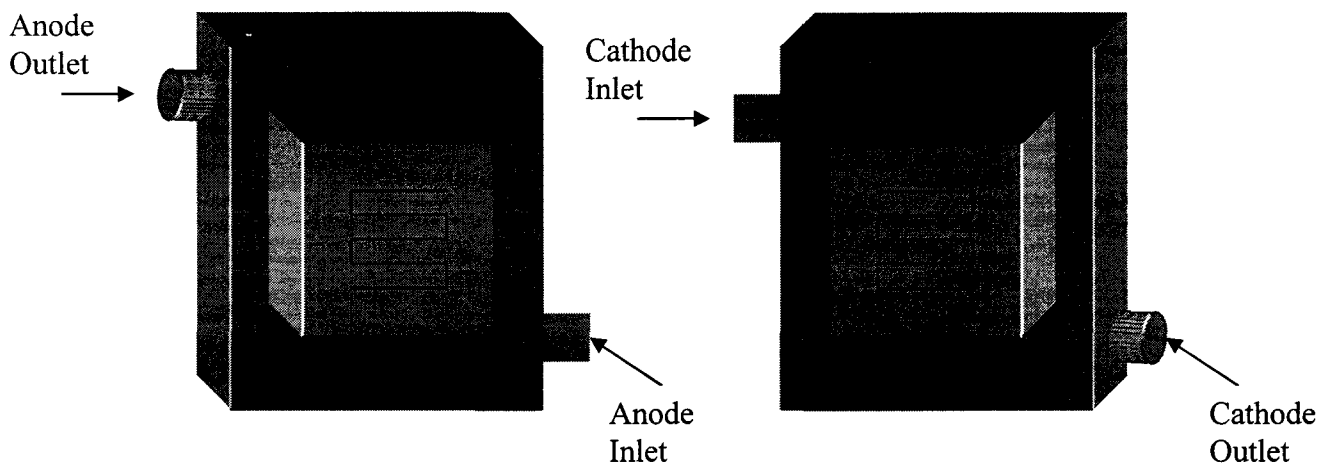

Figure 2.1 Schematic diagram of a fuel cell with serpentine flow fields.

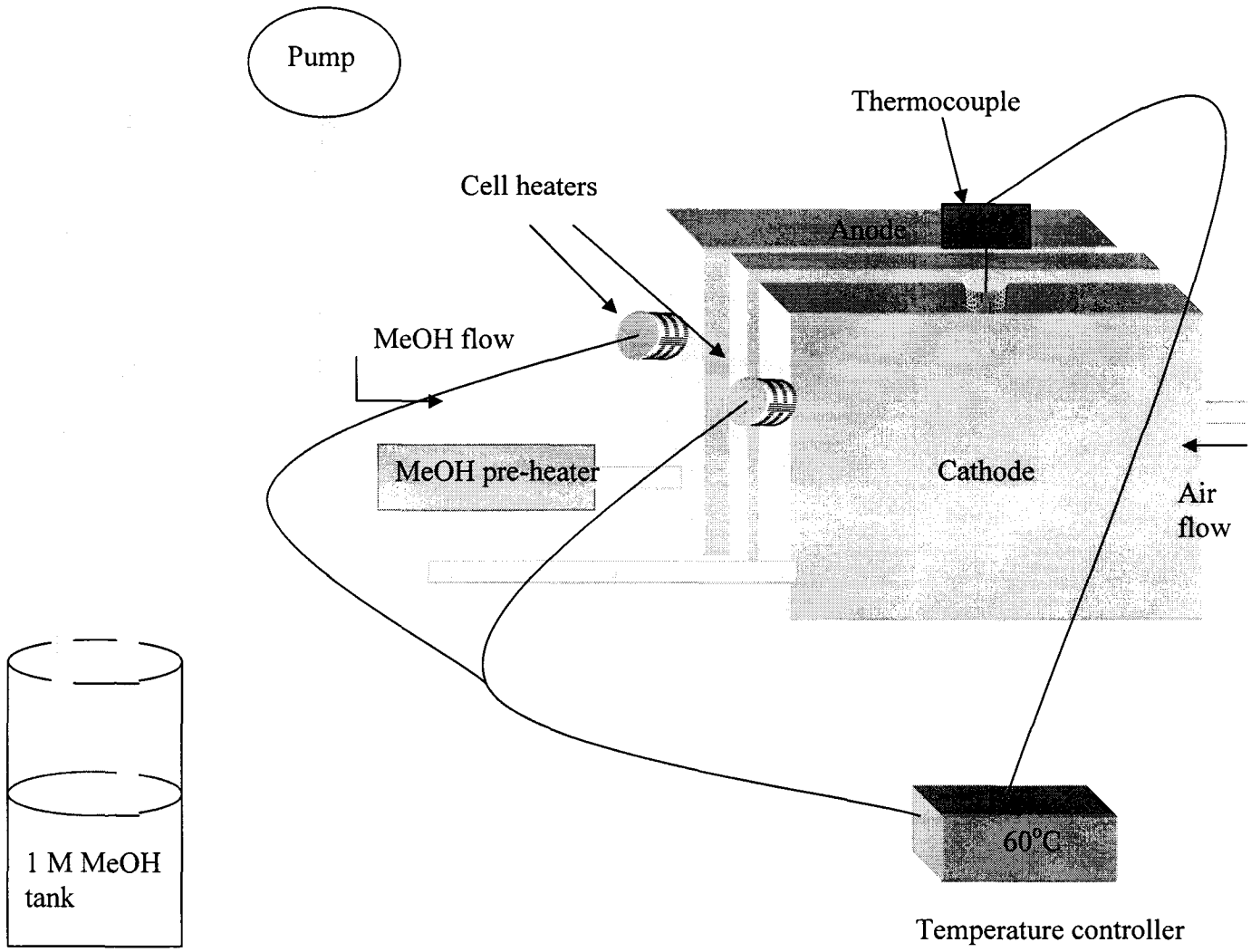

Figure 2.2 Schematic diagram of a DMFC testing system

References

[1]Aylward, W. M.; Pickup, P. G. *J. Solid State Electrochem.* **2004**, 8, 742

[2]E. B. Easton, Ph.D. Thesis, Memorial University of Newfoundland, Newfoundland (2003)

Chapter 3

Ion Exchange and Ion Transport Properties of Sulphonated Silica Sol-Gels

3.1 Introduction to Redox Probes in Sol-Gel Characterization

A wide variety of sol-gel materials have been investigated for electrochemical applications[1-13] and electrochemical methods have been used to characterize sol-gel processes and the properties of sol-gel materials.[5, 14-19] Typically, a redox probe is incorporated into the sol-gel matrix and its electrochemistry is monitored. This allows the extraction of information concerning the sol and gel structures, the mobility of entrapped species, and the extent of intermolecular interactions.[20] Sol-gels provide both molecular accessibility and rapid mass transport via diffusion because their structures are composed of three-dimensional networks of nanometer-sized particles surrounded by a continuous mesoporous volume.[3]

The concentration of redox probe exposed to the sol-gel network can be accurately controlled so that the partition coefficient for the probe in the sol-gel can be easily determined using chronoamperometry (CA) or chronocoulometry (CC).[1, 20] The partition coefficient is the ratio of the concentrations of the same molecular species in two different phases and is given by $K_p = [\text{molecule}]_{\text{phase1}} / [\text{molecule}]_{\text{phase2}}$. Using data extracted from the Cottrell Equation, eq. 1.4, applied to the CA or CC one can also accurately measure the diffusion coefficient, which describes the rate of diffusion of particles, for the redox probe inside the sol-gel matrix.[1, 20]

In this chapter, two strategies for incorporating electroactive probes into the sol-gel network and experiments which provide insight into the ion exchange and ion transport properties of the sol-gels are described.

In the first strategy, cyclic voltammograms (CV) of bare and gel-modified carbon fiber paper (CFP) electrodes were obtained in 0.1 M KNO_3 (aq) containing $Ru(NH_3)_6^{3+}$. In the second strategy, gel-modified CFP electrodes were pre-loaded with $Ru(NH_3)_6^{3+}$ by soaking them in solutions of $Ru(NH_3)_6^{3+}$ + 0.1 M CF_3CO_2Na (aq) of various redox probe concentrations for 24 hours. CV, CA, and CC measurements were then obtained for the loaded gel-modified CFP electrodes in 0.1 M CF_3CO_2Na (aq).

The effects of sulphonate concentration, sol-gel shrinkage, sol-gel solvent and sol-gel catalyzation on the ion exchange and ion transport properties are also discussed in this chapter.

Part of the work described in this chapter has been published in ref 21.

3.2 Experimental

3.2.1 Preparation of Hydrogel Modified Carbon Fiber Paper Electrodes

CF_3CO_2Na (aq) solutions were prepared by the neutralization of a CF_3CO_2H solution with NaOH (aq). The $Ru(NH_3)_6^{3+}$ redox probe was found to be unstable in solutions where the pH was greater than 8, therefore a slight excess of acid was used in all experiments to give a solution with pH ~ 3.3.[22]

A clear and colorless silica sol was prepared by adding a mixture of 0.6 mL of 2-(4-chlorosulfonylphenyl) ethyl-trichlorosilane (50 % in CH_2Cl_2) and 2.4 mL of methanol (or 2-propanol; see Section 3.3.6) to 1.5 mL TMOS, 1.3 mL deionized water and 0.3 mL 0.1 M HCl (aq) (or 0.1 M NaOH (aq); see Section 3.3.7) in a round bottom flask and heating at reflux for 1.5 hours. The reaction mixture was then sealed in a vial for 2 to 3

days at ambient temperature to gel. The mass of the mixture typically decreased by 30 % during preparation of the gel due to loss of the HCl and solvents.

In the experiments described below (except for in Section 3.3.3 where the amount of sulphonated silane was varied in the gels), the gel had an initial solvent content (MeOH, H_2O, CH_2Cl_2) of ca. 80 mass % and a calculated dry equivalent mass (EW) of ca. 733 $g \cdot mol^{-1}$ $-SO_3^-$, as shown in eqs 3.1 and 3.2. The CH_2Cl_2 (initially ca. 5 mass %) was presumably lost during refluxing and gelation, while residual MeOH would be replaced by water during the electrochemical experiments.

Percent solvent = (mass solvent / mass sol) x 100% Eq. 3.1

where the mass of solvent was 3.92 g as determined from volumes and densities of the reagents and the mass of the sol was 5 g.

EW = mass gel/ mol SO_3^- Eq 3.2

The dry mass of gel (0.88 g) was obtained after drying the gel for ca. 3 weeks, at which time the gel had shrunk to approximately a third of its original volume as solvent was lost from the pores. The moles of SO_3^- were calculated from the volume (50% by volume of 0.6 mL) and density (1.4 g/mL) of the sulphonated silane used (MW = 338.11 g/mol).

In preliminary experiments, films of the gel were prepared on polished glassy carbon disc electrodes by spin coating and their voltammetry was investigated in a solution of 1 mM $Ru(NH_3)_6^{3+}$ in 0.1 M KNO_3 (aq). Voltammograms of modified electrodes were not significantly different from those of bare carbon electrodes, and visual inspection following these experiments revealed that the gel separated from the electrode over the course of the experiments. Use of Triton-X to pre-treat the electrode[16]

did not help. This problem was overcome by using carbon fiber paper to make gel modified carbon fiber paper (CFP; Toray-090; thickness = 0.3 mm) working electrodes. These were prepared by suspending strips (ca. 5.5 mm x 40 mm) of CFP in a freshly prepared sol until complete gelation. Approximately 5 mm of each strip was immersed in the gel. The height was measured after removal from the gel using a ruler. Upon removing the CFP from the gel, excess gel on the surface of the electrode was mechanically scraped off. The amount of gel dispersed within the porous carbon matrix was determined from the increase in the mass of the electrode using the density of 1.09 $g \cdot cm^{-3}$ which had been determined for a bulk sample of the hydrogel aged for ca. 1 week in a sealed vial.

For a typical ca. 5.1 mm x 5.5 mm modified electrode area, this procedure resulted in the uptake of an average (for 13 electrodes) mass of gel corresponding to a volume of ca. 6.4 mm^3. This is the same as the void volume of the CFP (6.4 mm^3 based on 78 % porosity[23]), indicating complete filling of the pores with the gel. Average values are used because it is hard to reproduce the electrode areas.

The gels used in the work reported here were prepared and aged for several days in closed vials. Aging of the gels for longer periods or exposure to the atmosphere resulted in slow shrinkage due to loss of solvent. To prevent loss of solvent and possible collapse of the gel structures, the gel modified CFP electrodes were immersed in electrolyte + redox probe solutions within ca. 3 minutes of being removed from the vial containing the gel. The effects of gel shrinkage on the ion exchange and ion transport properties are discussed in Section 3.3.5.

3.2.2 Electrochemical Measurements

Electrochemical measurements were performed at ambient temperature in a 3 compartment conventional glass cell with an Ag/AgCl reference electrode and platinum wire auxiliary electrode. Solutions were purged with nitrogen for fifteen minutes before each experiment.

3.3 Results and Discussion

3.3.1 Ion Exchange and Stability

Figure 3.1 shows cyclic voltammograms of bare and gel-modified CFP electrodes in 0.1 M KNO_3 (aq) containing $Ru(NH_3)_6^{3+}$. The $Ru(NH_3)_6^{3+}$ electrochemistry was reversible (the peak separation is due to the solution resistance – see below) at the gel-modified electrode and peak currents were much larger than observed at the bare electrode, indicating that the $Ru(NH_3)_6^{3+}$ became concentrated in the gel by ion-exchange. The current amplitude in the CVs for the $Ru(NH_3)_6^{3+/2+}$ redox probes at the gel-modified electrode increased with time for ca. 5 hours and were then stable for at least another hour. In longer term experiments it was found that the $Ru(NH_3)_6^{3+}$ in 0.1 M KNO_3 (aq) solution was unstable and came out of solution, and so further experiments were conducted with CF_3CO_2Na (aq)[22] as the supporting electrolyte. The $Ru(NH_3)_6^{3+}$ complex stayed in solution over a period of several months using this electrolyte.

Figure 3.2 shows voltammograms, in a solution containing no redox probe, of a gel-modified CFP electrode that had been pre-loaded with $Ru(NH_3)_6^{3+}$ by soaking it in a

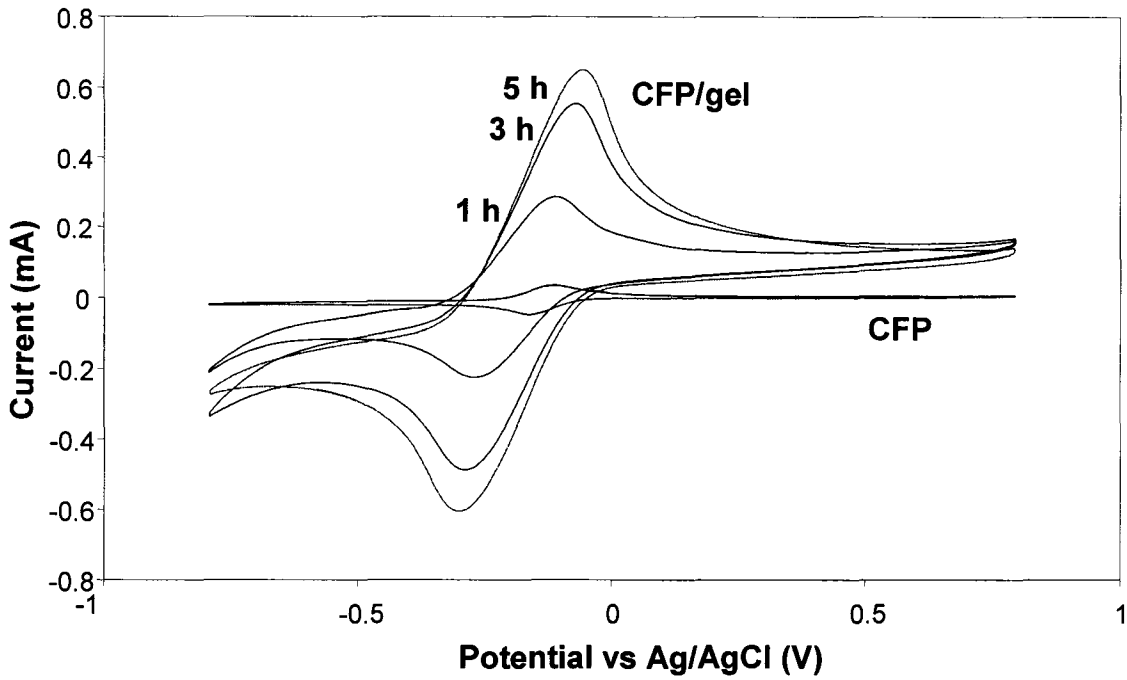

Figure 3.1 Cyclic voltammograms (10 $mV \cdot s^{-1}$) of gel loaded and bare CFP electrodes in 0.1 M KNO_3 (aq) containing 1 mM $Ru(NH_3)_6^{3+}$. Voltammograms at ~ 1h, 3h and 5 h in the solution are shown for the gel electrode.

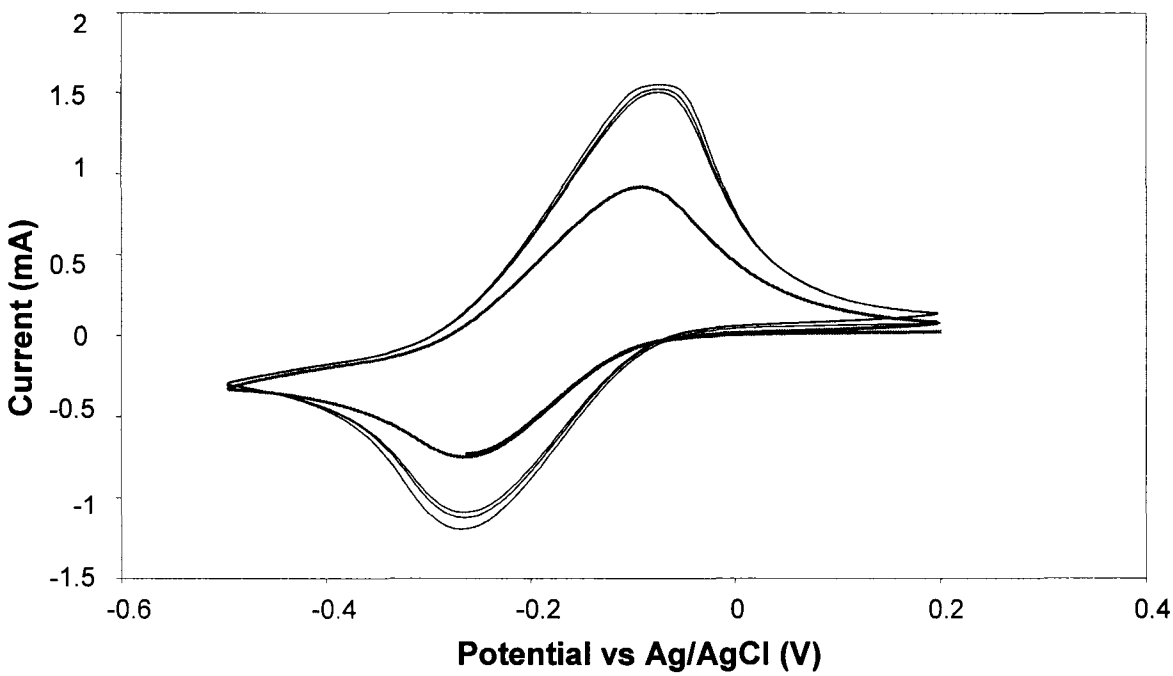

Figure 3.2 Cyclic voltammograms (10 $mV \cdot s^{-1}$) of a $Ru(NH_3)_6^{3+}$ loaded (1 mM; 24 h) CFP/gel electrode in 0.1 M CF_3CO_2Na (aq). The initial three scans are shown, together with a steady state voltammogram (bold) after 5 h.

1 mM $Ru(NH_3)_6^{3+}$ + 0.1 M CF_3CO_2Na (aq) solution for 24 hours. Again, large reversible $Ru(NH_3)_6^{3+}$ waves were seen, indicating concentration of $Ru(NH_3)_6^{3+}$ in the gel by ion-exchange. These waves decreased in height over a period of ca. 3 hours as the $Ru(NH_3)_6^{3+}$ diffused out of the gel,

$$n[Ru(NH_3)_6^{3+}]_{gel} \overset{k}{\leftrightarrow} (n-x)[Ru(NH_3)_6^{3+}]_{gel} + x[Ru(NH_3)_6^{3+}]_{soln},$$

and then remained stable for at least two more hours.

Voltammograms like those shown in Figs 3.1 and 3.2 exhibited linear relationships between peak currents and the square root of scan rate as shown in Figure 3.3, indicating diffusion control of the current.[26] Thus the charges under the voltammograms do not allow estimation of the concentration of $Ru(NH_3)_6^{3+}$ in the gel, even at scan rates as low as 1 $mV \cdot s^{-1}$. This is primarily a consequence of the thickness of the gel layer.[21] Concentrations and partition coefficients were therefore determined by chronocoulometry (see Section 3.3.2).

The larger than theoretical (59 mV) peak separations observed in Figs 3.1 and 3.2 are due to the uncompensated solution resistance, measured to be 75 Ω by impedance. This was measured using a gel-modified electrode, and it is reasonable to assume that some small portion of this resistance may in fact be due to resistance in the gel as well as in the solution. This has a pronounced effect here because of the high currents generated by the three dimensional CFP/gel electrode, relative to a planar modified electrode. In order to demonstrate and minimize the effect of the solution resistance, the concentration of the supporting electrolyte, CF_3CO_2Na (aq), was increased to 1 M. As can be seen in Figure 3.4, this decreased the peak to peak separation, but led to excessive leaching of the

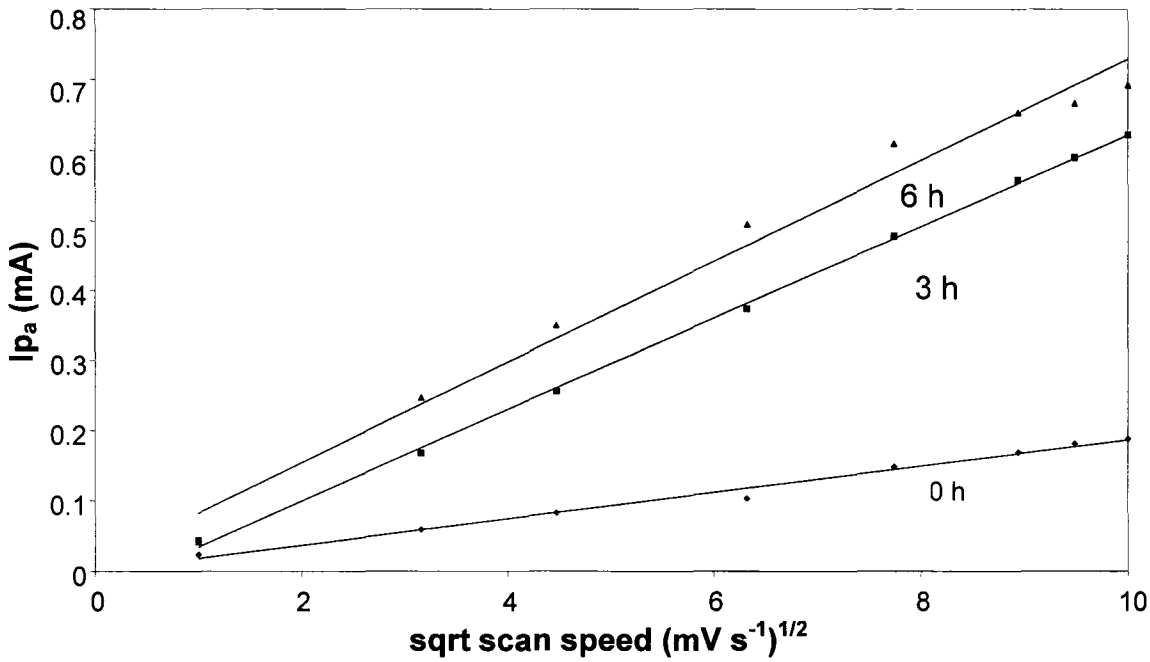

Figure 3.3 Peak current vs (scan speed)$^{1/2}$ for a CFP electrode in 1 mM $Ru(NH_3)_6^{3+}$ redox probe in 0.1 M CF_3CO_2Na (aq). Data shown are for 0 h, 3 h and 6 h of immersion in the redox probe solution.

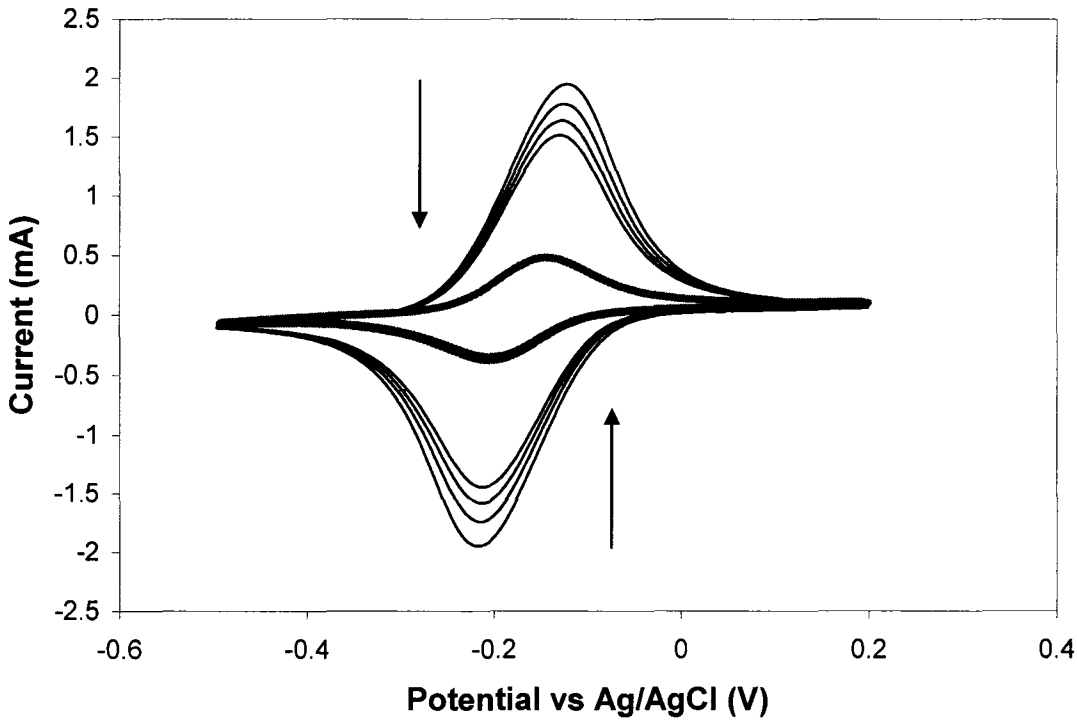

Figure 3.4 Cyclic voltammograms (10 $mV \cdot s^{-1}$) of a $Ru(NH_3)_6^{3+}$ loaded (1 mM; 24 h) CFP/gel electrode in 1 M CF_3CO_2Na (aq). The initial four scans are shown, together with a voltammogram (bold) recorded after 75 minutes.

$Ru(NH_3)_6^{3+}$ probe from the gel. The peak current decreased to half of its original value in only 15 minutes, and continued to decrease with time.

The effect of the solution resistance was further demonstrated by obtaining cyclic voltammograms with iR compensation using this option on the EG&G potentiostat, as shown in Figure 3.5. These voltammograms clearly show how subtracting part of the solution resistance yielded CVs with closer to the theoretical peak separation.

The pH of the electrolyte solution was also found to strongly influence the voltammetric behavior of the $Ru(NH_3)_6^{3+}$-loaded CFP/gel electrodes and hence the effect of pH on the ion-exchange voltammetry was studied.[27] The results shown above were obtained with a slightly acidic (pH ~ 3.3) CF_3CO_2Na (aq) electrolyte. When a higher pH (~8) solution was used, the characteristic $Ru(NH_3)_6^{3+}$ peaks were absent. Electrolyte solutions with pHs between the range of 3 and 4 displayed cyclic voltammograms with reversible but largely separated peaks for the $Ru(NH_3)_6^{3+}$ probe. At pH below 2, cyclic voltammograms were obtained with very well defined $Ru(NH_3)_6^{3+}$ peaks with smaller peak separations. However, the diffusion coefficients obtained for the redox probe in electrolyte solutions between pH 3-4 were all similar and easy to reproduce while those obtained for solutions at pH < 2 were significantly larger and not as reproducible. Therefore, a CF_3CO_2Na (aq) electrolyte with a pH ca. 3.3 was prepared. Figure 3.6 shows the difference in voltammograms obtained for the various different pH values for the electrolyte.

As shown in Fig 3.6, I_{pa} initially decreased with increasing pH because of a decrease in the conductivity of the electrolyte as the concentration of protons in solution

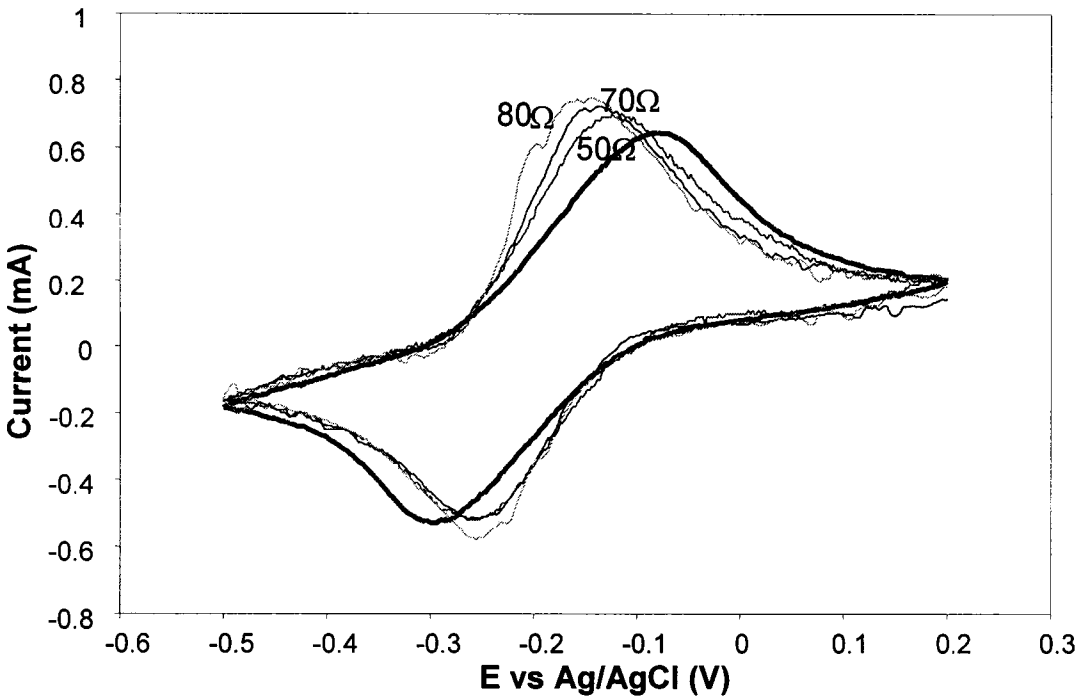

Figure 3.5 IR compensated cyclic voltammograms (10 $mV \cdot s^{-1}$) of a $Ru(NH_3)_6^{3+}$ loaded (0.5 mM; 24 h) CFP/gel electrode in 0.1 M CF_3CO_2Na (aq). Values for built-in iR compensation are shown on the plot. The CV having no iR compensation is shown in bold.

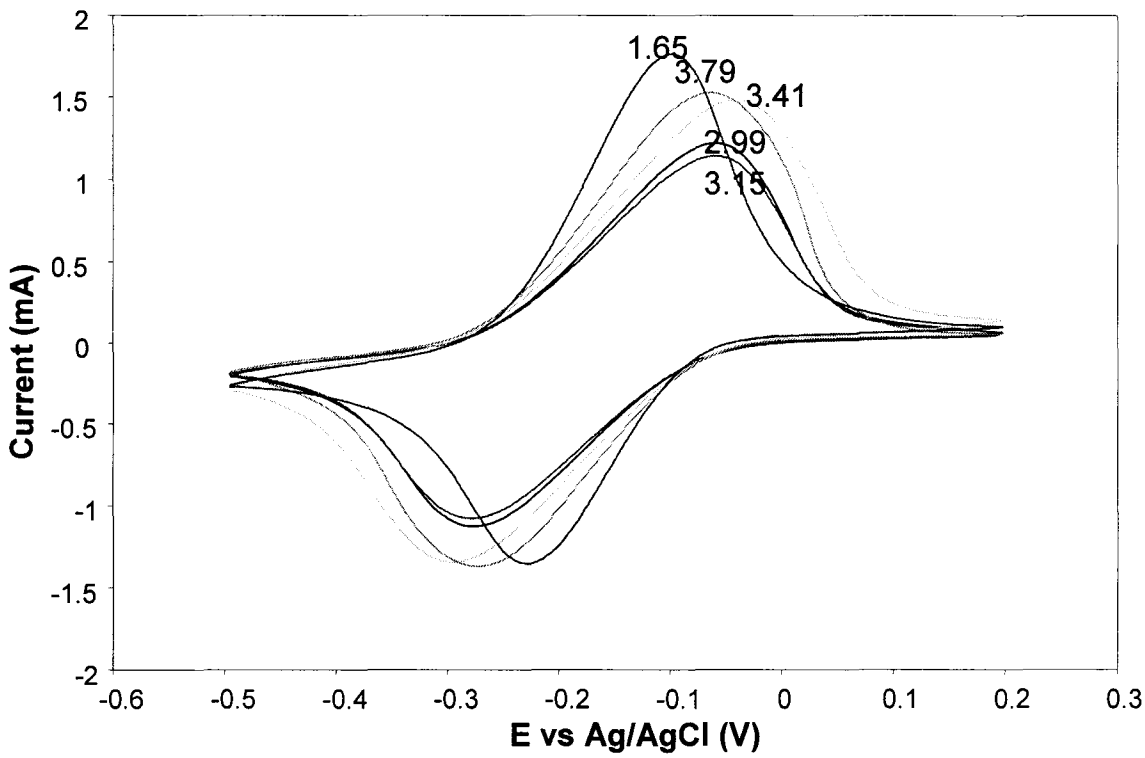

Figure 3.6 Cyclic voltammograms (10 $mV \cdot s^{-1}$) of a $Ru(NH_3)_6^{3+}$ loaded (ca. 3 mM; 24 h) CFP/gel electrode in 0.1 M CF_3CO_2Na (aq) as a function of electrolyte pH.

decreased. A minimum was reached at pH = 3.15, after which Ip_a increased with increasing pH indicating that the deprotonation of the surface silanol groups strengthened the interactions between the positively charged $Ru(NH_3)_6^{3+}$ probe and the negatively charged sol walls.[27] Silica-based materials are also known to be less stable at extreme pHs.[27]

The gel modified electrodes showed no deterioration over several days of use in acidic solution and could be re-loaded with $Ru(NH_3)_6^{3+}$ following leaching and reused. Figure 3.7 shows the excellent agreement between voltammograms obtained for a freshly loaded CFP/gel electrode and that of the same electrode re-loaded with $Ru(NH_3)_6^{3+}$ and used several days later. The high stability of the modified electrode is related to the mechanical and chemical stability of the silicate matrix and the possible interaction of the Ru-complex with the silanol and/or sulphonate groups.[26]

3.3.2 Partition Coefficients

Concentrations of $Ru(NH_3)_6^{3+}$ in gels that had been equilibrated in solutions containing various concentrations of $Ru(NH_3)_6^{3+}$ in 0.1 M CF_3CO_2Na (aq) were determined from the limiting charge values obtained from chronocoulometry in 0.1 M CF_3CO_2Na (aq) containing no $Ru(NH_3)_6^{3+}$ probe. Figure 3.8 shows a typical charge vs. time plot. Although these data have been corrected by subtraction of the background currents measured at bare CFP electrodes, the charge continues to rise linearly at long times, indicating the presence of additional background currents. These may be due to

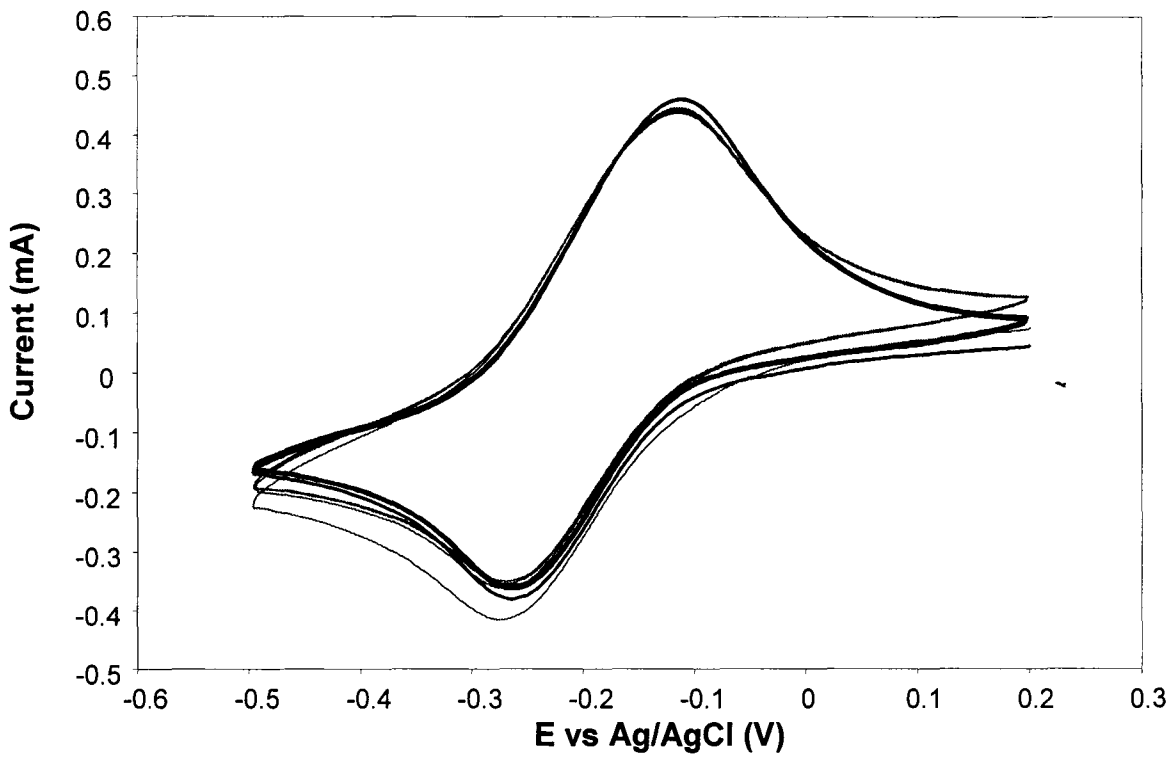

Figure 3.7 Cyclic voltammograms (10 $mV \cdot s^{-1}$) of a $Ru(NH_3)_6^{3+}$ re-loaded (ca. 0.5 mM; 24 h) CFP/gel electrode in 0.1 M CF_3CO_2Na (aq). Shown in bold is the original cyclic voltammogram for the $Ru(NH_3)_6^{3+}$ loaded CFP/gel electrode.

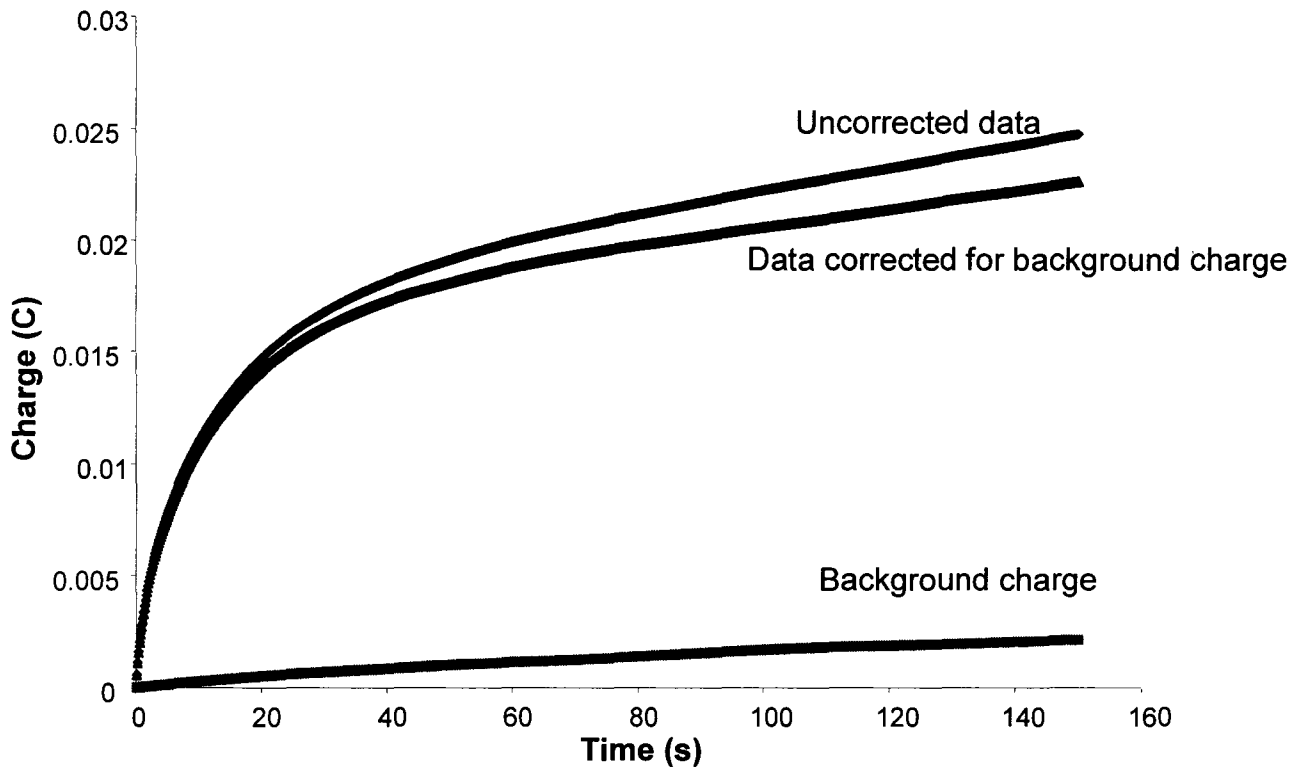

Figure 3.8 Chronocoulometric plot for a –0.4 V to +0.2 V potential step on a $Ru(NH_3)_6^{3+}$ loaded (1 mM; 24 h) CFP/gel electrode in 0.1 M $CF_3CO_2Na_{(aq)}$. Data for the same experiment on a bare CFP electrode have been subtracted as a background correction.

$Ru(NH_3)_6^{3+}$ that is either in dense poorly accessible regions of the gel, to the presence of methanol in the sol-gel matrix, or to the bulk solution. In order to estimate the concentration of $Ru(NH_3)_6^{3+}$ in the gel available for facile electrochemistry, this contribution to the final charge was neglected. This is the most appropriate concentration to use in kinetic analyses but it may underestimate the partition coefficients by ca. 20-30 %.

Table 3.1 shows partition coefficients ($K_p=[Ru(NH_3)_6^{3+}]_{gel}/[Ru(NH_3)_6^{3+}]_{solution}$) for $Ru(NH_3)_6^{3+}$ in the gel. Over the range of solution concentrations studied, the concentration of $Ru(NH_3)_6^{3+}$ in the gel increased linearly with increasing solution concentration and then became non-linear and saturated as solution concentration was increased. The saturation behaviour indicates that no further $Ru(NH_3)_6^{3+}$ could be concentrated into the gel. The partition coefficient was approximately constant at ca. 36 ±8 which is the average of 13 measurements obtained on 13 different modified electrodes.

The concentration of sulphonate groups in the gel can be estimated to be ca. 0.3 M based on the mass and approximate composition of the gel (shown below). This is only 3 times the maximum $Ru(NH_3)_6^{3+}$ concentration of 0.10 M reported in Table 3.1 for the gel, indicating that essentially all of the sulphonate sites are associated with the Ru complex at the highest loading used.

$[SO_3^-]$ = mol SO_3^- / volume of sol remaining after reflux Eq. 3.3

Table 3.1. Partition coefficients for $Ru(NH_3)_6^{3+}$ and diffusion coefficients for $Ru(NH_3)_6^{2+}$ in gels loaded from different concentrations of $Ru(NH_3)_6^{3+}$ in 0.1 M CF_3CO_2Na(aq).

$[Ru(NH_3)_6^{3+}]_{soln}$ / mM	$[Ru(NH_3)_6^{3+}]_{gel}$ / mM	K_p	D_{2+} / 10^{-8} cm^2 s^{-1}
0.5	12.7	25.3	11
1.00	22.8	22.8	5.2
1.21	30.8	25.5	4.0
1.42	42.4	29.9	4.2
1.50	44.6	29.8	5.1
1.94*	96.5, 99.3	49.7, 51.1	4.5, 3.8
2.00*	78.3, 80.0	39.2, 40.0	4.1, 4.2
2.45*	92.2, 94.0	37.6, 38.4	5.3, 4.1
2.97*	102, 104	34.2, 34.9	4.0, 3.9

* duplicate measurements

where the mol of SO_3^- is determined from the volume (50%) and density (1.4 g/ml) of the sulphonated silane (MW = 338.11 g/mol) and the volume of sol remaining after reflux is ca. 4.3 mL after loss of CH_2Cl_2 and some methanol (see experimental).

3.3.3 Apparent Diffusion Coefficients for $Ru(NH_3)_6^{3+/2+}$ in the Gel

The Faradaic current that flows when a redox species undergoes reversible electron-transfer at an electrode surface provides a direct measure of the apparent diffusion coefficient (D_{app}) of the redox species.[24] This can best be determined from chronoamperometry, or chronocoulometry for a planar electrode. Figure 3.9 shows a typical chronoamperometry (Cottrell) plot obtained for a $Ru(NH_3)_6^{3+}$-loaded CFP/gel electrode in 0.1 M CF_3CO_2Na (aq) when stepped from –0.4 V to 0.2 V. The current at the shortest times is limited by the solution resistance, as described below*, but then there is a linear I vs. $t^{-1/2}$ region that appears to fit the Cottrell equation nicely. At long times, the current falls sharply due to depletion of $Ru(NH_3)_6^{2+}$ within the finite volume of the gel.[28] Application of the Cottrell equation to the intermediate linear region gave a D_{app} value of ca. 1 x 10^{-7} $cm^2 \cdot s^{-1}$, which would correspond to a diffusion layer thickness ($\delta = (\pi Dt)^{1/2}$) of ca. 5.5 μm at t = 1s. Since this is much larger than 10 % of the radius (4.2 μm) of the fibers of the CFP, the use of the Cottrell equation, which assumes linear diffusion, is invalid.[28] The Cottrell equation is only valid for times up to ca. 10 ms, and at such short times, the current is limited by the solution resistance.[28]

---

*The maximum current obtained by Ohm's Law for this potential step (-0.4 V to 0.2 V, a 0.6 V potential) and R_u of 75 Ω is i = V / R = 0.6 V / 75 Ω = 8 mA.

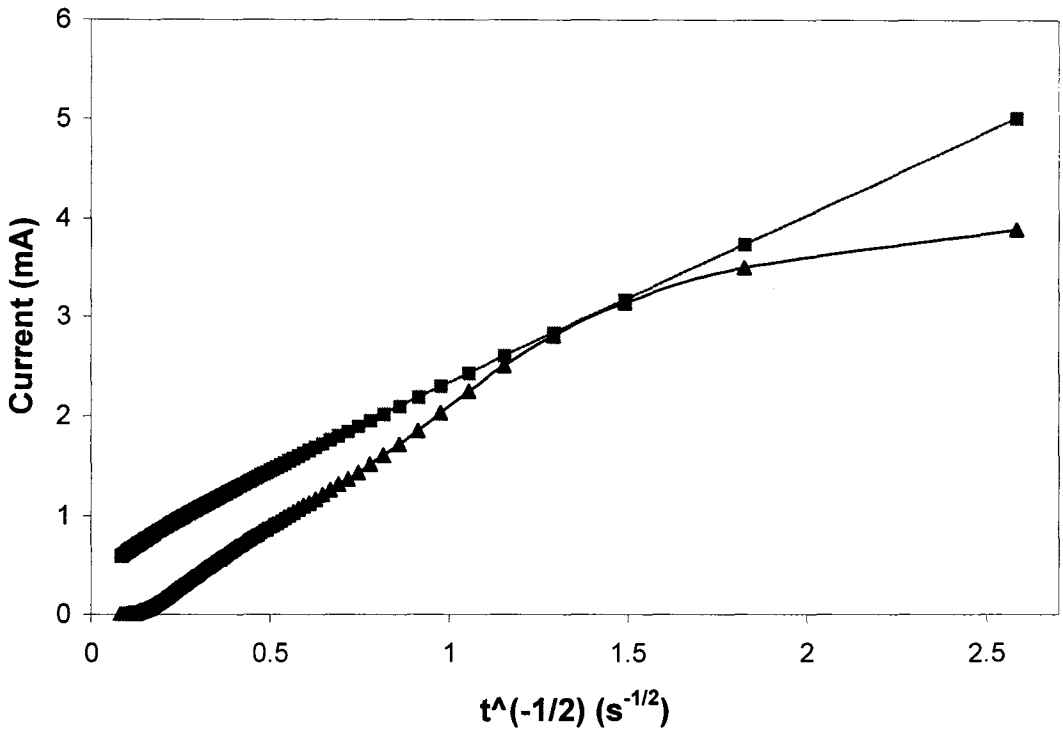

Figure 3.9 Chronoamperometric plot (triangles) for a –0.4 V to +0.2 V potential step on a $Ru(NH_3)_6^{3+}$ loaded (1 mM; 24 h) CFP/gel electrode in 0.1 M CF_3CO_2Na (aq). Squares are data calculated from Eq. 1.4.

The chronoamperometric response for diffusion to a cylindrical microelectrode of radius r, can be represented by the following equation[24]

$$i = (nFAD_{app}C/r)[2\exp(-0.05\pi^{1/2}\tau^{1/2})/\pi^{1/2}\tau^{1/2} + 1/\ln(5.2945 + 0.7493\tau^{1/2})] \quad \text{Eq 3.4}$$

where $\tau = 4D_{app}t/r^2$. Since the concentration (C) of $Ru(NH_3)_6^{2+}$ in the gel is known, and the total area of the fibers (average = 5.3 ± 0.2 cm^2) can be calculated from the fiber radius (r) of 4.2 μm determined by SEM and the total volume of the carbon fibers (electrode volume x (1 – porosity)), D_{app} can be obtained by manual fitting of this equation to the experimental data at short times. At longer times (> 1 s), the finite distance between fibers leads to more rapid depletion of $Ru(NH_3)_6^{2+}$ than predicted by the semi-infinite diffusion assumption implicit in Eq. 3.4, and the experimental current falls below the calculated current.

The apparent diffusion coefficients for the ruthenium complex in the gel-modified electrode, as determined from Eq. 3.4 fitted to the data $t^{-1/2}$ = ca. 1.25-1.5 on Fig. 3.9, were 3.4 x 10^{-8} $cm^2 \cdot s^{-1}$ for the $Ru(NH_3)_6^{2+}$ ion (-0.4 V to 0.2 V step) and 1.5 x 10^{-8} $cm^2 \cdot s^{-1}$ for $Ru(NH_3)_6^{3+}$ (0.2 V to –0.4 V step). The larger D_{app} for the less highly charged ion indicates dominance by molecular diffusion, rather than electron hopping. Similar behavior was reported by Buttry and Anson[22, 25] for $Ru(NH_3)_6^{3+/2+}$ in Nafion films coated on pyrolytic graphite electrodes. They believed that the diffusion of this complex proceeded by physical motion, thereby giving two distinct D_{app} values for the differently charged species.[22]

Measured values of D_{app} for the $Ru(NH_3)_6^{3+}$ probe in the gel were independent of probe concentration in the gel over the range of 10 to 100 mM, as shown in Table 3.1. The average was $(3.3 \pm 1.1) \times 10^{-8}$ $cm^2 \cdot s^{-1}$.

3.3.4 Effects of Gel Aging and Shrinkage on Ion Exchange and Ion Transport Properties

One of the primary concerns associated with the application of sol-gel hosts is the long-term stability of the materials. As the sols aged, they became more viscous and solidified to a hard, rubber-like gel in ca. 4 to 5 days. Further aging beyond this point resulted in a very brittle glass-like material as the gel underwent synerisis structure collapse. Microstructural changes in the pore structure can alter the nature of the entrapment of redox probes in the sol-gel matrix.[15]

To measure how aging affected the sulphonated silica sol-gel properties, a large batch of the gel was prepared and separated into several smaller vials. Into each of these vials was placed a strip of CFP and the gels inside were allowed to dry in open air. At various times during the aging process, the gel-impregnated CFP electrodes were removed and the CV and CA were measured. Figure 3.10 shows the cyclic voltammograms of typical sulphonated silica sol-gels as a function of aging time. The basic shape of the cyclic voltammograms remained the same over a period of two months, but there was a significant decrease in the $Ru(NH_3)_6^{3+/2+}$ peak heights.

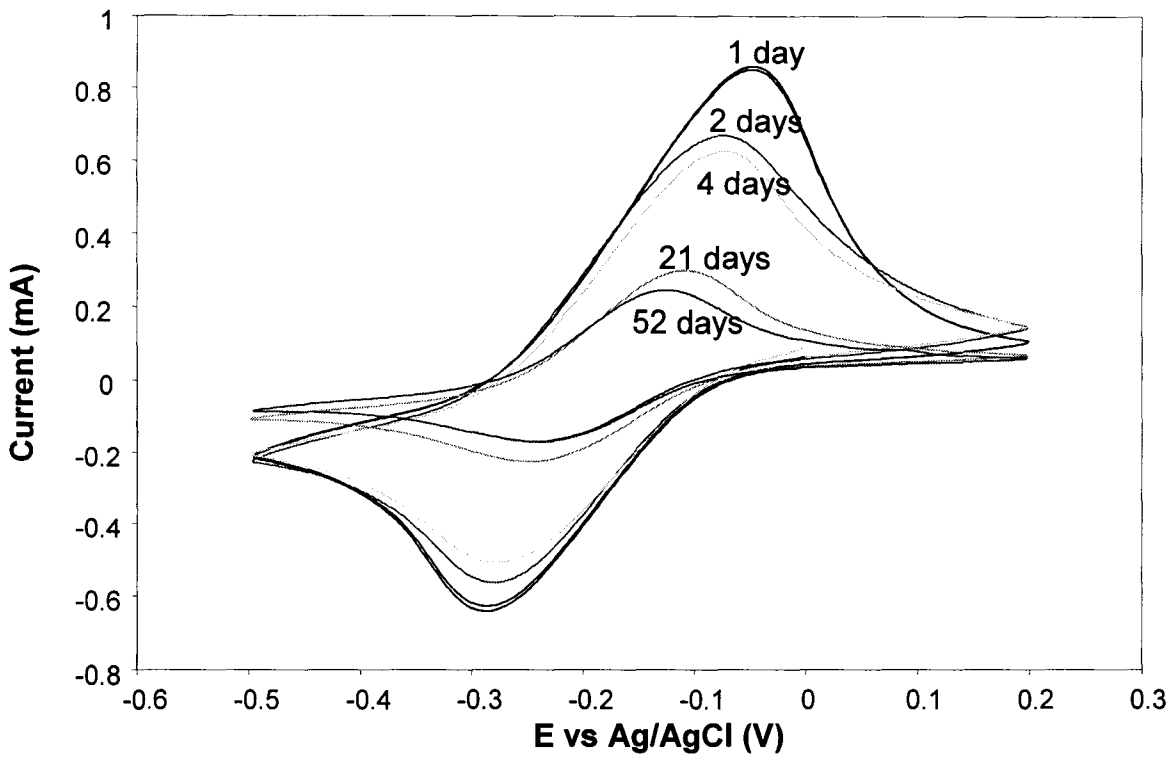

Figure 3.10 Cyclic voltammograms (10 $mV \cdot s^{-1}$) of $Ru(NH_3)_6^{3+}$ loaded (ca. 1 mM; 24 h) CFP/gel electrodes in 0.1 M CF_3CO_2Na (aq) as a function of gel aging. Aging times are indicated on the plot.

While the apparent diffusion coefficient steadily dropped from ca. $5x10^{-8}$ $cm^2 \cdot s^{-1}$ for the gel aged for 1 day to $7x10^{-9}$ $cm^2 \cdot s^{-1}$ for the gel aged for 52 days, the partition coefficient showed no such dependence on the gel aging and remained constant at ca. 30.

Due to the constraints of pore structures and surface interactions, diffusion in sol-gel solids can be significantly more complex than in liquids.[5] Since the gel was ca. a twentieth of its original size by day 52, the relatively small drop in D_{app} and constant partition coefficient can be explained as follows. D_{app} decreases as the gel dried because of a decrease in the porosity of the gel, and/or an increase in the extent of intermolecular interactions between the probe and the gel matrix due to the increase in surface area-to-volume ratio.[5] However, as the gel dried and shrank in size, it lost some of its solvent to evaporation and therefore an apparent increase in the concentration of the entrapped redox probe inside the gel matrix was observed.[5]

Quantitative analyses were not performed for gels aged in sealed vials as a function of time. As the gels aged in sealed vials the sol-gel solvent required significantly longer time (months instead of weeks) for solvent evaporation and subsequent collapse of the gel matrix.

3.3.5 Effects of Sol-Gel Sulphonate Concentration on Ion Exchange and Ion Transport Properties

The effect of sulphonate concentration on ion exchange and ion transport properties in the ormosil gels was determined by preparing gels with varying amounts of the sulphonated silane while the remainder of the gel components remained constant.

As the sulphonate concentration was increased, the amount of SO_3^- sites available for ion exchange with the ruthenium complex also increased. As a result, the sols displayed a continuous increase in D_{app} and K_p as the amount of sulphonated silane in the sols was increased, as shown in table 3.2. This increase continued until a composition was reached which produced unstable sols. These sols (at twice the original amount of sulphonated silane) took significantly longer to gel and did not yield easily reproducible CVs or charges from chronoamperometry. Increasing the organosilane content in the synthesis of sol-gels is reported as leading to less ordered and less open structures.[11] Walcarius and Delacôte[12] have reported that the aggregates for materials containing higher organic group loadings were much larger than for those of lower loading.[12] Furthermore, they ascribed this phenomenon to the increased hydrophobicity of the hybrids compared to those materials containing no or little organic moieties.[12]

3.3.6 Effects of Solvent on Sol-Gel Ion Exchange and Ion Transport Properties

While sol-gels can be prepared without the addition of solvents, besides the water required for the sol-gel reaction itself, the initial reaction mixture is a two-phase system that must be vigorously mixed or sonicated in order to achieve a homogeneous sol.[20] Therefore, additional co-solvents are commonly added to homogenize the reaction mixture or to assist with dissolution of dopants. The nature of these co-solvents can greatly influence the sol-gel reactions.[29, 30] It has been reported in the literature that sol-gels prepared with isopropanol as the mutually miscible solvent display pore sizes that are larger than those obtained using other solvents.[31]

Table 3.2 Diffusion and partition coefficients for $Ru(NH_3)_6^{2+}$ in gels of varying $[SO_3^-]$. As the amount of sulphonate silane increases in the gel, the $[SO_3^-]$ increases.

$[Ru(NH_3)_6^{3+}{}_{soln}]$ / mM	Gel Composition $SiO_2 : SO_3^-$ mol ratio	D_{2+} / 10^{-8} $cm^2 \cdot s^{-1}$	K_p
ca. 1.0	1 : 0	8 ± 2	0.2 ± 0.01
	33.4 : 1	2.1 ± 0.5	13.0 ± 0.4
	11.8 : 1	3.8 ± 0.9	25 ± 1
	*9.3 : 1	5 ± 1	23 ± 1
	7.5 : 1	5 ± 1	42 ± 1
	6.4 : 1	11 ± 3	47 ± 1
	5.2 : 1	Not reproducible	Not reproducible

*Duplicate measurements made. See section 3.3.3

In this work sols were prepared with isopropanol as the mutually miscible solvent. A comparison of the CVs, D_{app} and K_p parameters with those obtained from previous experiments with sols made using methanol was performed. These results are summarized in Fig 3.11 and Table 3.3. The data show that the nature of the co-solvent did not have a large effect on the ion exchange or ion transport properties in these sols. There does appear to be an increase in K_p, but this is within the range observed for gels prepared with methanol (see Table 3.1).

3.3.7 Effects of the Sol-Gel Catalyst on Ion Exchange and Ion Transport Properties

The sol-gel process is a two-step inorganic polymerization (see Section 1.1) process occurring in the liquid state. The resulting sol-gel structure/texture is largely dependant on the relative rates of the hydrolysis and polycondensation reactions. Under conditions that favor hydrolysis, condensation is the rate-limiting step and small hydroxylated oligomers predominate, yielding polymer-like gels with relatively small pores. Alternately, when high condensation rates are favored, the resulting gel network consists of interconnected colloidal particles and large pores.[3, 20]

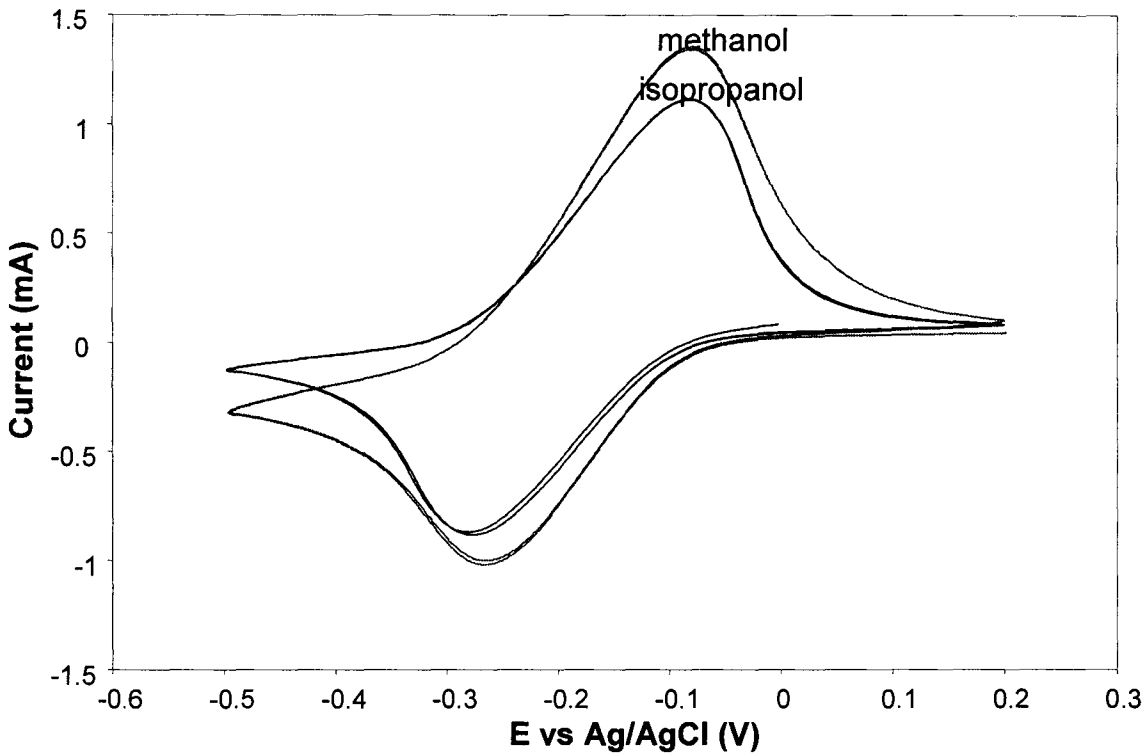

Figure 3.11 Cyclic voltammograms (10 $mV \cdot s^{-1}$) of $Ru(NH_3)_6^{3+}$ loaded (ca. 1 mM; 24 h) CFP/gel electrodes in 0.1 M CF_3CO_2Na (aq). The solvent used in preparing the sol-gel is shown on the plot.

Table 3.3 Diffusion and partition coefficients for $Ru(NH_3)_6^{2+}$ in gels prepared with different solvents.

Gel Solvent	**$[Ru(NH_3)_6^{3+}]_{soln}$ mM**	**$[Ru(NH_3)_6^{3+}]_{gel}$ mM**	**K_p**	**D_{2+} / 10^{-8} $cm^2 \cdot s^{-1}$**
Methanol	1.0	22.8	22.8 ± 0.7	5 ± 1
Isopropanol	0.78	32.3	41 ±1	7 ± 2

Because silicon alkoxide precursors have a low electrophilicity and their coordination number is stable (because the silicon precursor and product oxide have the same coordination number, N =4), the hydrolysis of $Si(OR)_4$ is slow and the rates of the polymerization reactions in these alkoxides are mainly controlled by acid or base catalysis.[3] Under acid-catalyzed conditions, condensation reactions are rate limiting and therefore gels compromised of very small particle sizes are formed.[20] This minimizes light scattering effects and gives rise to optically transparent gels.[20] Under base-catalyzed conditions, hydrolysis is the rate-limiting step and gels composed of larger, denser particles with lower surface area and high porosities are formed.[20] These gels are preferable for applications such as catalysis, where accessibility of substrates to supported metal centers is essential and optical transparency is expendable.[20]

The sulphonated silica sol-gels prepared in this work by acid catalysis ($HCl_{(aq)}$) were clear and colorless while those prepared under basic conditions ($NaOH_{(aq)}$) were white and opaque. The D_{app} values obtained for the base catalyzed gels were an order of magnitude larger than those obtained for the acid catalyzed gels described above and are shown in Table 3.4. The cyclic voltammograms for a base-catalyzed sol-gel is compared to that of an acid catalyzed sol-gel in Fig 3.12. Acid catalysis resulted in gels with smaller particle sizes that can fit more tightly together in the gel matrix. However, base catalysis resulted in gels with larger pore sizes that could fit more of the redox probe inside the gel matrix and allowed for easier physical diffusion of the probe.

Table 3.4 Diffusion and partition coefficients for $Ru(NH_3)_6^{2+}$ in gels prepared with different sol-gel catalysts.

Gel Catalyst	**$[Ru(NH_3)_6^{3+}]_{soln}$ mM**	**$[Ru(NH_3)_6^{3+}]_{gel}$ mM**	**K_p**	**D_{2+} / 10^{-8} $cm^2 \cdot s^{-1}$**
HCl (aq)	1.0	22.8	22.8 ± 0.7	5 ±1
NaOH (aq)	1.3	10.5	8.2 ± 0.2	57 ± 14

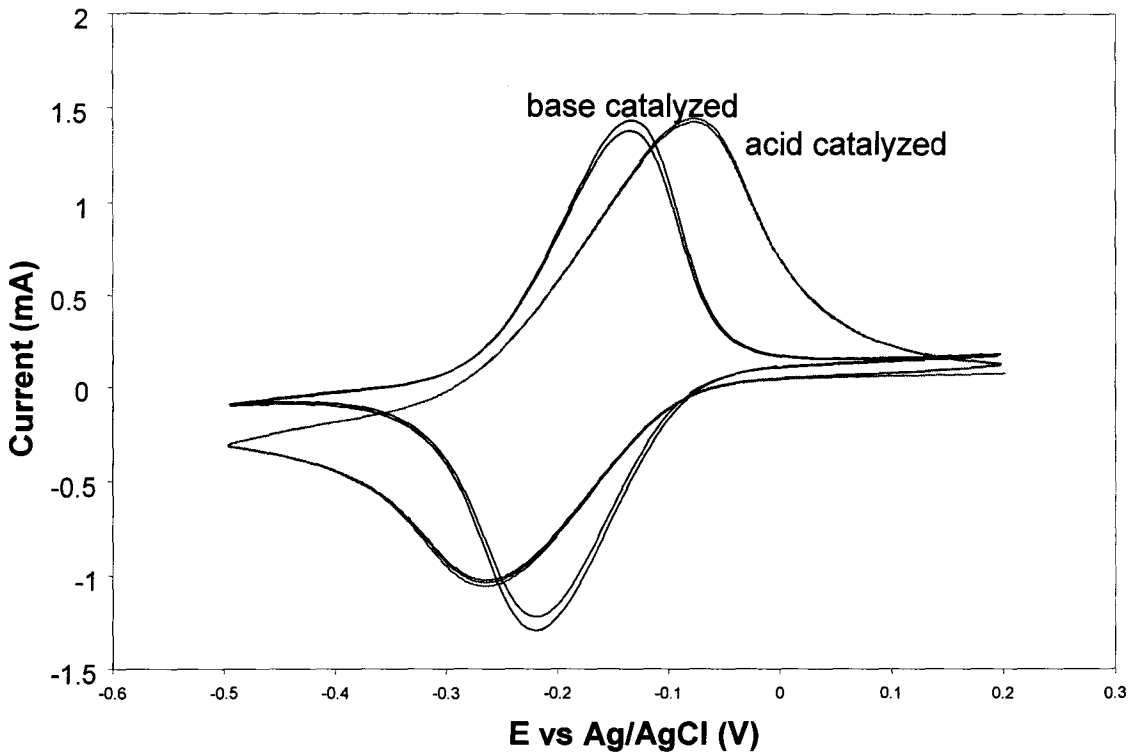

Figure 3.12 Cyclic voltammograms (10 $mV \cdot s^{-1}$) of $Ru(NH_3)_6^{3+}$ loaded (ca. 1 mM; 24 h) CFP/gel electrodes in 0.1 M CF_3CO_2Na (aq). The sol-gel catalysts used in preparing the sol-gel are shown on the plot.

3.4 Conclusions

Stable silica films were formed within the matrix of carbon fiber paper electrodes. $Ru(NH_3)_6^{3+}$ redox probes entrapped within the silicate matrix after the sol-gel process served as probes to obtain information about the environment, stability, partitioning of ions into the pores of the sol-gel matrix, diffusion coefficients of the redox probes and degree of leaching from the sol-gel.

Diffusion in porous sol-gels can be significantly more complex than that in solution due to the intermolecular interactions between the host matrix and the diffusing species along with the constrained environment of the sol-gel pores.[5] The ormosil hydrogels studied in this work exhibited excellent ion exchange and ion transport properties, and were very stable in electrochemical studies so long as care was taken to avoid gel shrinkage as it aged.[21] This stability was shown both by aging of the hydrogels to a collapsed structure and by re-loading the same gel-modified electrodes for electrochemical studies. Cyclic voltammetry with $Ru(NH_3)_6^{3+/2+}$ as a redox probe showed reversible behaviour of the probe in the gel matrix. Gel-modified carbon fiber paper electrodes did not show any deterioration over a period of days in the electrolyte solution.

$Ru(NH_3)_6^{3+}$ partitioned strongly into the gel with essentially all of the gel's sulphonate sites being available for ion exchange. The ion exchange process was facile and could be reversed by immersing the gel in a concentrated electrolyte solution containing no $Ru(NH_3)_6^{3+}$. Transferring the $Ru(NH_3)_6^{3+}$-loaded modified electrode to an analyte free electrolyte solution resulted in a significant decrease in peak currents when

continuing to cycle the potential. This decrease is due to the leaching of the electroactive cations out of the gel film into the external solution as a consequence of ion exchange for the electrolyte cation. Tonle et al. have reported similar findings in their work with $Ru(NH_3)_6^{3+}$-loaded clay modified electrodes and report that complete disappearance of the voltammetric peaks was not observed.[32] The new equilibrium established between their clay-bound $Ru(NH_3)_6^{3+}$ species and the supporting electrolyte cations is known to be affected by the supporting electrolyte concentration and the nature of the electrolyte cations.[32]

Furthermore, both maximal and equilibrium steady-states were again obtained when performing a second "accumulation-depletion" sequence in cyclic voltammetry with the same gel-modified electrode, having peak currents of the same intensities as those sampled during the first sequence.[32] This is similar to the behaviour observed for the hydrogels prepared in this work when re-loading a used gel-modified electrode with $Ru(NH_3)_6^{3+}$ to study its electrochemistry. This indicates that no significant structural changes in the gel occurred during the electrochemical measurements.[32]

The diffusion coefficients for the redox probe ions in the gel were high for an ion-exchanger, compared to Nafion for example, indicating that the gel had a well hydrated and open structure.

The effects of electrolyte concentration and pH, sol-gel aging, sol-gel sulphonate concentration, sol-gel solvent and sol-gel catalyst on the ion exchange and ion transport properties were studied.

The significance of these results can be illustrated by a comparison with Nafion, in which $Ru(NH_3)_6^{3+/2+}$ exhibits a D_{app} value of only ~$2x10^{-9}$ $cm^2 \cdot s^{-1}$.[25] Nafion has a dry equivalent mass of ~1100 g/mol SO_3^- and a hydration level of ~30%, while the gel reported here had a D_{app} of $4.9x10^{-8}$ $cm^2 \cdot s^{-1}$, a dry equivalent mass of 733 g/mol SO_3^- and a hydration level of ~80%. The gel is clearly a superior matrix for ion transport and showed good stability over time. Supporting the gel within a carbon fiber matrix is an important aspect of this stability.

References

[1]Collinson, M.M.; Howells, A.R. *Anal. Chem.*, **2000**, 72, 702A

[2]Lev, O.; Wu, Z.; Bharathi, S.; Glezer, V.; Modestov, A.; Gun, J.; Rabinovich, L.; Sampath, S. *Chem. Mater.*, **1997**, 9, 2354

[3] Rolison, D.R.; Dunn, B. *J. Mater. Chem.*, **2001**, 11, 963

[4]Robinovich, L.; Lev, O. *Electroanal.*, **2001**, 13, 265

[5]Kanungo, M.; Collinson, M.M. *Anal. Chem.*, **2003**, 75, 6555

6Sadki, S.; Sallard, S.; Oms, O.; Mutin, P. H.; Leclercq, D.; Vioux, A.; Audebert, P. *Talanta*, **2004**, 66, 1

[7]Audebert, P.; Griesmar, P.; Sanchez, C. *J. Meterials Chem.*, **1991**, 1, 699

[8]Audebert, P.; Griesmar, P.; Hapiot, P.; Sanchez, C. *J. Materials Chem.*, **1992**, 2, 1293

[9]Kanungo, M.; Collinson, M. M. *Langmuir*, **2005**, 21, 827

[10]Liu, A.; Zhou, H.; Honma, I. *Electrochemistry Communications*, **2005**, 7, 1

[11]Walcarius, A.; Delacôte, C.; Sayen, S. *Electrochimica Acta*, **2004**, 49, 3775

[12]Walcarius, A.; Delacôte, C. *Chem. Mater.*, **2003**, 15, 4181

[13]Walcarius, A.; Mandler, D.; Cox, J. A.; Collinson, M. M.; Lev, O. *J. Materials Chem.*, **2005**, 15, 3663

[14]Dvorak, O.; De Armond, M.K. *J. Phys. Chem.*, **1993**, 97, 2646

[15]Collinson, M.M.; Wang, H.M.; Makote, R.; Khramov, A. *J. Electroanal. Chem.*, **2002**, 519, 65

[16]Collinson, M.M.; Rausch, C.G.; Voigt, A. *Langmuir*, **1997**, 13, 7245

[17]Hsueh, C.C.; Collinson, M.M. *J. Electroanal. Chem.*, **1997**, 420, 243

[18]Cox, J.A.; Wolkiewicz, A.M.; Kulesza, P.J. *J. Solid State Electrochem.*, **1998**, 2, 246

[19]Howells, A.R.; Zambrano, P.J., Collinson, M.M. *Anal. Chem.*, **2000**, 72, 5265

[20]Watton, S.P., Taylor, C.M.; Kloster, G.M., Bowman, S.C. Coordination Complexes in Sol-Gel Silica Materials in *Progress in Inorganic Chemistry,* Vol. 51, ed. Kenneth D. Karlin, **2003**, 333-420

[21]Aylward, W. M.; Pickup, P. G. *J. Solid State Electrochem.* **2004**, 8, 742

[22]Buttry, D.A.; Anson, F.C. *J. Electroanal. Chem.*, **1981**, 130, 333

[23]Toray Industries Inc. 2004. Torayca website. http://www.torayca.com/index2.html

[24]Bard, A.J.; Faulkner, L.R. *Electrochemical Methods: Fundamentals and Applications*, **2001**, 2nd edn. Wiley, New York, pg 174-175

[25]Buttry, D.A.; Anson, F.C. *J. Am. Chem. Soc.*, **1983**, 105, 685

[26]Salimi, A.; Hallaj, R.; Amini, M. K. *Analytica Chimica Acta*, **2005**, 534, 335

[27]Lin, C.-L.; Tien, P.; Chau, L.-K. *Electrochimica Acta*, **2004**, 49, 573

[28]Daum, P.; Murray, R. W. *J. Phys. Chem.*, **1981**, 85, 389

[29]Alber, K.S.; Cox, J. A. *Mikrochim. Acta*, **1997**, 127, 131

[30]Durakpasa, H.; Breiter, M. W.; Dunn, B. *J. Sol-Gel Sci. and Tech.*, **1994**, 2, 251

[31]Montoya, I.A.; Viveros, T.; Dominquez, J. M.; Canales, L. A.; Schifter, I. *Catalysis Letters*, **1992**, 15, 207

[32]Tonle, I. K.; Ngameni, E.; Walcarius, A. *Electrochimica Acta*, **2004**, 49, 3435

Chapter 4:

Surface Interactions Between a Sol-Gel Matrix and Redox Probes

4.1 Introduction to Surface Interactions of Functionalized Sol-Gels

Modified electrodes containing ion-exchange films have given rise to a new analytical technique known as ion-exchange voltammetry.[1] This technique takes advantage of the preconcentration capabilities of the coating for electroactive ionic species.[2] Ion-exchangers based on silica present other attractive properties, such as thermal stability, durability with organic solvents and oxidizing agents, rigidity and ease of surface modification with a variety of functional groups.[2,3] The low loading capacity, relatively weak binding strength and low selectivity of these materials can be overcome by introducing organic functions into the materials by functionalization with, for example organosilanes.[1] Coating thin films onto many electrode surfaces can easily be achieved by use of the sol-gel process.[4]

Recently there has been considerable attention with regards to the use of sol-gel materials as host matrices for the encapsulation of many small molecules, including active proteins, enzymes and organic and organometallic molecules.[5,6,7] For example, the incorporation of small molecules into the porous matrices of sol-gels results in the fabrication of novel materials including nonlinear optical materials, catalytic supports, optical sensors and amperometric sensors.[7]

The gel microstructure and its affect on the stability and activity of entrapped reagents is poorly understood. As sol-gels dry, solvent evaporates, the gel shrinks, the surface-area-to-volume ratio in the pores increases, and interactions between entrapped reagents and the walls of the host becomes more important.[5] It is important to understand how molecules diffuse in sol gel materials in order to develop procedures to alter the rate

at which reagents diffuse in a solid host and improve the performance of sol-gel based devices.[5]

Information about the diffusion of molecules into or within sol-gel matrices can be obtained by using electrochemical voltammetric or amperometric methods and redox active probes (see Chapter 3). In this work, redox probes of different charges and sizes were physically doped into sulphonated silica sols, which were impregnated into CFP electrodes. Cyclic voltammetry and chronoamperometry, in 0.1 M CF_3CO_2Na (aq), were used to study the stability and electroactivity of redox probes encapsulated in the gel matrices in order to obtain insight into the nature of their entrapment. Ruthenium (III) hexamine, $Ru(NH_3)_6^{3+}$, and ruthenium (II) tris(bipyridine), $Ru(bpy)_3^{2+}$, were selected for this work because of their similar charges but differing sizes, whereas ferricyanide, $Fe(CN)_6^{3-}$, was used to study the affect of similar size, but opposite charge, on diffusion within the matrix.

4.2 Experimental

Redox probes of $Ru(NH_3)_6Cl_3$, $Ru(bpy)_3Cl_2$ and $Fe(CN)_6K_3$ were prepared in 0.1 M CF_3CO_2Na (aq) as described in Chapter 3.

In this study, the sol-gel modified CFP electrodes (see Section 3.2.1) were soaked in 1 mM solutions of each of the redox active species for 24 hours. The sulphonated silica sol-gel was of the same composition as described in Chapter 3 (SiO_2:SO_3H ratio = 9.3:1). After loading, the modified electrodes were rinsed with deionized water and cyclic voltammetry and chronoamperometry in 0.1 M CF_3CO_2Na (aq) was used to

characterize the extent to which the sol-gel matrix incorporates the various redox probes. The sol-gel matrix contains silanol groups and sulphonate groups, giving the walls a negative charge. The sol-gel modified electrodes should therefore act in a cation exchange capacity.

4.3 Results and Discussion

4.3.1 $Ru(NH_3)_6^{2+/3+}$

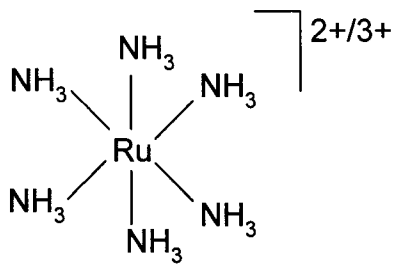

The work performed on the gel-modified CFP electrodes using a $Ru(NH_3)_6^{2+/3+}$ redox probe to monitor ion transport and ion exchange was presented in Chapter 3. Described below is a condensed summary as relevant for direct comparison with the other redox probes to study the issue of surface interactions between the sol-gel matrix wall and the probe.

The electrochemical behaviour of ruthenium (III) hexamine was first evaluated at bare and unfunctionalized silica-modified electrodes to establish a baseline for comparison with the sulphonate-modified electrode. Figure 4.1 shows the CVs for the three different electrode materials.

A comparison of the bare electrode response to $Ru(NH_3)_6^{2+/3+}$ with the sol-gel modified electrodes, as shown in Fig 4.1, indicates that $Ru(NH_3)_6^{3+}$ was preconcentrated

into the silica film to enhance the current by about 17 times. Furthermore, the addition of the sulphonate functionality to the sol-gel matrix enhanced the current by about 38 times. This behaviour is attributed to the interaction of positively charged $Ru(NH_3)_6^{2+/3+}$ with the negatively charged silanol and sulphonate groups within the silica sol-gel film.[1,2] Note that in these and experiments with $Ru(bpy)_3^{3+}$ and $Fe(CN)_6^{3-}$, the bare electrode was rinsed with deionized water following immersion in the probe solution, and CVs were recorded in solutions that did not contain the probe.

The large peak to peak separations that were observed were attributed to the large uncompensated solution resistance (see Chapter 3). The peak currents gradually diminished over time as the redox probe leached out of the sol matrix into the electrolyte solution.

Voltammograms exhibited linear relationships between peak currents and square root of scan rate (see Figure 3.3 and Figure 4.2), indicating diffusion control of the current.[8] Therefore, the integrated current densities in the voltammograms do not allow estimation of the concentration of $Ru(NH_3)_6^{3+}$ in the gel, even at scan rates as low as 1 $mV \cdot s^{-1}$. This is primarily a consequence of the thickness of the gel layer.[9] Concentrations and partition coefficients were therefore determined by chronocoulometry, as shown in Fig 4.3 and discussed in Section 3.3.2 and summarized in Table 4.1 (see page 95).

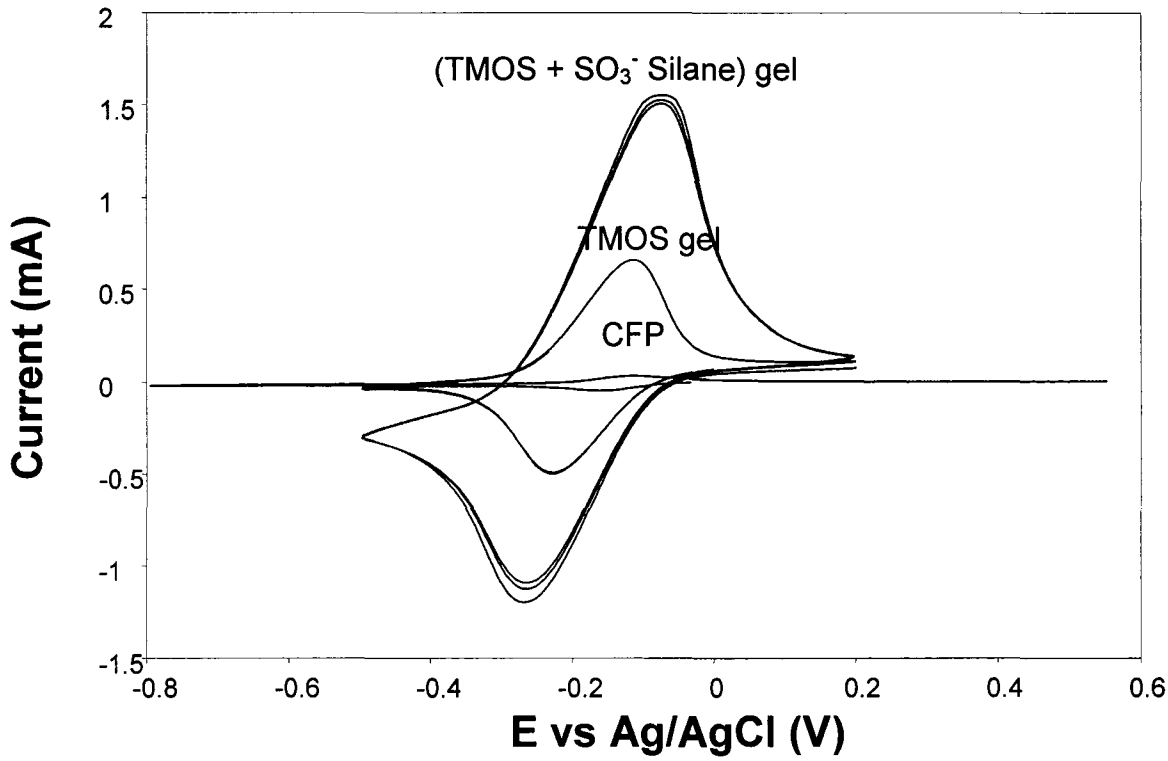

Figure 4.1 Cyclic voltammograms (10 $mV \cdot s^{-1}$) of $Ru(NH_3)_6^{3+}$ loaded (1 mM; 24 h) CFP and CFP/gel electrodes in 0.1 M CF_3CO_2Na (aq).

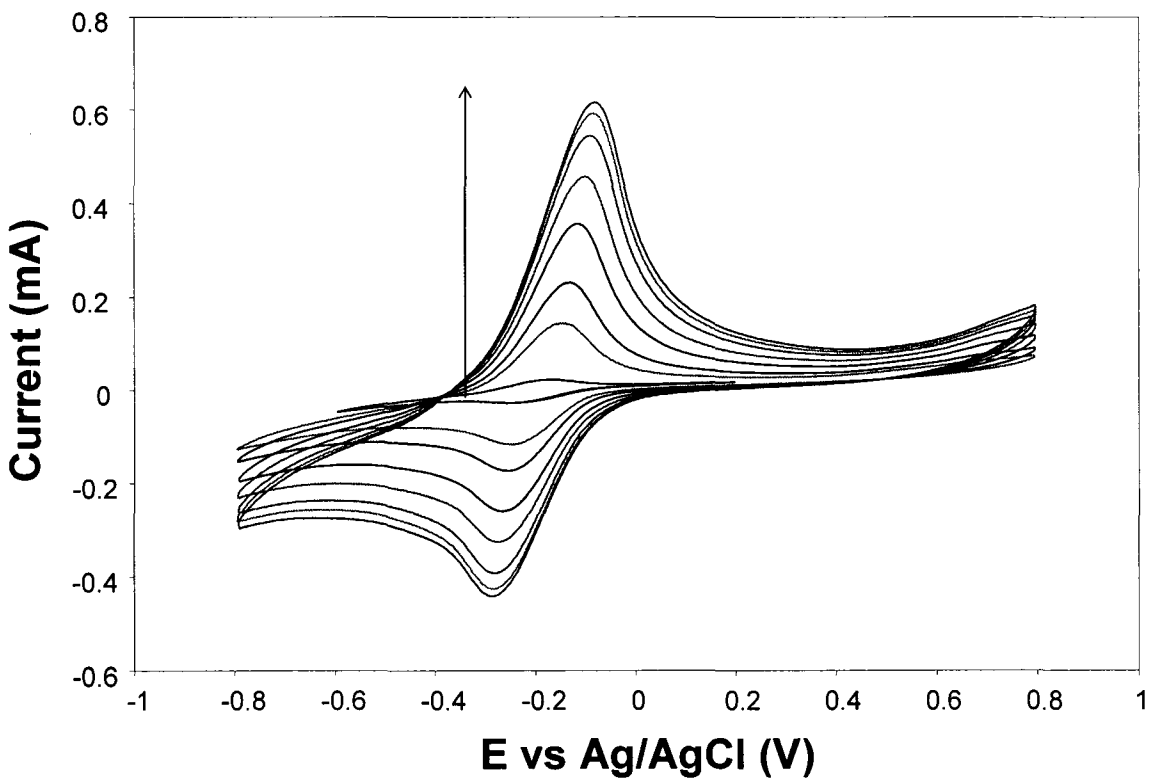

Figure 4.2 Cyclic voltammograms of a (TMOS + SO_3^- Silane) gel loaded CFP electrode in 0.1 M CF_3CO_2Na (aq) containing 1 mM $Ru(NH_3)_6^{3+}$ as a function of scan speed (1, 10, 20, 40, 60, 80, 90, 100 $mV \cdot s^{-1}$). Voltammograms at ca. 3 h in the solution are shown.

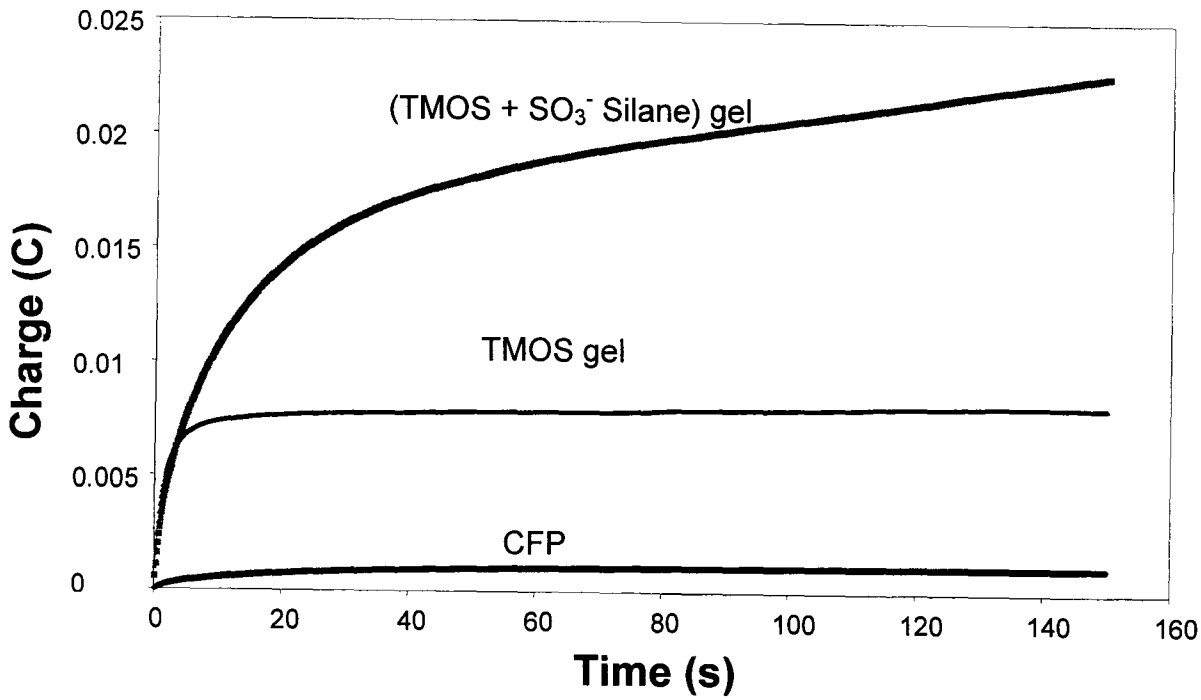

Figure 4.3 Chronocoulometric plots for –0.4 V to +0.2 V potential steps on $Ru(NH_3)_6^{3+}$ loaded (1 mM; 24 h) CFP and CFP/gel electrodes in 0.1 M CF_3CO_2Na (aq).

4.3.2 $Ru(bpy)_3^{2+/3+}$

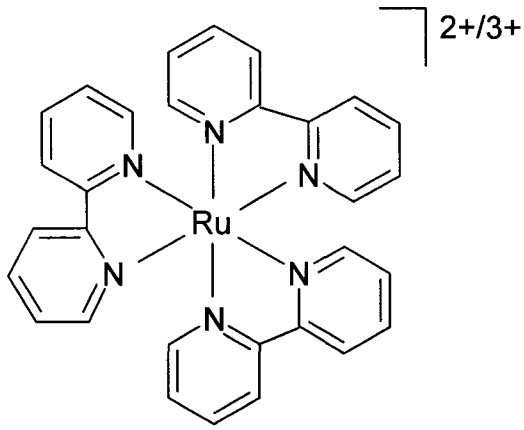

The relative sizes of the redox probes and how they affect transport issues through a sol-gel film was studied by investigating the transport properties of $Ru(bpy)_3^{2+}$ (radius ca. 6 Å),[10] which is significantly bulkier than $Ru(NH_3)_6^{3+}$ (radius ca. 2.1 Å).[11] The polypyridyl complexes of ruthenium, especially $Ru(bpy)_3^{2+}$ are well suited for reporting matrix-dopant interactions when incorporated into sol-gels because they are stable in the 2+ and 3+ oxidation states and display reversible electrochemistry.[12]

A comparison of the bare electrode response to $Ru(bpy)_3^{2+/3+}$ with the sol-gel modified electrodes was performed and the CVs are shown in Figure 4.4. The results are qualitatively similar to those found for the $Ru(NH_3)_6^{3+/2+}$. The $Ru(bpy)_3^{2+/3+}$ preconcentrates into the silica film to enhance the current by about 16 times. The addition of the sulphonated functionality to the sol-gel matrix enhances the current slightly further. This behaviour is due to the interactions between the positively charged redox probe and the negatively charged groups inside the sol-gel. Since $Ru(bpy)_3^{3+}$ is larger than $Ru(NH_3)_6^{3+}$ it is hindered to a greater extent than the smaller probe and is therefore unable to physically diffuse to as great an extent into the sol-gel network.[7]

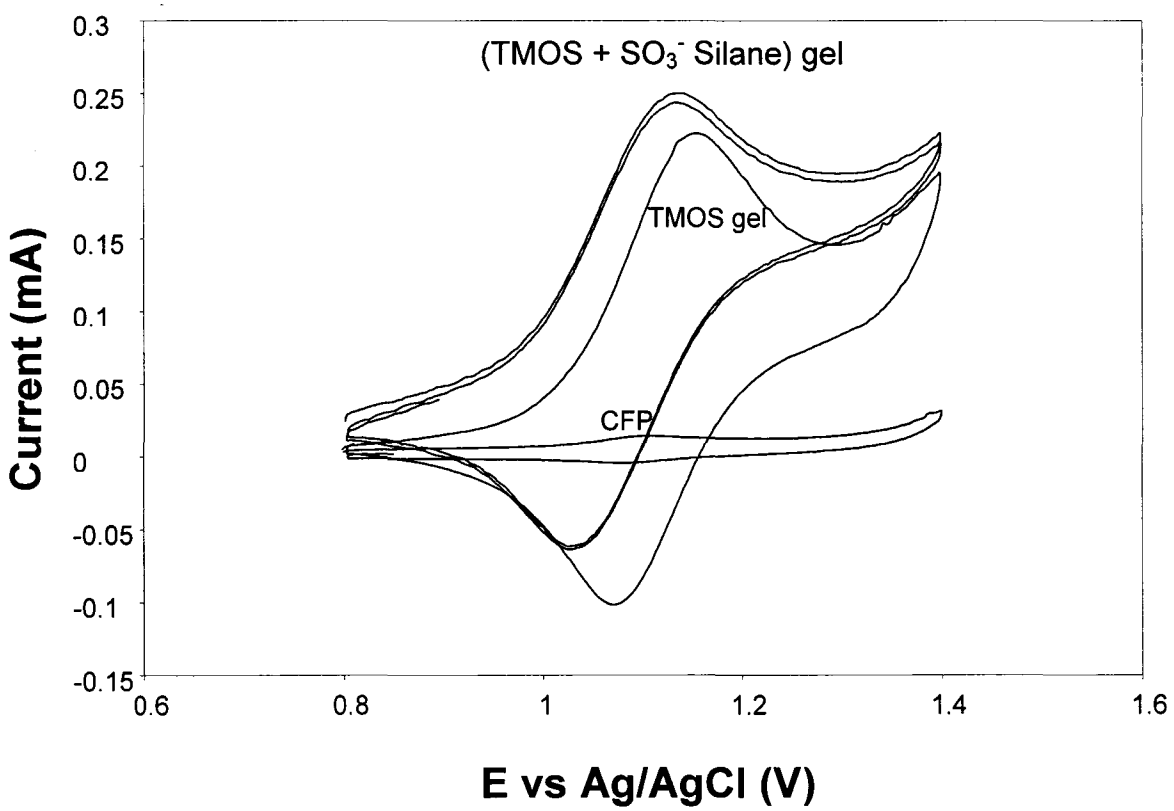

Figure 4.4 Cyclic voltammograms (10 $mV \cdot s^{-1}$) of $Ru(bpy)_3^{3+}$ loaded (1 mM; 24 h) CFP and CFP/gel electrodes in 0.1 M CF_3CO_2Na (aq).

The CVs show larger than normal peak separations attributable to the uncompensated solution resistance. There is a peak shift towards lower potential in the sulphonated gel. This indicates that there is a small stabilizing effect of the $Ru(bpy)_3^{3+}$ cations by the negatively charged SO_3^- sol-gel walls.[1] With time, the redox probe leached out of the matrix into the electrolyte solution, as observed by the decrease in currents shown in Fig 4.5 and confirmed visually by the appearance of an orange color in the supporting electrolyte over time. When compared to the $Ru(NH_3)_6^{3+}$ redox probe, significantly less leaching for the larger $Ru(bpy)_3^{2+}$ probe was observed presumably because the diffusion of the probe in the sol-gel network is hindered.

The voltammograms shown in Fig 4.6 exhibited a linear relationship between peak currents and the square root of scan rate as shown in Figure 4.7, indicating diffusion control of the current.[8] The amount of redox probe incorporated into the sol-gel matrices (see Table 4.1) was obtained by analysis of the chronocoulometry plots shown in Fig 4.8.

4.3.3 $Fe(CN)_6^{3-/4-}$

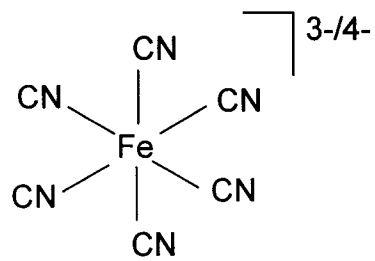

Figure 4.9 shows a comparison of the bare electrode response to $Fe(CN)_6^{3-/4-}$ with those for the sol-gel modified electrodes. The lack of development of large, well-defined

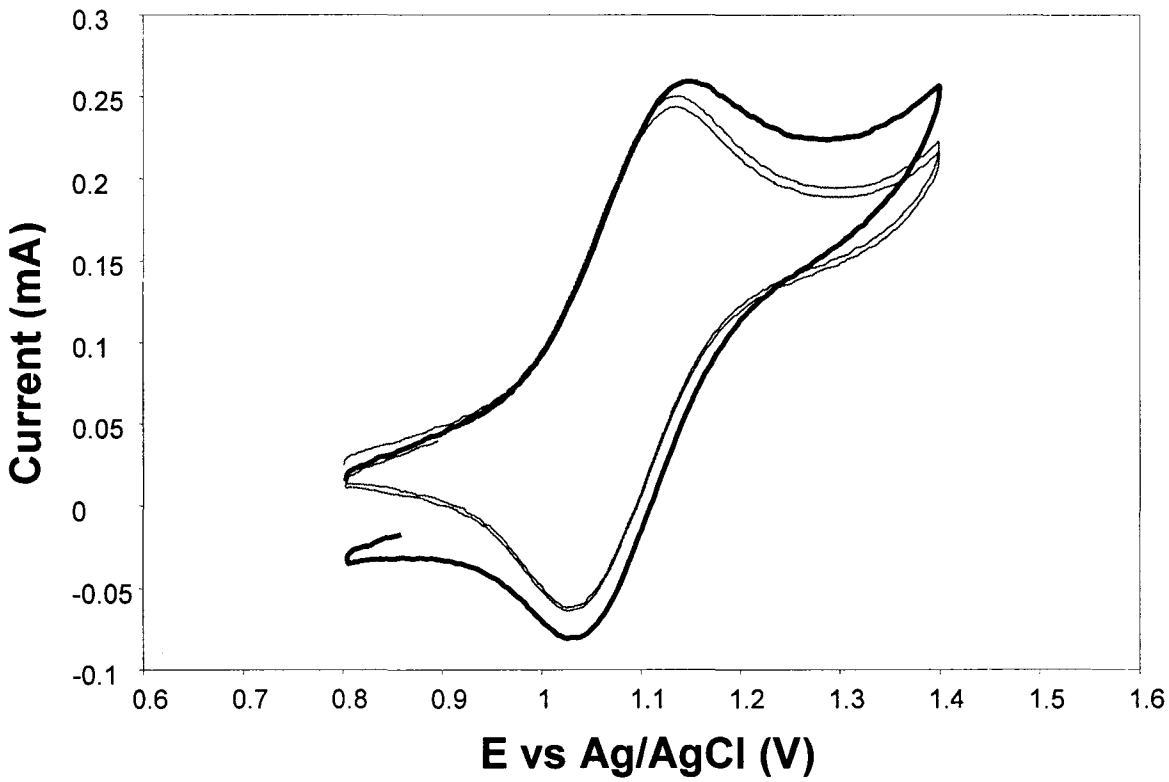

Figure 4.5 Cyclic voltammograms (10 $mV \cdot s^{-1}$) of a $Ru(bpy)_3^{3+}$ loaded (1mM; 24 h) CFP/(TMOS + SO_3^- Silane) gel electrode in 0.1 M CF_3CO_2Na (aq). The initial scan is shown in bold, together with a voltammogram recorded after 30 min.

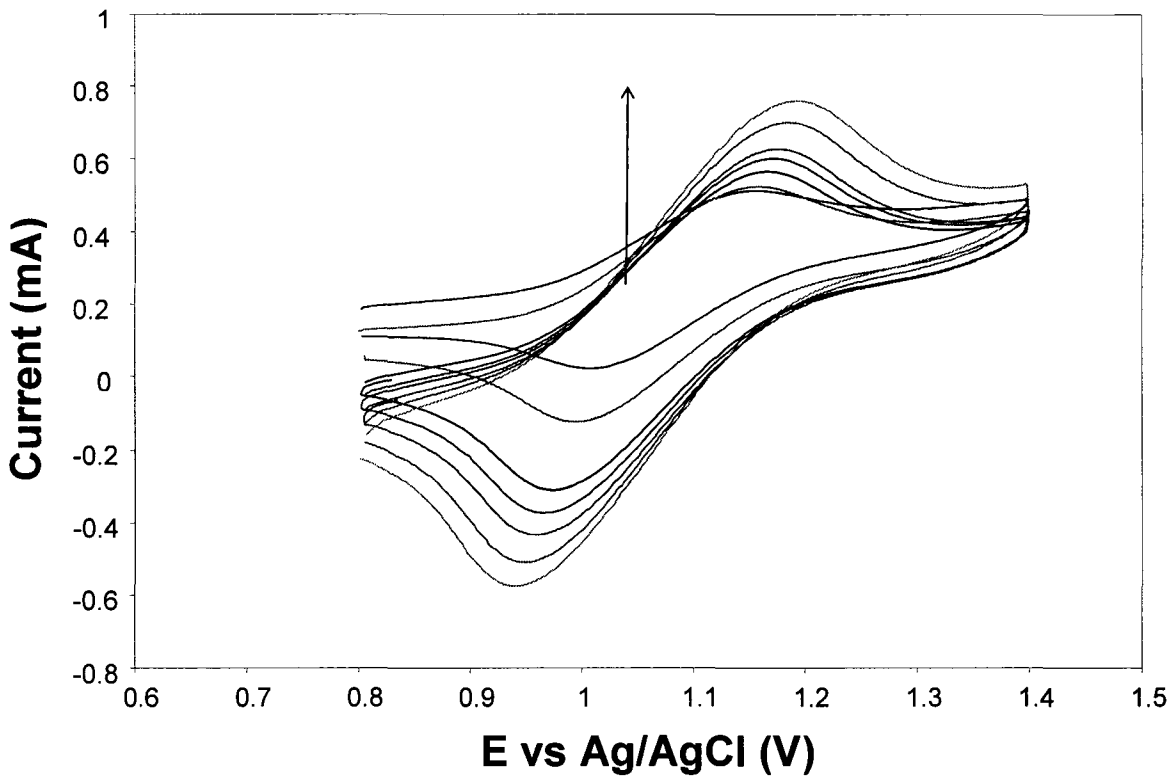

Figure 4.6 Cyclic voltammograms of a $Ru(bpy)_3^{3+}$ loaded (1mM; 24 h) CFP/(TMOS + SO_3^- Silane) gel electrode in 0.1 M CF_3CO_2Na (aq) as a function of scan speed (10, 20, 40, 50, 60, 80, 100 $mV \cdot s^{-1}$).

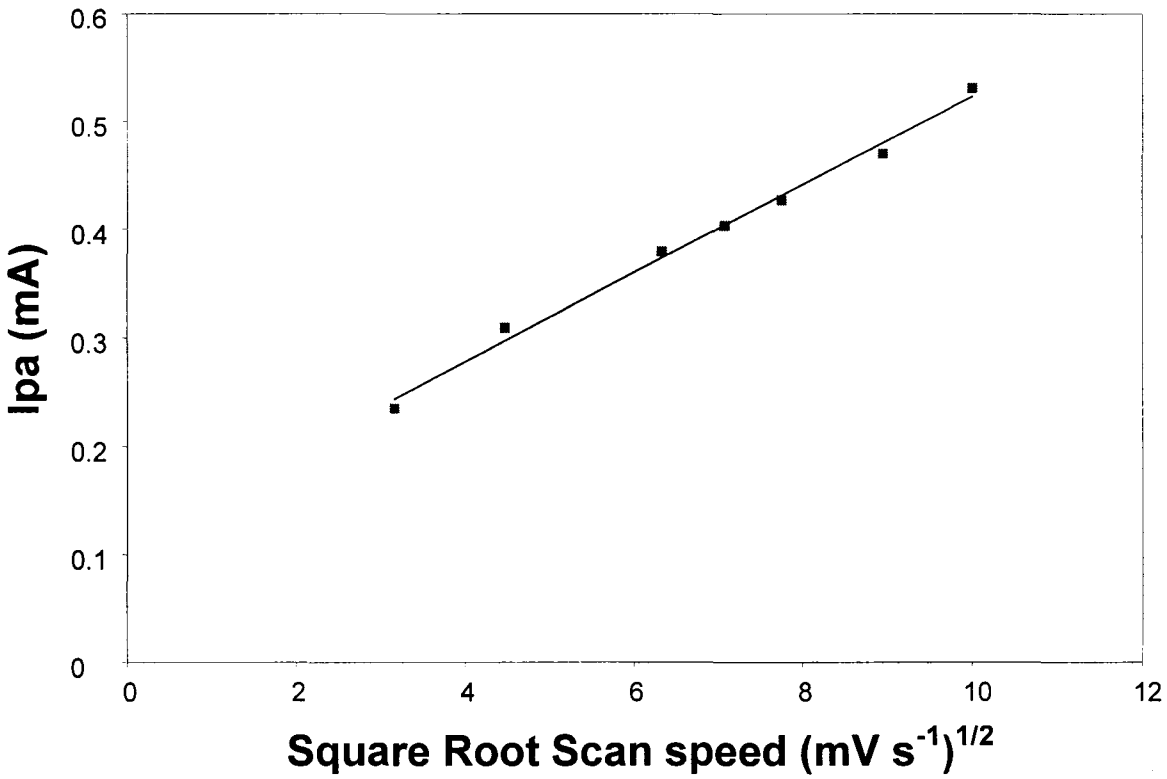

Figure 4.7 Peak current vs square root of scan speed for a $Ru(bpy)_3^{3+}$ loaded CFP/(TMOS + SO_3^- Silane) gel electrode in 0.1 M CF_3CO_2Na (aq).

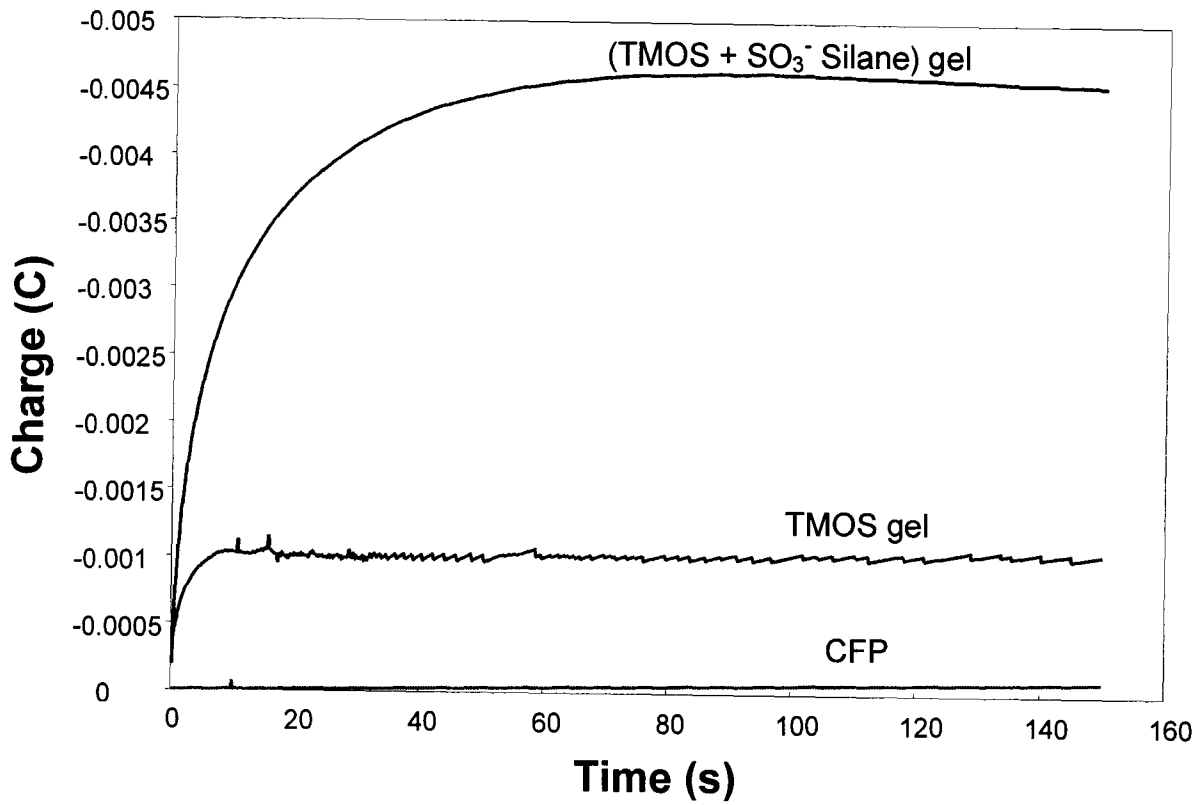

Figure 4.8 Chronocoulometric plots for 1.4 V to 0.8 V potential steps on $Ru(bpy)_3^{3+}$ loaded (1 mM; 24 h) CFP and CFP/gel electrodes in 0.1 M CF_3CO_2Na (aq).

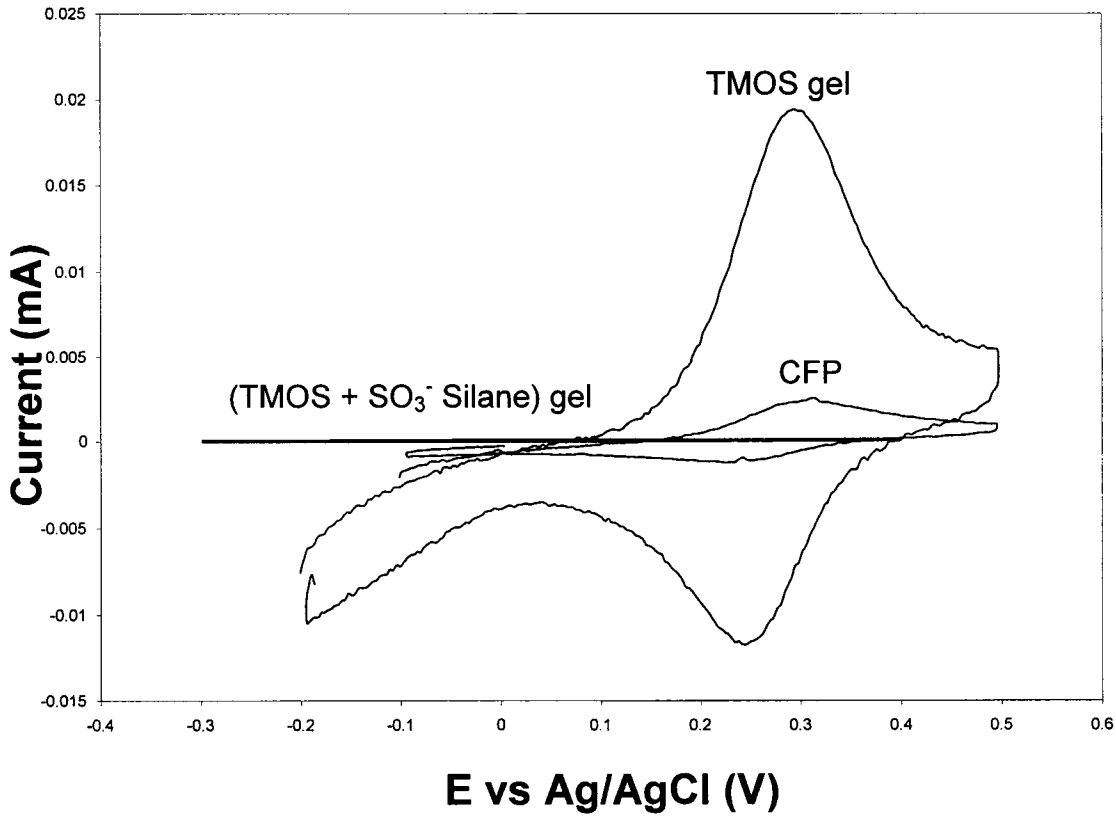

Figure 4.9 Cyclic voltammograms (10 $mV \cdot s^{-1}$) of $Fe(CN)_6^{4-}$ loaded (1 mM; 24 h) CFP and CFP/gel electrodes in 0.1 M CF_3CO_2Na (aq).

redox peaks indicates a resistance to diffusion of this complex into the (TMOS + SO_3^- Silane) sol-gel modified electrode.[8] This can be explained by the negatively charged silica or SO_3^- surfaces within the confining regions of the sol-gel which provide an electrostatic barrier to diffusion once the complex reaches the interior pores.[12] Despite this resistance, some $Fe(CN)_6^{3-}$ probe did penetrate into the pores of the sol-gel network, as evidenced by the small redox peaks present in Fig 4.9. Furthermore, the presence of the sulphonate groups in the (SO_3^- Silane + TMOS) gels hindered the diffusion of the negative probe into the network to a greater extent than that shown for the TMOS gel.

Work done by Tonle et al. on clay-modified electrodes show similar results.[1] The presence of their negatively charged clay film at the electrode surface prevented the free access of the negatively charged $Fe(CN)_6^{3-}$ electroactive probe to the electrode surface. Their results, however, show that the permselectivity is not absolute, as a small cathodic signal was observed with a wave shape suggesting the existence of small pinholes or cracks in the clay through which the $Fe(CN)_6^{3-}$ can diffuse.[1]

Cyclic voltammograms shown in Figure 4.10 displayed linear relationships between square root of peak currents and scan rate as shown in Figure 4.11, indicating diffusion control of the current.[8] The amount of redox probe incorporated into the sol matrix (Table 4.1) was obtained by analysis of the chronocoulometry plots shown in Fig 4.12.

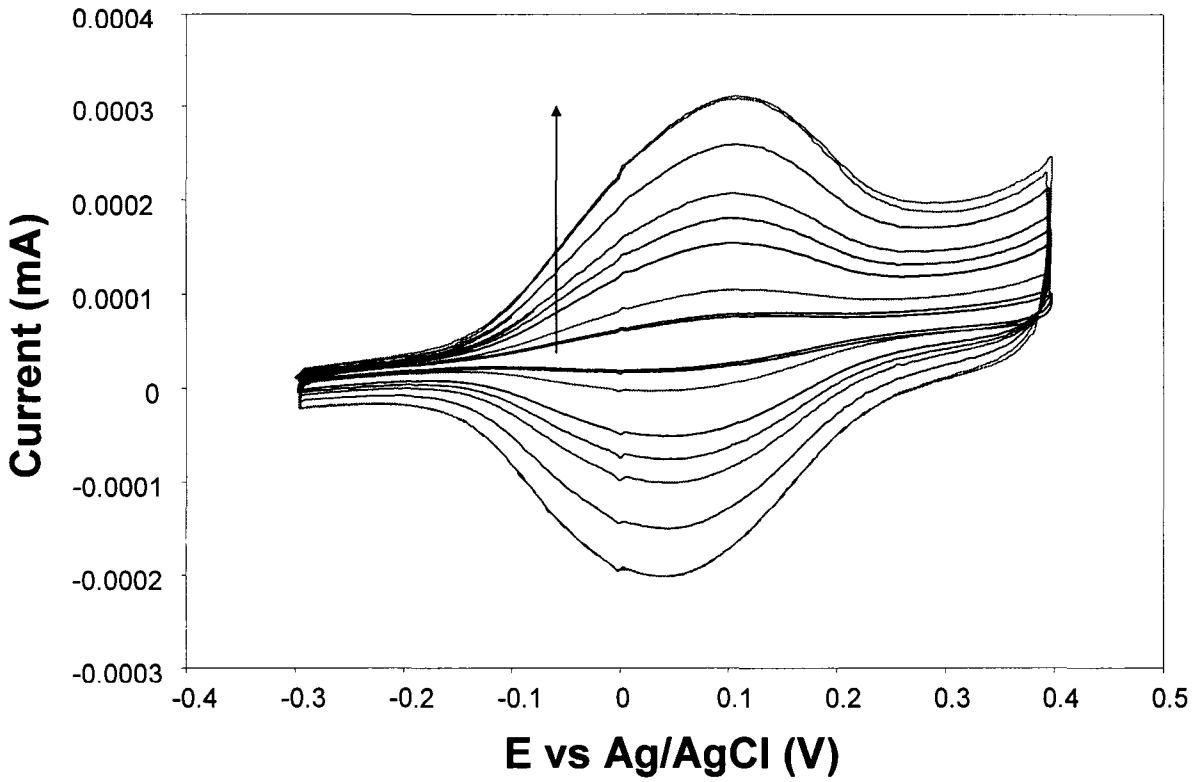

Figure 4.10 Cyclic voltammograms of a $Fe(CN)_6^{3-}$ loaded (1mM; 24 h) CFP/(TMOS + SO_3^- Silane) gel electrode in 0.1 M CF_3CO_2Na (aq) as a function of scan speed (10, 20, 40, 50, 60, 100 $mV \cdot s^{-1}$).

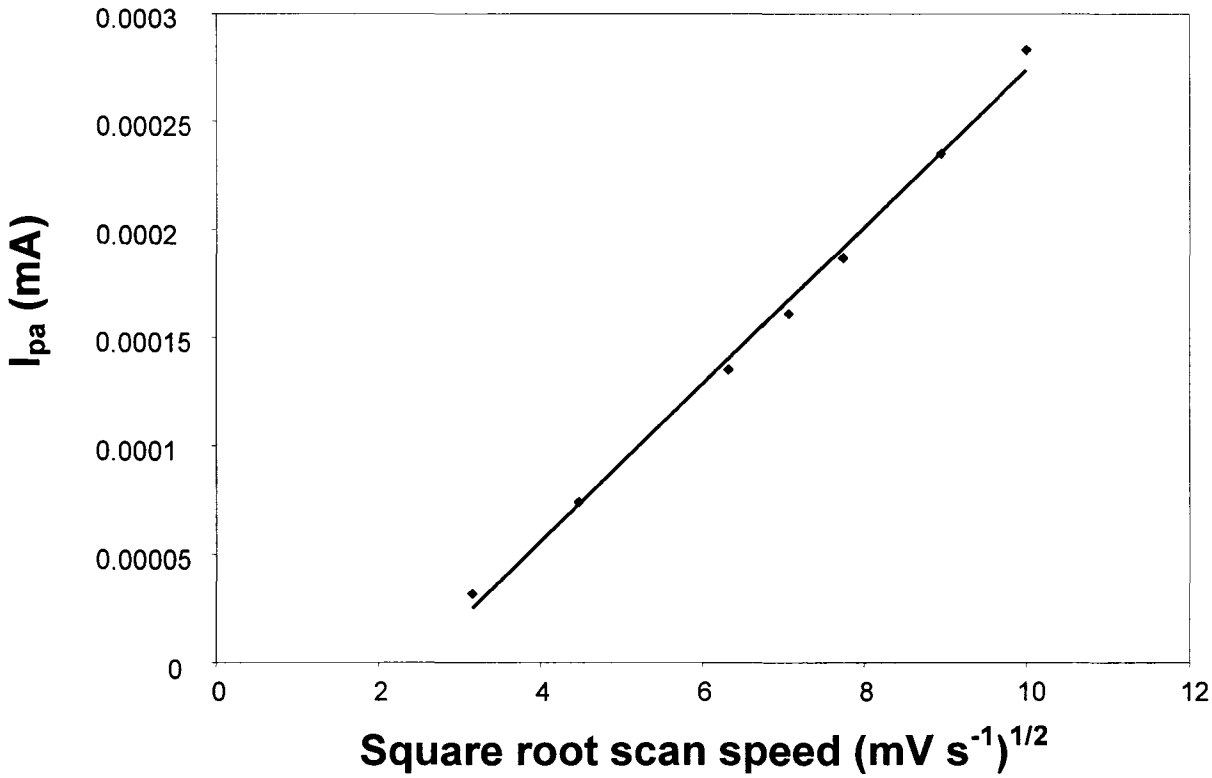

Figure 4.11 Peak current vs square root scan speed for a $Fe(CN)_6^{3-}$ loaded CFP/(TMOS + SO_3^- Silane) gel electrode in 0.1 M CF_3CO_2Na (aq).

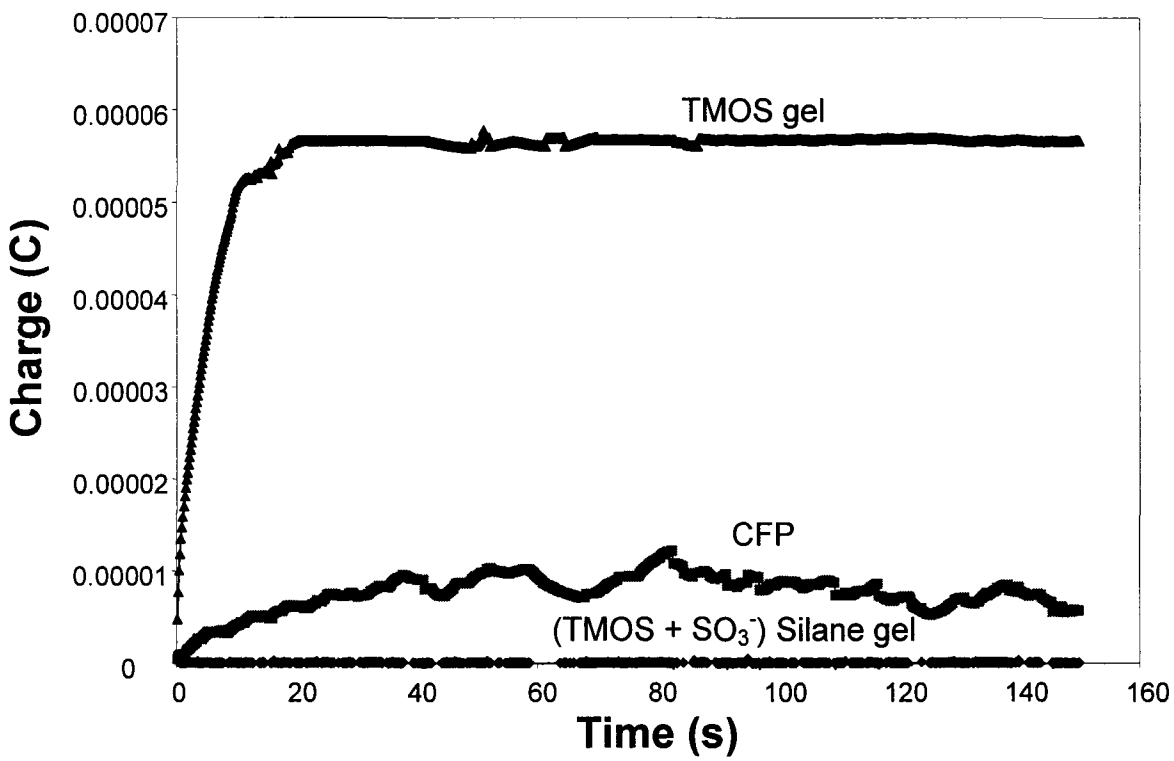

Figure 4.12 Chronocoulometric plots for -0.2 V to +0.5 V potential steps on $Fe(CN)_6^{3-}$ loaded (1 mM; 24 h) CFP and CFP/gel electrodes in 0.1 M CF_3CO_2Na (aq).

4.3.4 Discussion

Small redox-active molecules can be incorporated within sulphonated silica hosts prepared by a sol-gel process after gelation. Figure 4.13 shows CVs for sol-gel modified electrodes soaked in each of the three redox probes: $Ru(NH_3)_6^{2+/3+}$, $Ru(bpy)_3^{2+/3+}$ and $Fe(CN)_6^{3-/4-}$ at the same concentrations and for the same amount of time. By monitoring the effects of size and charge of the redox probes on encapsulation into the host matrices, specific information can be obtained about their stability and diffusion behaviour in the sol network.[7]

Diffusion in porous solids is much more complicated than that measured in solution because of potential interactions between the entrapped guest and the walls of the porous network, and because of confinement effects.[5] Transport within sol-gel films is often quantified in terms of an apparent diffusion coefficient, D_{app}, to account for the reduced accessible volume, interactions with pore walls, and exclusion effects.[3]

For silica-based sol-gels, the pore walls contain many different functional groups, including siloxane (Si-O-Si), silanol (Si-OH) and siloxide (SiO^-) groups. In addition to these groups, the sulphonated silane used here provides SO_3^- sites as well as hydrophobic organic (ethylbenzene) functionality at the pore walls. Since the isoelectric point of silica is ca. pH = 2, the walls of the silica sol-gels are negatively charged at the pH of 3.3 used here.[5] Gel encapsulation of the two cations is significant, as predicted based on electrostatic charge interactions.

It was expected that more of the smaller $Ru(NH_3)_6^{3+}$ probe could fit into the pores of the sol matrix, which is supported by the larger concentrations of that probe in the sol

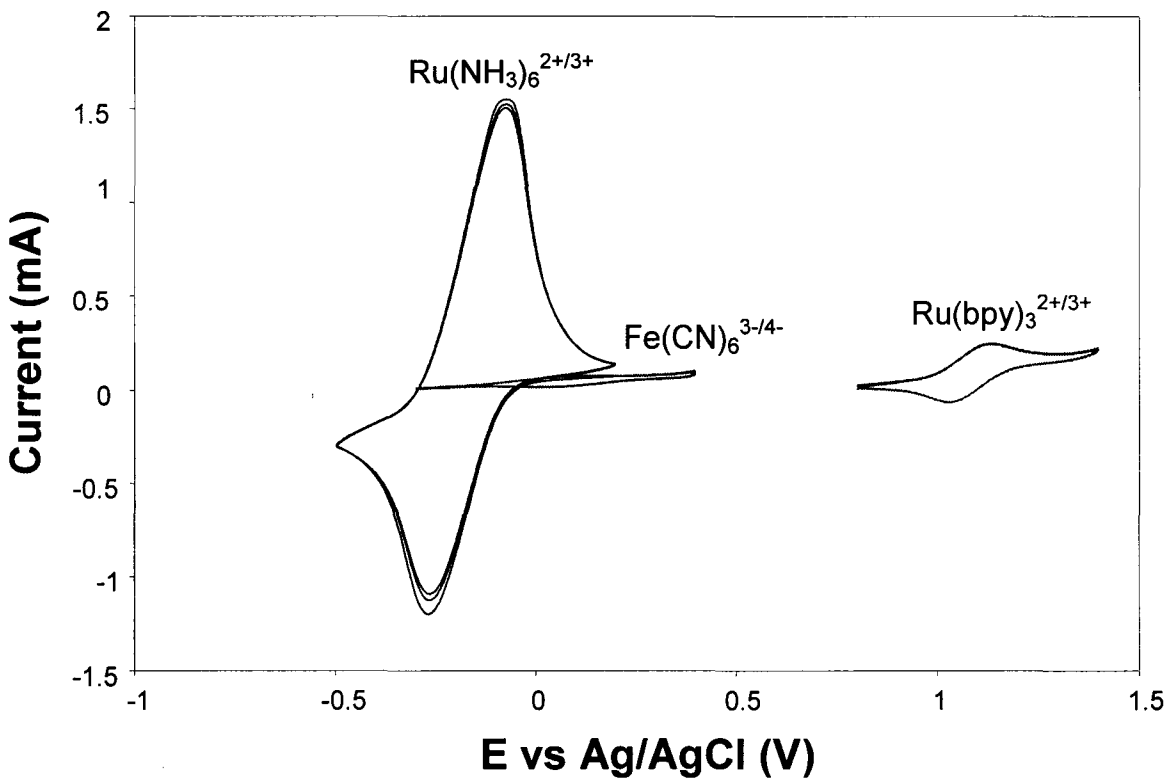

Figure 4.13 Cyclic voltammograms (10 $mV \cdot s^{-1}$) of $Ru(NH_3)_6^{3+}$, $Ru(bpy)_3^{3+}$ and $Fe(CN)_6^{4-}$ loaded (1 mM; 24 h) CFP/(TMOS + SO_3^- Silane) gel electrodes in 0.1 M CF_3CO_2Na (aq). The $Fe(CN)_6^{3-/4-}$ plot is enlarged 1000 times.

network obtained from chronocoulometry, as shown in Table 4.1 and in Fig 4.13. $Ru(bpy)_3^{2+}$ is more than twice the size of $Ru(NH_3)_6^{3+}$ and this would hinder diffusion of the $Ru(bpy)_3^{2+}$ probe in the sol-gel network.[7]

The "electroactive fraction" of an encapsulated redox probe consists of those species adsorbed on the pore walls or trapped within microchannels near the electrode surface which can therefore diffuse easily to the electrode surface to undergo electron transfer.[7] Collinson et al. have reported that only small fractions of entrapped dopants within a silica host are electroactive.[7] This is indicative of large portions of the electroactive probes residing in collapsed pores or trapped within regions of the matrix that is inaccessible for electron exchange with the electrode.[7] Increasing pore size in the sol matrix by base catalysis or increasing hydration of the sol film may result in increasing the mobility of dopants inside a sol network and hence increase the redox probes' electroactivity.[6,12]

The distinct differences observed between the oppositely charged complexes in the voltammetric waveshape can provide information concerning diffusion. All of the redox probes studied here showed typical cyclic voltammograms with Faradaic peak currents proportional to the square root of scan rate, indicative of semi-infinite diffusion at the electrode.[12]

The stability of the redox probes incorporated into the sulphonated silica sol network is complex. The steady decrease in Faradaic current with time for the ruthenium-soaked gel-modified electrodes in solution is most likely due to the redox probe diffusing out of the films and into the solution and not very likely to be due to film

Table 4.1. Partition coefficients and diffusion coefficients for redox probes in CFP and probe impregnated gel-modified electrodes.

Redox Probe	Electrode	$[probe]_{soln}$ mM	$[probe]_{gel}$ mM	Kp	D_{app} 10^{-8} $cm^2 \cdot s^{-1}$
$Ru(NH_3)_6^{2+/3+}$	CFP	1	3.2	3.2	7.2
	TMOS Gel	1	16.1	16.1	6.3
	SO_3^- Gel	1	22.8	22.8	5.2
$Ru(bpy)_3^{2+/3+}$	CFP	1	0.07	0.07	22
	TMOS Gel	1	0.9	0.9	20
	SO_3^- Gel	1	3.8	3.8	9.1
$Fe(CN)_6^{3-/4-}$	CFP	1	0.008	0.008	4.0
	TMOS Gel	1	0.06	0.06	1.4
	SO_3^- Gel	1	0.0001	0.0001	0.9

instability.[7] The films appeared to be intact upon removal from solution, and in fact, can be re-loaded with redox probe to obtained similar currents (see Chapter 3). Leaching of small molecules from silicate matrices has been reported in the literature and remains one of the biggest obstacles to their use as sensors.[1, 7, 13 - 16]

The anionic species $Fe(CN)_6^{3-}$ showed very little Faradaic current, indicative of very little incorporation of the redox probe into the sol-gel matrix. The results indicate a permselective behavior based on either favorable or unfavorable electrostatic interactions.[1,12] The negative walls of the sol-gel matrix act as a cation-exchanger accumulating the positive cation redox probes while rejecting the negative anion species.

Repulsive interactions between redox sites in the sol-gel film is also a possibility and is confirmed in the CVs by the larger than theoretical peak width at half height.[2]

Information about the ion exchange equilibria can be obtained from observing the shifts of the formal potentials for the redox probes in the sol-gel films relative to that of dissolved probes[2], as shown in Table 4.2.

The formal potentials for gel-encapsulated $Ru(NH_3)_6^{2+/3+}$ and $Ru(bpy)_3^{2+/3+}$ are approximately the same as those obtained in solution for $Ru(NH_3)_6^{2+/3+}$ and $Ru(bpy)_3^{2+/3+}$ in 0.1 M KNO_3 (aq) at bare glassy carbon electrodes. Similar results were reported by Collinson et al.[7] for the same redox probes in a TMOS-based sol-gel.

There is a negative shift of ca. 100 mV for gel-encapsulated $Fe(CN)_6^{3-/4-}$ relative to that of $Fe(CN)_6^{3-/4-}$ in solution. This indicates that the oxidized species binds to the sol-gel more strongly than the reduced form.[2] The hydrophobic interactions between the

Table 4.2 Formal potentials for $Ru(NH_3)_6^{2+/3+}$, $Ru(bpy)_3^{2+/3+}$ and $Fe(CN)_6^{3-/4-}$ in 0.1 M KNO_3 (aq) at bare glassy carbon, CFP and CFP/gel modified electrodes.

Redox Probe	$E^{o'}_{soln}$ (V)	$E^{o'}_{CFP}$ (V)	$E^{o'}_{TMOS\ gel}$ (V)	$E^{o'}_{SO3-\ gel}$ (V)
$Ru(NH_3)_6^{2+/3+}$	-0.17	-0.13	-0.17	-0.17
$Ru(bpy)_3^{2+/3+}$	1.10	1.11	1.12	1.08
$Fe(CN)_6^{3-/4-}$	0.205	0.27	0.29	0.10

Note: $E^{o'}$ values for $Ru(NH_3)_6^{2+/3+}$ and $Ru(bpy)_3^{2+/3+}$ are taken from reference 7, $E^{o'}$ for $Fe(CN)_6^{3-/4-}$ is from reference 2.

negatively charged sol-gel electrode and the anionic probe can contribute to the Donnan potential (the potential present at the interface between polyelectrolyte coatings on electrodes and the solutions in which they are used) and as such a shift in the apparent formal potential is observed.[18] The peak shifts can therefore be explained as a combination of equilibria shifts and electrostatic interactions.

Proper design of the sol-gel matrix by using suitable materials can fine-tune the permeability of the sol-gel film. One could expect to create anion exchange properties to the gel modified electrodes simply by introducing a positive charge to the gel walls. This could be done by protonation of the organofunctional groups or by using a grafting process involving the reaction of γ-aminopropyltriethoxysilane with the surface silanol groups of the gel.[1,4] Lin et al. prepared anion-exchange sol-gel films by covalently attaching propyl-N,N,N-trimethylammonium ($-N(CH_3)_3^+$) to a silica matrix[2] in a manner similar to this work. It is also possible to develop functionalized ORMOSILs using reactive precursors, such as 3-glycidoxypropyltrimethoxysilane and 2-(3,4-epoxycyclohexyl)ethyltrimethoxysilane to design films with selective ring opening reactions in the presence of Lewis acids or bases.[17] This could further expand the range of potential applications of such materials.

4.4 Conclusions

Redox molecules entrapped into the gel modified CFP electrodes can serve as probes to obtain valuable information about the gel environment, the entrapment and the degree of leaching.

The ion-exchange and permselective properties of ORMOSIL films can be easily tailored through the sol-gel process. In this work, the sulphonated silica hydrogel offers highly porous volumes which enable a percentage of the entrapped $Ru(NH_3)_6^{2+/3+}$ probe to be mobile and readily able to exchange electrons with the electrode surface. The bulkier $Ru(bpy)_3^{2+/3+}$, while displaying favorable electrostatic interactions with the sol-gel matrix, is sterically hindered from diffusing into the sol-gel to as great of an extent as the smaller $Ru(NH_3)^{2+/3+}$ probe.

The negatively charged SO_3^- groups associated with the sulphonated sol-gels studied here provide cation exchange properties to the modified CFP/gel electrodes which inhibit incorporation of anions, such as $Fe(CN)_6^{3-/4-}$.

References

[1]Tonle, I. K.; Ngameni, E.; Walcarius, A. *Electrochimica Acta*, **2004**, 49, 3435

[2]Lin, C-L.; Tien, P.; Chau, L-K. *Electrochimica Acta*, **2004**, 49, 573

[3]McKenzie, K.J.; Niedziolka, J.; Paddon, C.A.; Marken, F.; Rozniecka, E.; Opallo, M. *Analyst*, **2004**, 129, 1181

[4]Wei, H.; Collinson, M. M. *Analytica Chimica*, **1999**, 397, 113

[5]Kanungo, M.; Collinson, M. M. *Langmuir*, **2005**, 21, 827

[6]Liu, A.; Zhou, H.; Honma, I. *Electrochemistry Communications*, **2005**, 7, 1

[7]Collinson, M. M.; Rausch, C. G.; Voigt, A. *Langmuir*, **1997**, 13, 7245

[8]Salimi, A.; Hallaj, R.; Amini, M. K. *Analytica Chimica Acta*, **2005**, 534, 335

[9]Aylward, W. M.; Pickup, P. G. *J. Solid State Electrochem.* **2004**, 8, 742

[10]Rillema, D. P.; Jones, D. S.; Levy, H. A. *J. C. S. Chem. Comm.*, **1979**, 849

11Zheng, C.; McCammon, J. A.; Wolynes, P. G. *Proc. Natl. Acad. Sci.*, **1989**, 86, 6441

[12]Watton, S.P., Taylor, C.M.; Kloster, G.M., Bowman, S.C. Coordination Complexes in Sol-Gel Silica Materials in *Progress in Inorganic Chemistry* Vol. 51, ed. Kenneth D. Karlin, **2003**, 333-420

[13]Avnir, D. *Acc.Chem. Res.*, **1995**, 28, 328

[14]Lev, O.; Tsionsky, M.; Rabinovich, L.; Glezer, V.; Sampath, S.; Pankratov, I.; Gun, J. *Anal. Chem.*, **1995**, 67, 22A

[15]Samuel, J.; Polevaya, Y.; Ottolenghi, M.; Avnir, D. *Chem. Mater.*, **1994**, 6, 1457

[16]Kraus, S. C.; Czolk, R.; Reichert, J.; Ache, H. J. *Sens. Actuators B*, **1993**, 15-16, 199

[17]Pandey, P. C.; Upadhyay, S.; Upadhyay, B. C.; Tripathi, V. S. *J. Sol-Gel Science and Technology*, 2005, 33, 25

[18]Naegeli, R.; Redepenning, J.; Anson, F. C. *J. Phys. Chem.*, **1986**, 90, 5227

Chapter 5:

Ionic Conductivity of Sulphonated Silica Sol-Gels

5.1 Introduction to Ionic Conductivity of Sol-Gels

The sol-gel process has been used to produce new materials with varying amounts and sizes of pores and water remaining in the solids.[1] These porous and water-containing properties can be utilized to prepare solid materials with high ionic conductivity. Highly proton conducting materials have attracted much attention because of their potential use in environmentally friendly energy sources such as fuel cells.[1] The wide composition flexibility, ease of fabrication and high ionic conductivity coupled with low electronic conductivity of the silica sol-gel matrix have contributed to their applications in areas such as solid electrolytes and sensors.[2-8] Although there are non-sol-gel ionic conductive materials that exhibit higher conductivity, the easy processibility of sol-gel materials provide a distinct advantage.[2]

With the development of solid-state batteries it was inevitable that a trend would emerge towards solid-state technology in electrochemical energy engineering.[16] As a result, methods for the characterization of systems with solid-solid or solid-liquid interfaces have been developed for electrochemical and materials scientists. EIS may be used to investigate solid or liquid materials.[17]

Electrical resistance is the fundamental measurement used to study the motion of ions in solution and is generally measured using a conductivity cell in one arm of a resistance bridge,[18] as shown in Fig 5.1. Alternating currents must be used to avoid electrolysis and polarization. A balance point is then obtained when the resistances $R_1/R_2 = R_3/R_4$ (or substituting impedance for resistance since an AC current is used).

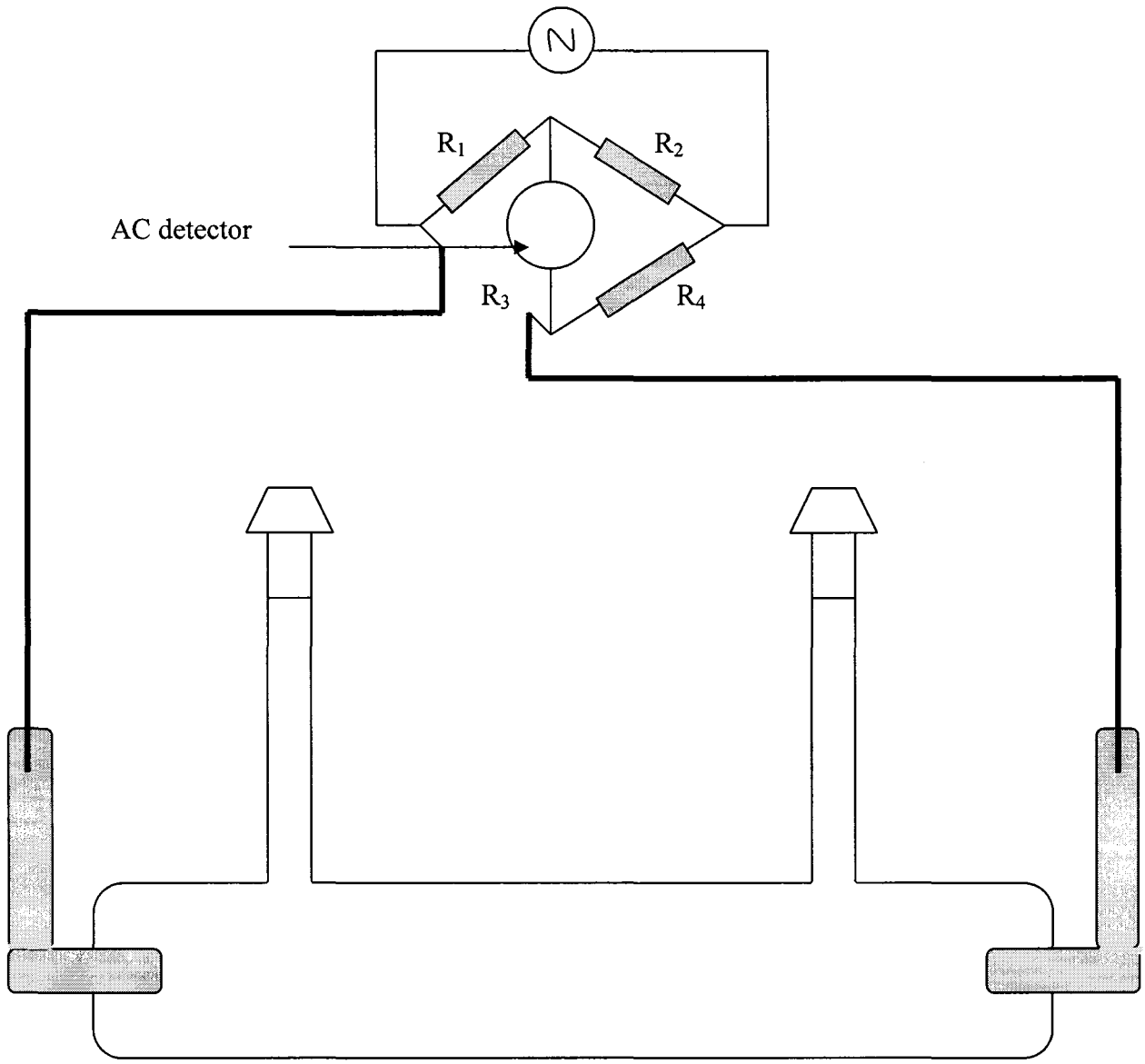

Figure 5.1 Conductivity cell for an electrolyte solution.

Conductance is the inverse of resistance and is expressed in siemens, S. Conductivity, κ, is expressed as $S \cdot m^{-1}$ or $S \cdot cm^{-1}$.

Impedance spectroscopy (see Section 1.7) has been effectively used in the past to probe the chemical and structural changes which occur during the sol-gel process.[1,2,10,11] Impedance spectroscopy is also able to measure the bulk resistance of a sol-gel.[2,11] By measuring the frequency dependence of the impedance one can readily separate the bulk and interfacial contributions to the resistance.[1] Therefore EIS has been extensively employed for determining the ionic conductivity of sol-gels.[11-15]

Dry silica has a low mobility of protons making it a poor ionic conductor.[2,9] These materials can be made more ionically conductive by incorporating electrolytes into a sol-gel network, with appropriate inorganic and organic dopants and with covalently linked aminosilane and other ORMOSILs.[2]

The work presented here reports the ionic conductivity of (TMOS + SO_3^- Silane) sol-gels.

5.2 Experimental

5.2.1 Preparation of 2-Electrode Cell Assembly for Solid State Impedance

To obtain conductivity measurements of gels in the solid state, it was necessary to design a 2-electrode conductivity cell assembly that would enable collection of impedance data without a liquid electrolyte. This was achieved by dipping two identical pieces of CFP (ca. 5 cm long) into a vial of sol and holding them in place until the sol gelled. The CFP electrodes were positioned 1 cm apart and such that they were face to

face to one another. To strengthen the CFP electrodes, each was wrapped in ca. 5 cm of copper foil, leaving 1 cm of the CFP exposed on the bottom. The connections to the Solartron 1250 frequency response analyzer were made using alligator clips attached to the top end copper foil of each electrode. The vial was covered with parafilm while the sol was left to age. See Figure 5.2 below for a schematic of the set-up.

The conductivity cell described above was calibrated using a solution of known conductivity. For the purposes of this work, a 0.1001 M KCl (aq) solution was prepared using deionized water and placed in a similar cell to that used for the gels. The impedance of the KCl (aq) solution was measured using the Z Plot software. The calibration constant, C, for the cell was determined using equation 5.1:[18]

$$C = \kappa^* \cdot R^* \qquad \text{Eq. 5.1}$$

given that the conductivity, κ^*, for a 0.1001 M KCl (aq) solution is 0.0258 $cm^2 \cdot \Omega^{-1}$ [18] and the resistance, R*, is obtained from the high frequency intercept of the impedance plot.

Simply measuring the high frequency impedance of the gels in a calibrated 2-electrode conductivity cell and substituting the value into a rearranged form of equation 5.1 yields conductivity values, κ, for the gels studied.

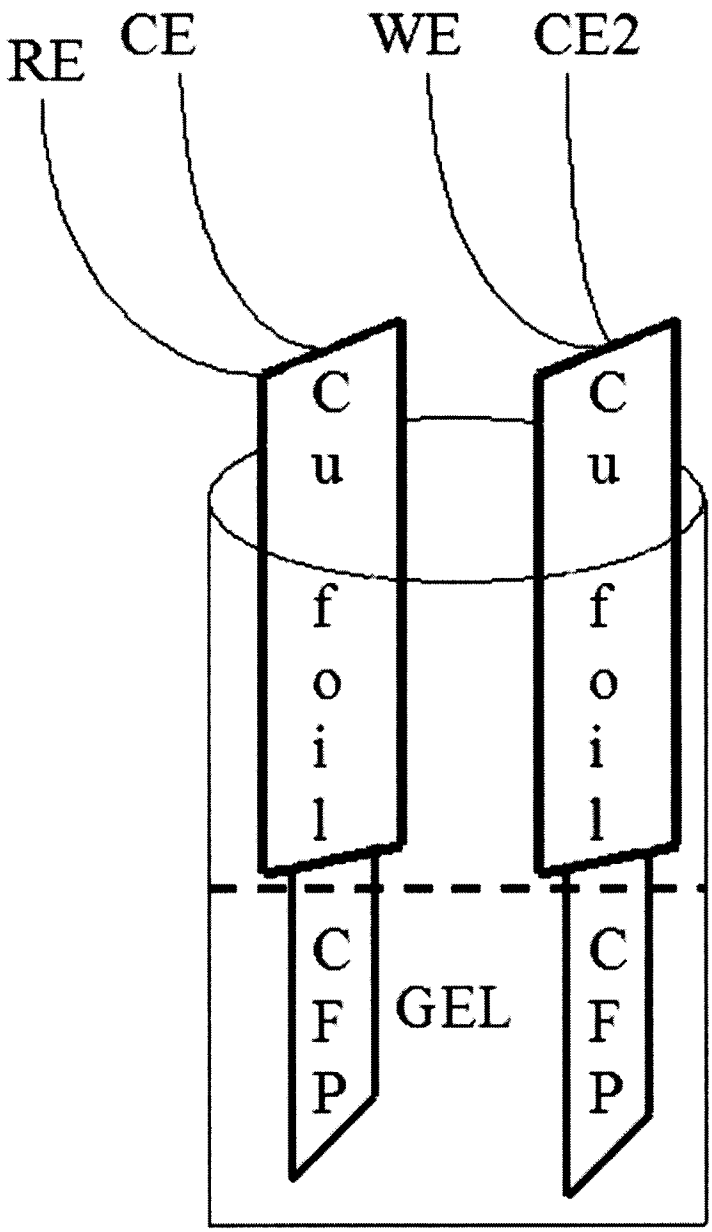

Figure 5.2 Two-electrode assembly for the impedance measurement of a solid hydrogel.

5.2.2 Ionic Conductivity for a Sulphonated Silica Hydrogel

TMOS: Sulphonated Silane (or TMOS:Nafion) hydrogels were prepared with SiO_2:SO_3^- molar ratios 9.3:1 were prepared as described in Chapter 3. The sols were placed in the 2-electrode assembly shown in Fig. 5.2 and their impedance measured over a period of several days while the sol aged.

In order to accurately measure the ionic conductivity of the gels, and not the conductivity due to hydrochloric acid from the sulphonated silane added to the sol-gels, it was necessary to extract the solid gels with deionized water for several days to flush the HCl (aq) out of the gel network. This was done by adding 3 mL of deionized water to the hydrogel and allowing it to equilibrate for approximately an hour before removing the external water solution. Impedance plots were measured and the procedure was repeated until plots were obtained with reproducible high frequency intercepts. Flushing of the gels with water had to be done slowly and carefully to avoid destroying the gel network. The re-hydrated gels were still rigid. However, if adequate time (several hours) was not allowed between extractions, the gel swelled with the water and eventually a bulk liquid phase dominated.

In all conductivity calculations, the R value used was obtained from the high frequency intercept of the last impedance plot measured after adequate rinsing with water (i.e. reproducible high frequency intercepts were obtained).

5.2.3 Rinsing of Hydrogels with Deionized Water

In order to evaluate the rinsing procedure used in the conductivity measurement, aged hydrogels were rinsed with 4 milliliters of deionized water to remove HCl (aq) from the pores of the gels. The water was allowed to equilibrate with the hydrogel (2.5 mL) for a period of 5 minutes, at which time a 50 μL sample of the water was removed and placed in 5 mL of deionized water in a clean flask. The pH of the deionized water containing 50 μL of rinse water was measured. The remainder of the rinse water was left on top of the hydrogel to continue equilibrating with the hydrogel and the procedure was repeated at 5 minute intervals, each time using a fresh 5 mL sample of deionized water in which to place the rinse water sample. The change in pH of the rinse water was monitored and subsequently the amount of HCl (aq) remaining in the hydrogel after rinsing was calculated, knowing that the hydrogel initially contained ca. 1 M HCl (aq).

5.3 Results and Discussion

5.3.1 Ionic Conductivity of Sulphonated Silica Sol-Gels

Figure 5.3 shows examples of Nyquist plots obtained before extraction and during aging while the gel was rinsed with deionized water. Figure 5.4 provides an expanded view of the high frequency region of Nyquist plots for a hydrogel before extraction and after the final rinsing with deionized water.

During the initial 5 minutes of equilibration with the deionized water, ca. 10 % of the acid was removed from the aged sol-gel. By 2 hours over 70 % of the acid was removed and by 2.5 hours over 90 % of the acid was removed from the gel. It is

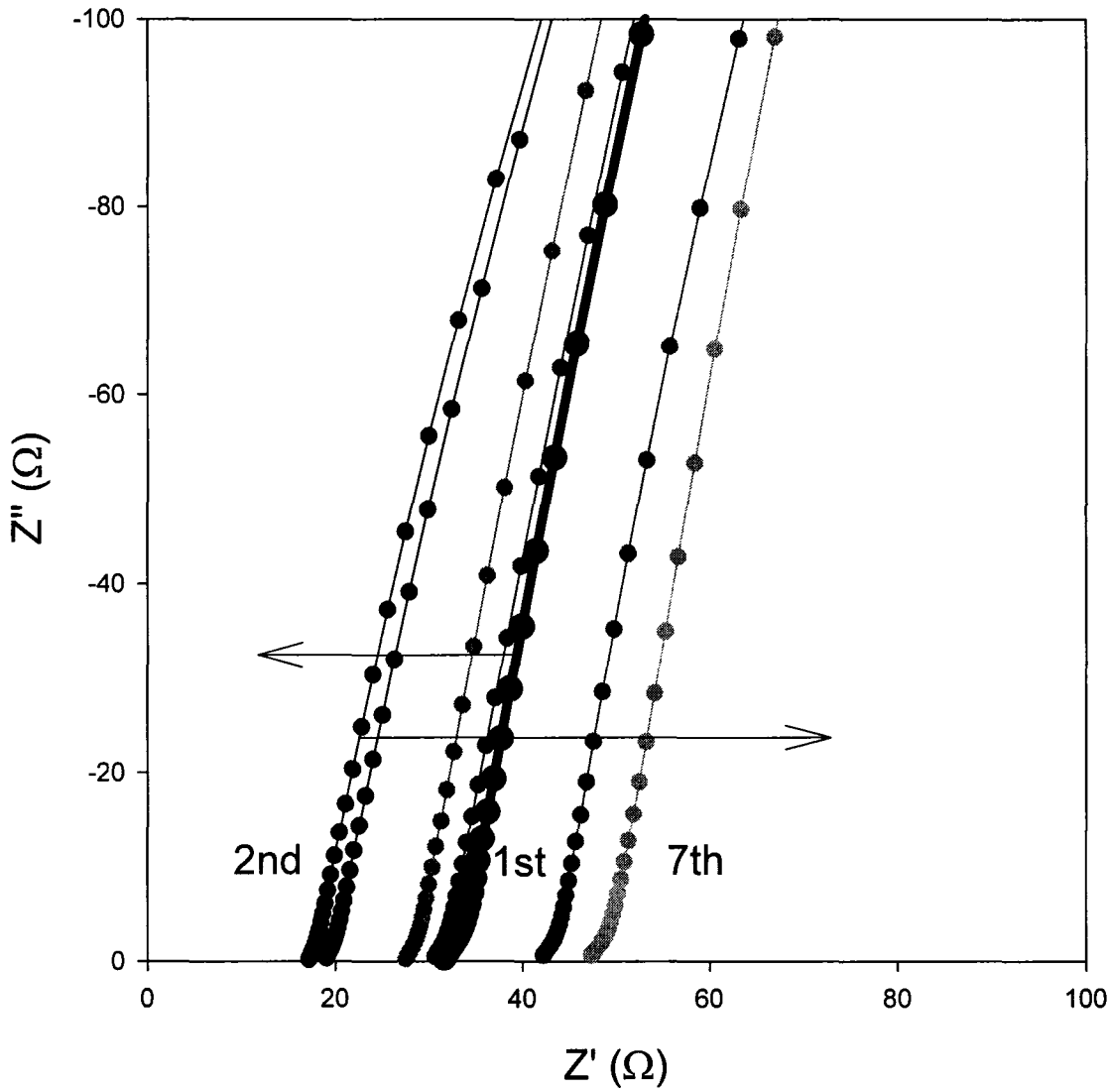

Figure 5.3 Nyquist plots of real impedance (Z') vs. imaginary impedance (Z") (65000 Hz → 0.1 Hz) for a sol in a 2-electrode cell with no added electrolyte before extraction with deionized water (shown in bold). Also shown are plots at different times during the extraction with deionized water.

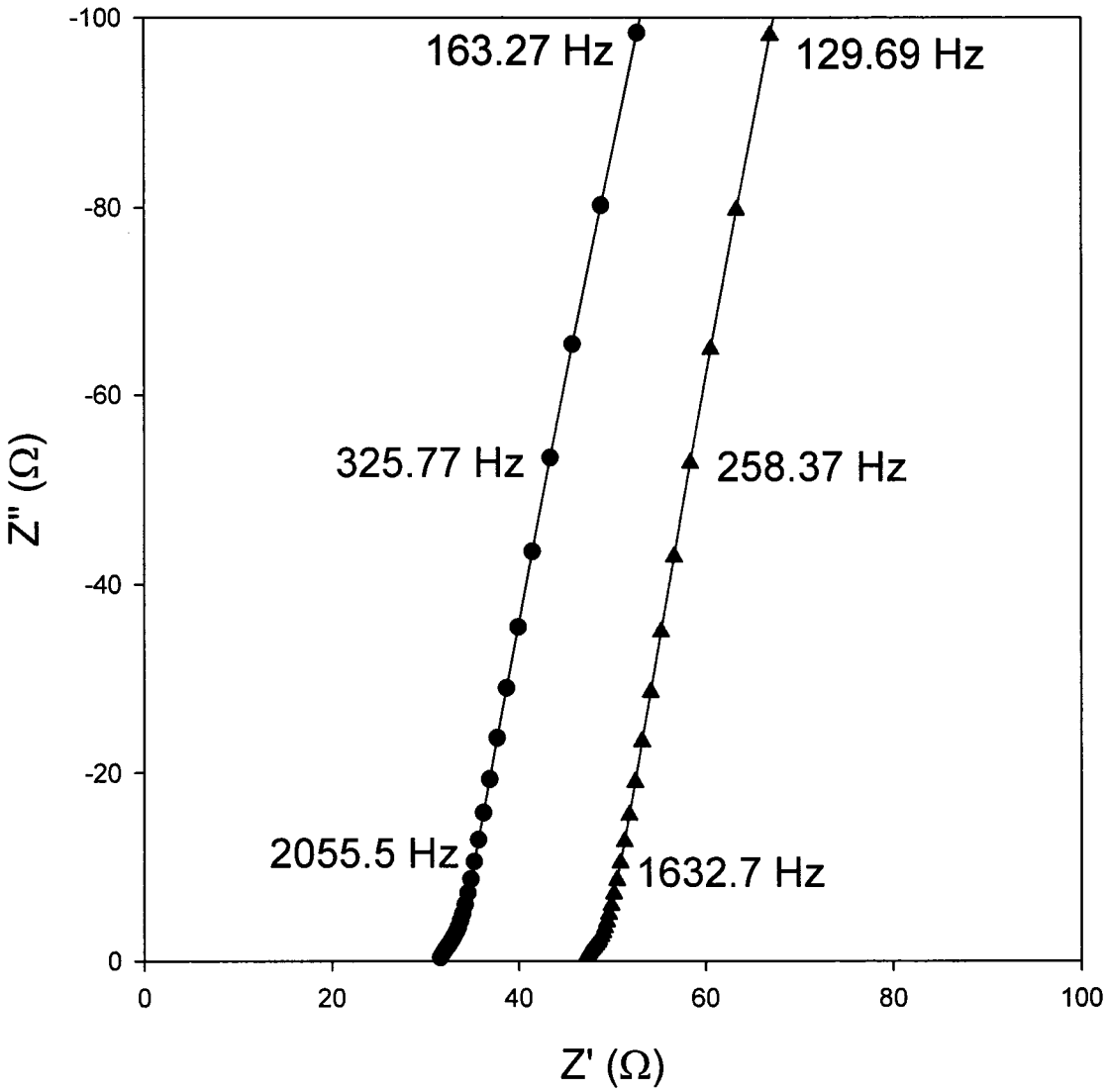

Figure 5.4 Nyquist plots showing high frequency intercepts for a sol (•) and an aged (1 week) hydrogel after extraction with 9 x 3 mL of deionized water over a period of 5 days (▲).

reasonable to assume that after a period of several days of extraction of the gel with deionized water left to equilibrate with the gel for an hour for each extraction that essentially all of the HCl (aq) was removed.

A summary of the pH changes as a function of rinsing is shown in Table 5.1.

Ionic conductivities were measured for a sulphonated silica sol-gel. For comparison, gels were prepared using Nafion in place of the sulphonated silane as the sulphonate source. In all cases, the SiO_2:SO_3^- mol ratio was maintained at 9.3:1. As well, TMOS gels (no sulphonate functionality) were also prepared and their ionic conductivities measured. Figure 5.5 shows Nyquist plots comparing the impedance for the two sulphonated silica sol-gels. Included on Figure 5.5 is the impedance measured for a 0.1001 M KCl solution used to calibrate the 2-electrode cell. Figure 5.6 shows a Nyquist plot for the TMOS gel.

The presence of the sulphonate groups greatly increases the ionic conductivity of the hydrogels, as evidenced by the decrease in high frequency real impedance intercepts for the sulphonated silane and Nafion-based hydrogels when compared to the TMOS gel as illustrated in Figs 5.5 and 5.6.

The (TMOS + Sulphonated Silane) hydrogel has a larger ionic conductivity over the Nafion-based gel based on the data shown in Fig 5.5. The sulphonated silane appears to be a better source of protons in a sol-gel network relative to Nafion.

Table 5.2 summarizes the results calculated for the ionic conductivities of these hydrogels. κ_i is the ionic conductivity measured for the sols when they are freshly made

Table 5.1 Amount of HCl (aq) in aged hydrogel as a function of rinsing with deionized water. The initial pH of the deionized water was 6.89. The aged gel contained ca. $2.5x10^{-3}$ mols HCl (aq).

Time (min)	pH 50 µL sample + 5 mL H_2O	Volume (mL) Rinse H_2O	Mols HCl (10^{-5}) 50 µL sample	% HCl removed
5	3.20	4.0	0.318	10.2
10	3.14	3.95	0.366	11.6
20	2.97	3.85	0.541	16.7
30	2.83	3.75	0.747	22.4
40	2.71	3.65	0.985	28.8
50	2.69	3.55	1.031	29.3
60	2.66	3.45	1.105	30.5
70	2.60	3.35	1.269	34.0
80	2.55	3.25	1.423	37.0
90	2.32	3.15	2.417	60.9
100	2.28	3.05	2.651	64.7
110	2.25	2.95	2.840	67.1
120	2.20	2.85	3.186	72.6
130	2.14	2.75	3.658	80.5
140	2.09	2.65	4.105	87.0
150	2.05	2.55	4.501	91.8

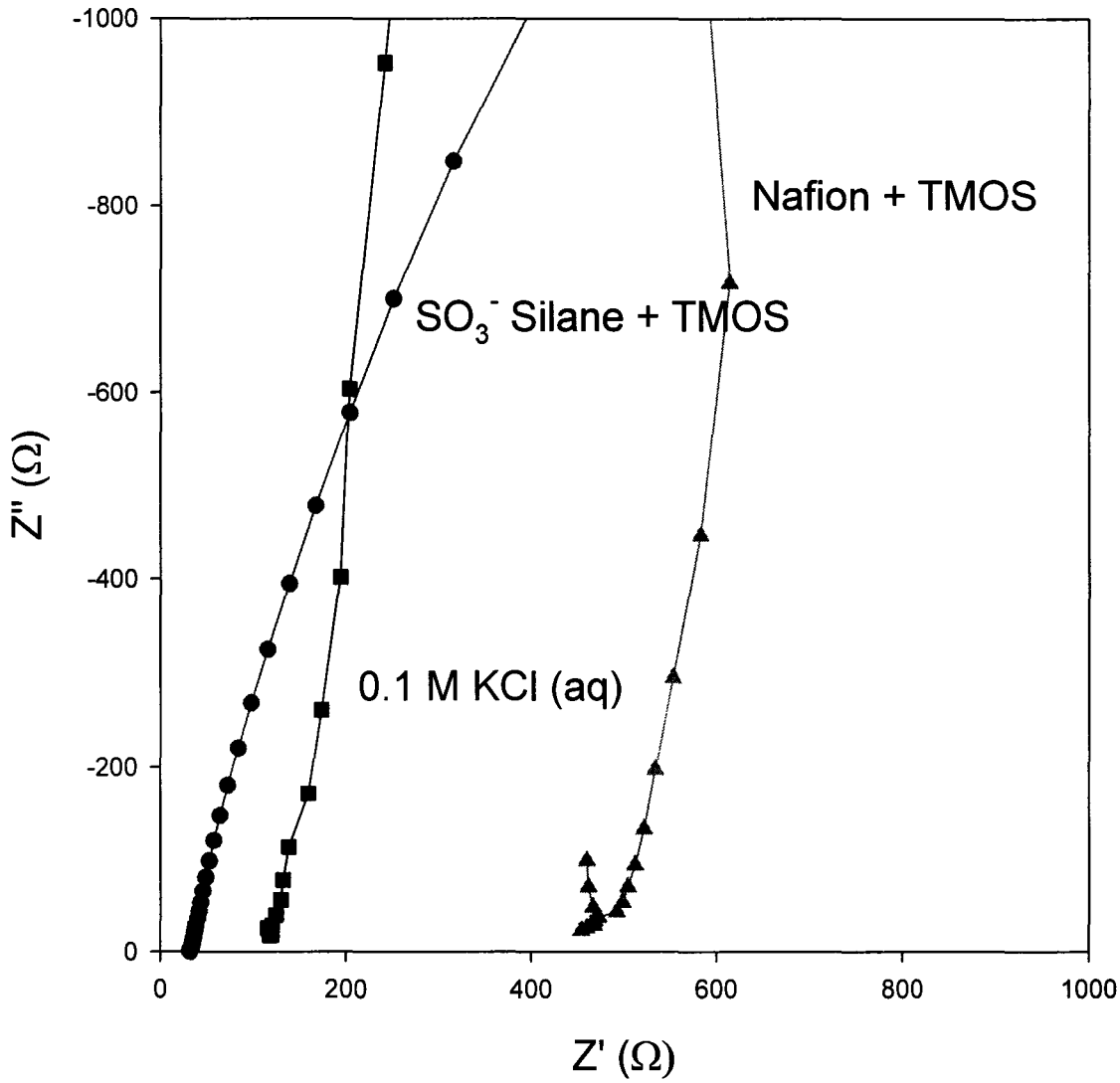

Figure 5.5 Nyquist plots showing the high frequency region for a (sulphonated silane + TMOS) hydrogel (•) and a (Nafion + TMOS) hydrogel (▲) after 5 days of rinsing with deionized water. Also shown is the impedance plot for a 0.1001 M KCl (aq) solution (■) used to calibrate the 2-electrode cell.

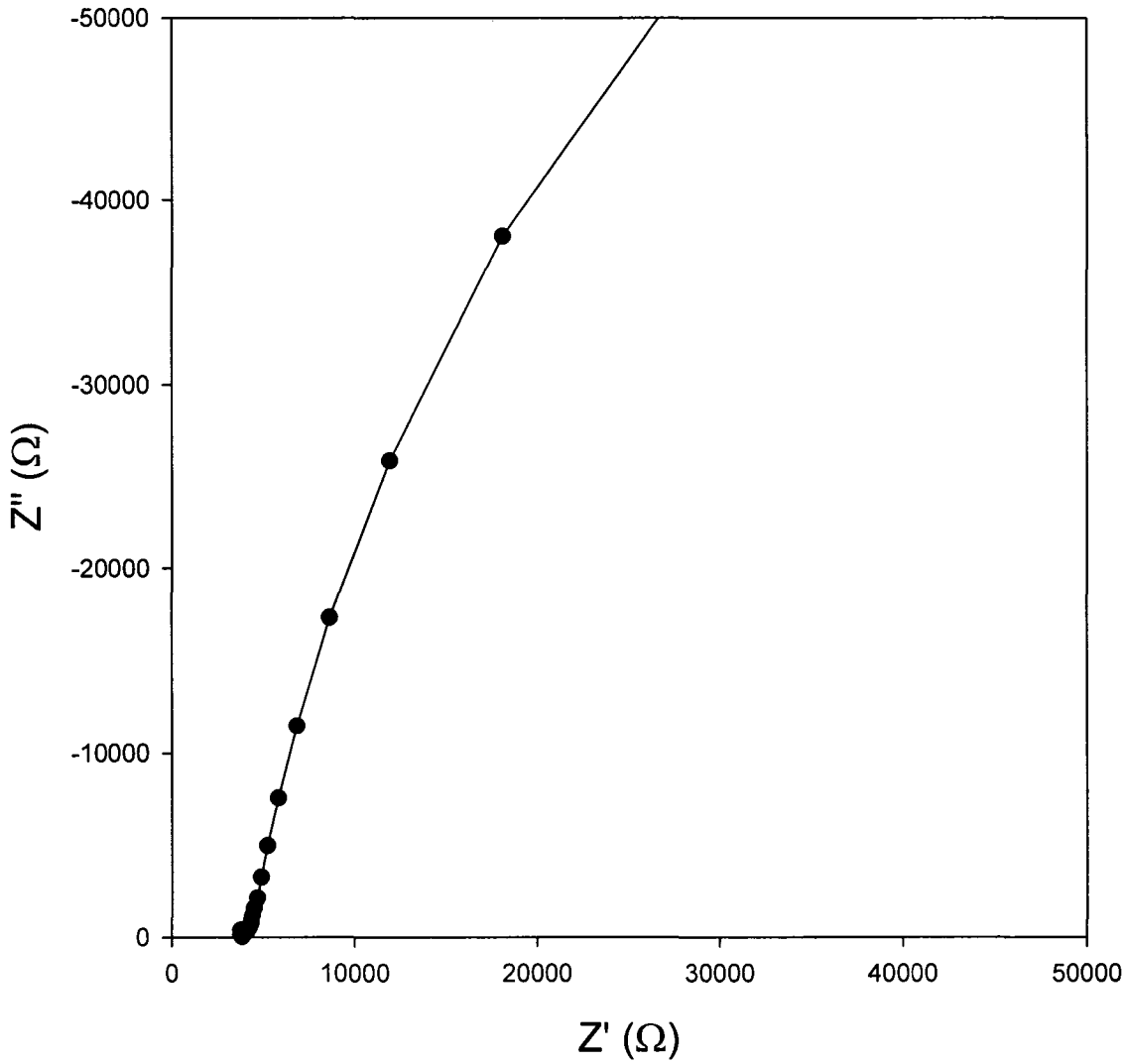

Figure 5.6 Nyquist plot showing the high frequency region for a TMOS hydrogel aged 1 week and subsequently rinsed for several days with deionized water.

Table 5.2 Summary of ionic conductivity results

Gel Composition	# Rinsing	κ_i ($S \cdot cm^{-1}$)	κ_f ($S \cdot cm^{-1}$)
TMOS	8	0.000791	0.000484
Nafion + TMOS	11	0.00753	0.00734
Silane + TMOS	9	0.0991	0.0561
(a)Nafion 115 membrane			0.2

(a) see reference 11

(i.e. liquid) while κ_f is the ionic conductivity as it was measured after the gel had aged (i.e. solid) and had been sufficiently extracted with deionized water.

5.3.2 Discussion

The ionic conductivities measured for the TMOS and (Nafion + TMOS) gels are comparable to ionic conductivities reported in literature for other sol-gels.[2,10-13] However, there are very few examples reported in literature of silica sol-gels with ionic conductivities approaching the value reported here for sulphonated silane + TMOS hydrogels.[1] These examples involve incorporating other metals into the silica sol-gels in order to achieve higher ionic conductivities. For example Nogami et al.[1] incorporated P_2O_5 into their silica gels to produce glasses with ionic conductivity of ca. 0.1 $mS \cdot cm^{-1}$ and Honma et al.[14] increased the conductivity (to > 10^{-2} $S \cdot cm^{-1}$) of their silica membrane by doping it with 12-phosphotungstic acid.

The high ionic conductivity observed for the sulphonated silica hydrogels is partly due to the presence of large amounts of water in the porous network.[1] Nogami et al have reported that the high proton conductivity exhibited in their P_2O_5-SiO_2 sol-gels is a result of the rapid proton mobility due to the coexistence of molecular water absorbed in the pores of the gels.[1] In addition, they stated that the proton conductivity was promoted by the dissociation of protons from the hydroxyl bonds and proton hopping between hydroxyl groups and water molecules.[1]

As shown below, ionic conductivity can proceed in two ways. Protons can hop from surface bound Si-OH groups to water molecules.

$$Si\text{-}OH + H_2O = SiO^- + H^+:H_2O \qquad \text{Eq.5.2}$$

Under these conditions, the proton motion is limited to hopping between the hydroxyl bond groups on the gel matrix and the surrounding water molecules. However, as the water content in the pore is increased, other water molecules act as further hopping sites for the proton transfer thus increasing the ionic conductivity.

$$H^+:H_2O + H_2O = H_2O + H^+:H_2O \qquad \text{Eq. 5.3}$$

Increasing the hydroxyl bonds and the absorbed water molecules in the pores, i.e. by increasing the surface area and volume of the pores, are ways to increase the conductivity of sol-gels. [1]

5.4 Conclusions

Ionic conducting silicate solids were synthesized using the sol-gel process. In this work, it was found that TMOS gels exhibited ionic conductivities of 4.8×10^{-4} $S \cdot cm^{-1}$. The addition of sulphonate functionality to the silica network significantly increased the ionic conductivity. SO_3^- groups were incorporated into the sol-gels by including either Nafion or a sulphonated silane into the sol-gel process. Gels prepared with Nafion exhibited ionic conductivities of 0.0073 $S \cdot cm^{-1}$ while those prepared with the sulphonated silane exhibited ionic conductivities of 0.056 $S \cdot cm^{-1}$. The larger ionic conductivities displayed by the (TMOS + Sulphonated Silane) gels over the (TMOS + Nafion) gels are due to the fact that the SO_3^- groups of the sulphonated silane are present on the surface of the sol-gel

pores while they are not for the Nafion-based gels. This allows for easier mobility of protons in the (TMOS + Sulphonated Silane) gels.

Sulphonated silica sol-gels benefit from the fact that they are ORMOSILs. It has been reported in the literature that the presence of organic-inorganic interfaces may assist in the solvation of ions.[12] This allows the protons to act as "free ions" and leads to an increase in ionic conductivity displayed by an amorphous solid.[2]

Impedance spectroscopy was a useful technique for obtaining ionic conductivities of solid samples.

References

[1]Nogami, M.; Tarutani, Y.; Daiko, Y.; Izuhara, S.; Nakao, T.; Kasuga, T. *Journal of the Electrochemical Society*, **2004**, 151, A2095

[2]Lev, O.; Wu, Z.; Bharathi, S.; Glezer, V.; Modestov, A.; Gun, J.; Rabinovich, L.; Sampath, S. *Chem. Mater.*, **1997**, 9, 2354

[3]Abe, Y.; Li, G.; Nogami, M.; Kasuga, T.; Hench, L. L. *J. Electrochem. Soc.*, **1996**, 143, 144

[4]Atik, M.; Pawlicka, A.; Aegerter, M. A. *J. Mater. Sci.*, **1995**, 14, 1486

[5]Forano, C.; Besse, J. P. *Mater. Chem. Phys.*, **1988**, 19, 567

[6]Tatsumisago, M.; Kishida, K.; Minami, T. *Solid State Ionics, Diffusion Reactions*, **1993**, 59, 171

[7]Eschenbaum, J.; Rosenberger, J.; Hempelmann, R.; Nagesgast, D.; Weidinger, A. *Solid State Ionics*, **1995**, 77, 222

[8]Abe, Y.; Hosono, H.; Akita, O.; Hench, L. L. *J. Electrochem. Soc.*, **1994**, 141, L64

[9]Watton, S. P.; Taylor, C. M.; Kloster, G. M.; Bowman, S. C. Coordination Complexes in Sol-Gel Silica Materials in *Progress in Inorganic Chemistry*, Vol. 51, ed. Kenneth D. Karlin. 2003, 333-420

[10]Pinol, S.; Najib, M.; Bastidas, D. M.; Calleja, A.; Capdevila, X. G.; Segarra, M.; Espiell, F.; Ruiz-Morales, J. C.; Marrero-Lopez, D.; Nunez, P. *J. Solid State Electrochem.*, **2004**, 8, 650

[11]Durakpasa, H.; Breiter, M. W.; Dunn, B. *Electrochimica Acta*, **1993**, 38, 371

[12]Mitra, S.; Sampath, S. *Macromolecules*, **2005**, 38, 134

[13]Li, Z.; Liu, H.; He, P.; Li, J. *J. Phys. Chem. B.*, **2004**, 108, 17512

[14]Honma, I.; Nakajima, H.; Nishikawa, O.; Sugimoto, T.; Nomura, S. *Solid State Ionics*, **2003**, 162, 237

[15]Huguenin, F.; Girotto, E. M.; Torresi, R. M.; Buttry, D. A. *J. Electroanal. Chem.*, **2002**, 536, 37

[16]Winter, M.; Brodd, R. J. *Chem. Rev.*, **2004**, 104, 4245

[17]MacDonald, J. R.; Johnson, W. B. Impedance Spectroscopy: Emphasizing Solid Materials and Systems, ed. Mac Donald, J. R. John Wiley & Sons, Inc., New York, 1987

[18]Atkins, P. Physical Chemistry, 5th ed. W. H. Freeman and Company, NY, 1994

Chapter 6:

Composites of a Sulphonated Silica Sol-Gel and a Conducting Polymer

6.1 Introduction to Conducting Polymers into Sol-Gel Hosts

The synthesis of organic/inorganic hybrid materials has received considerable attention because of the prospect of developing materials with unique micro/nanostructures and properties.[1, 2, 3, 4] One of the areas of interest is the synthesis of composites combining conducting polymers with metal oxides using the sol-gel process.[5, 6, 7, 8, 14] The goal behind the design of these materials is to incorporate the electronic conductivity of the conducting polymer into the ionic conducting network of the sol-gel to produce materials with redox characteristics that aid in rapid electron transfer at an electrode surface.[5] Chauby et al have electrochemically entrapped polyaniline into sol-gel films coated onto ITO glass plates for lactate biosensing[5] while Neves and Fonseca have electrochemically polymerized aniline in the pores of silica sol gel networks for use as cathodes in rechargeable lithium batteries.[6] Ballarin et al studied the electrosynthesis of polythiophene into silica sol-gel films using electrochemical, spectroscopic, and optoelectrochemical techniques as well as atomic force and scanning electron microscopy.[7]

It is critical to understand the mass/charge transport processes in conducting polymer + sol-gel films because the electrochemical switching of a conducting polymer film between the conducting (doped) and nonconducting (undoped) states involves both electron and ion transport within the film.[9]

In this chapter the synthesis of polypyrrole-gel (PPY/gel) composites and a study of ion transport in these materials in $NaClO_4$ (aq) and KCl (aq) employing cyclic

voltammetry and impedance spectroscopy is described. Scanning electron microscopy was used to perform an X-ray emission analysis on PPY/gel films.

Polypyrrole films doped with the sol-gel were prepared by electrochemical polymerization because this technique offers better control of the film thickness and morphology. In electropolymerization, a film of the electronically conductive polymer is deposited onto a supporting electrode surface by anodic oxidation of the monomer in the presence of an electrolyte. This can be achieved by using potentiostatic (constant potential), galvanostatic (constant current) or potentiodynamic (potential scanning) methods.[10] Aqueous electrolytes may be used in the electropolymerization of polypyrrole since pyrrole has a low oxidation potential. Since the intrinsic properties of polypyrrole are dependant on the electropolymerization conditions, it is necessary to understand the mechanism involved in the polymer film deposition.

The electropolymerization of pyrrole involves several steps.[10] The first step is the initiation step where the pyrrole monomer is oxidized at the electrode surface by loss of an electron and a radical cation is formed, as shown in Scheme 5.1:

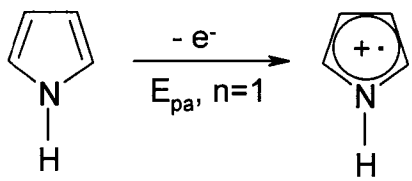

Scheme 6.1

The resonance forms of the cation are represented below:

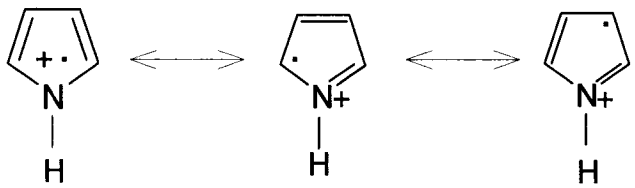

Scheme 6.2

The second step is the propagation step involving the dimerization between two radical cations and the subsequent loss of protons to form an aromatic dimer, as follows:

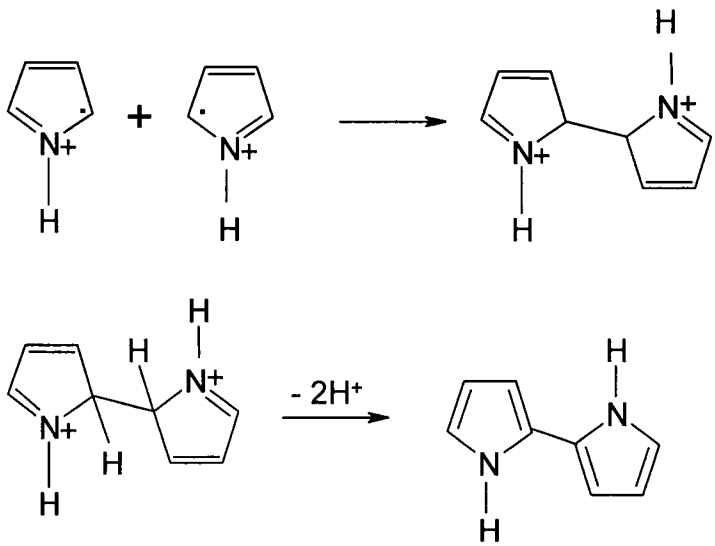

Scheme 6.3

Oxidation of the dimer produces a cation radical:

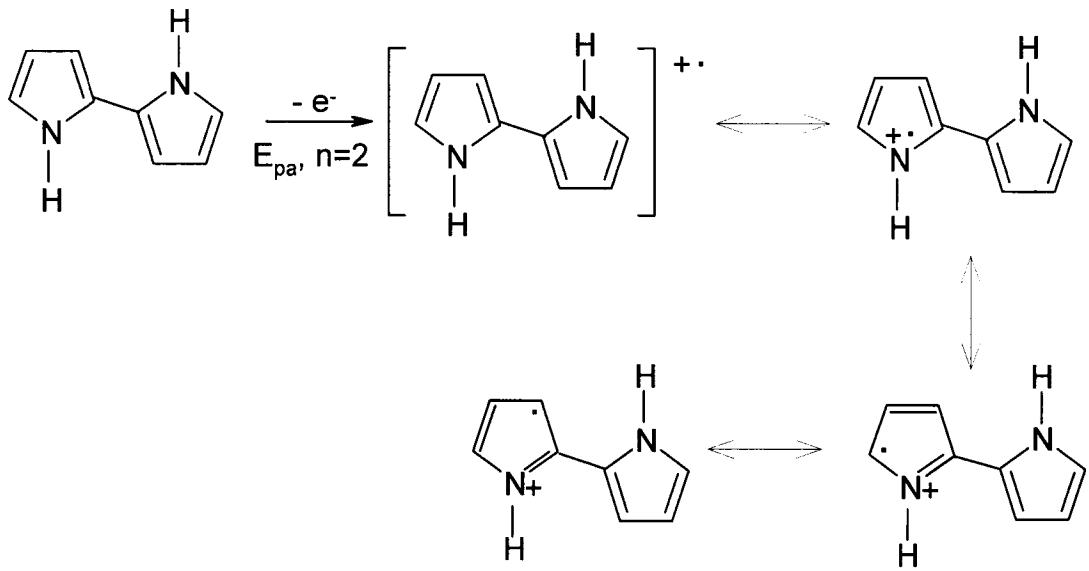

Scheme 6.4

The cation radical further reacts with monomer radical cation to form a trimer, which subsequently deprotonates to give a neutral trimer.

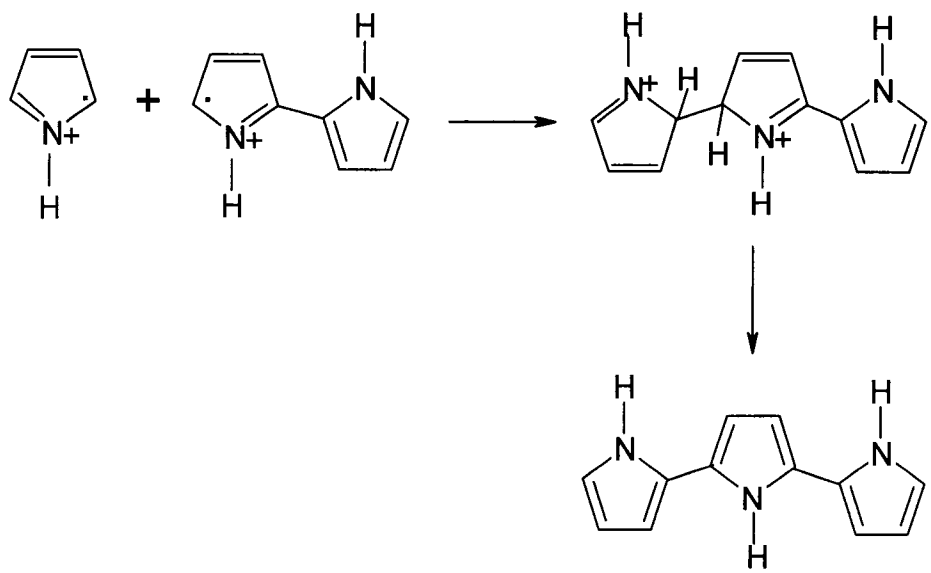

Scheme 6.5

The neutral dimer formed above undergoes oxidation to produce a radical cation (trimer), as described below:

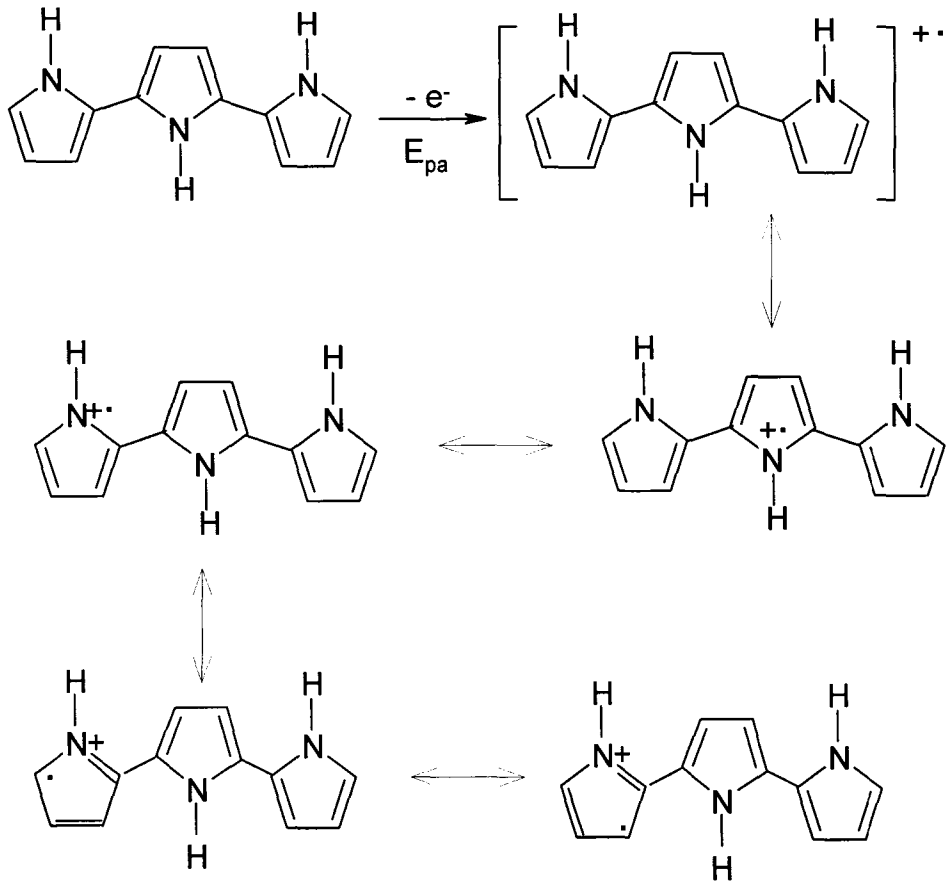

Scheme 6.6

This sequence of oxidation, coupling and deprotonation continues until the final polymer is obtained. The final polypyrrole product is abbreviated as:

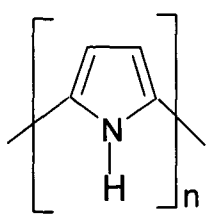

Scheme 6.7

A lowering of the oxidation potential occurs because of the extended conjugation of the polymer (when compared to the monomer). Therefore synthesis and doping of the polymer occur simultaneously. It has been reported that there is in fact a positive charge every 3 to 4 pyrrole units on the polymer chain.[10] This is balanced by the presence of an anion, and is shown below where A^- is the electrolyte anion.

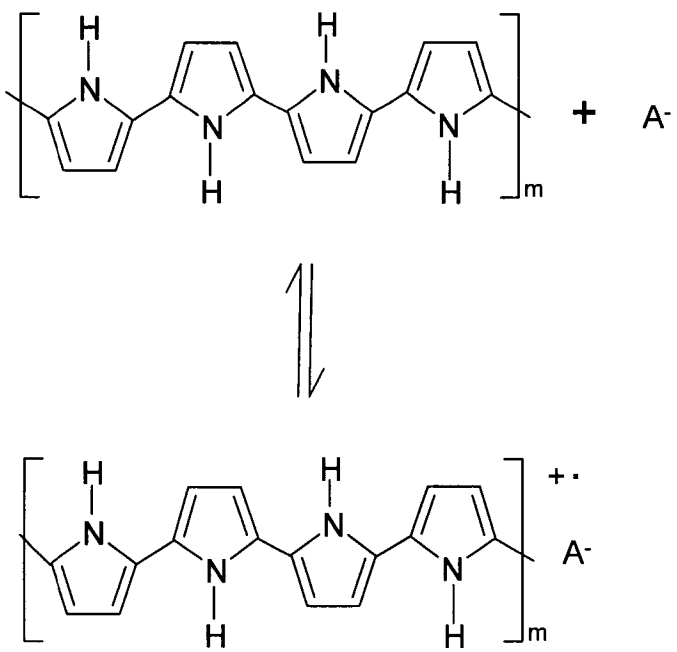

Scheme 6.8

Typically, the film consists of approximately 65% polymer and 35% anion (by mass).[10] The degree of electropolymerization, n, is dependant on current density, pH, monomer concentration and temperature.[10, 11]

Electrical conductivity is achieved in the film by p-doping (oxidation) which is followed by the insertion of anions or cations into the film. The charged species formed upon doping are able to move along the alternating double bonds in the conjugated polymer backbone, allowing electron transport.

Polypyrrole was the polymer of choice for this work because of it has excellent environmental stability, is easy to synthesize and it has higher conductivity than many other conductive polymers.[11]

6.2 Experimental

6.2.1 Preparation of Composites of a Sulphonated Silica Sol-Gel and Conducting Polypyrrole

Sulphonated silica sol-gels were prepared as described in Chapter 3 and allowed to age for several days. Once the gel was aged, it was washed repeatedly with deionized water to remove methanol and chloride ions in order to facilitate the polymerization of polypyrrole. After extensive washing, 3 mL of deionized water was left sitting in the vial with the gel until all of the water was absorbed by the gel and it turned liquid. This liquid gel was used as the electrolyte for the electropolymerization of polypyrrole. Polymer-gel composites were prepared electrochemically by applying a constant anodic current of 5 μA to a 0.0045 cm^2 Pt electrode in a small vial containing gel and pyrrole (ca. 0.1 M pyrrole in gel) under a N_2 (g) atmosphere. Cu wire was used as the counter electrode. The current was allowed to pass for 8 minutes. The cell potential during polymerization rapidly increased to about 0.40 V before remaining constant at 0.35 V for the duration of the polymerization. This indicates that the electrochemical polymerization was mainly determined by electron transfer control and the electropolymerization reaction commences instantaneously.[7] A black polymer-gel composite film was deposited on the

Pt disk electrode. The electrode was removed from the vial and the film rinsed with water and allowed to dry for 2 days.

6.2.2 Preparation of a Control Sol-Gel and PPY/Control Gel Film

A control sulphonated silica sol-gel was prepared by distilling a 2(4-chlorosulfonylphenyl) ethyl-trichlorosilane (50 % in CH_2Cl_2) + methanol solution to remove dichloromethane, methanol and HCl. The distilled silane (ca. 2 mL, liquid) was mixed with deionized water and 0.1 M HCl (aq) and allowed to age for several days. After aging for two weeks, the gel became very viscous and gel-like, but not solid. The control gel was further rinsed with deionized water to ensure all organic solvents were removed. Additional water was added to the vial to produce a liquid gel. A PPY/control gel film was deposited on a glassy carbon disk electrode by constant current of 100 μA for 8 minutes.

6.3 Results and Discussion

6.3.1 Cyclic Voltammetry

The electrochemical properties of the PPY/gel films were initially characterized by cyclic voltammetry in 0.2 M $NaClO_4$ (aq), as illustrated in Figure 6.1. A number of films were studied, but only the most comprehensive data set is described here. The two main peaks for the PPY/gel are centered at ca. –0.35 V and become more pronounced as the scan rate was increased.

Plots of peak potential and peak current vs. scan rate are shown in Fig 6.2 and Fig 6.3. There are significant peak separations, which increase with scan rate. Interestingly,

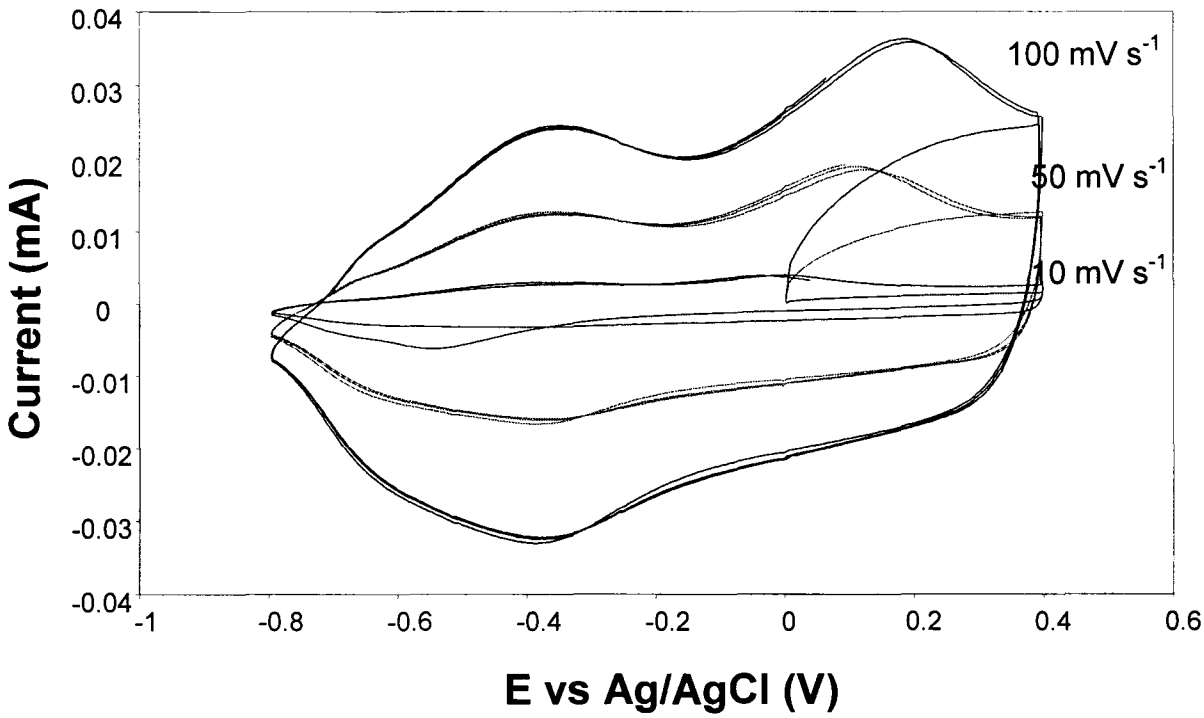

Figure 6.1 Cyclic voltammograms of a PPY/gel coated Pt electrode in 0.2 M $NaClO_4$ (aq). Scan rates in $mV \cdot s^{-1}$ are indicated.

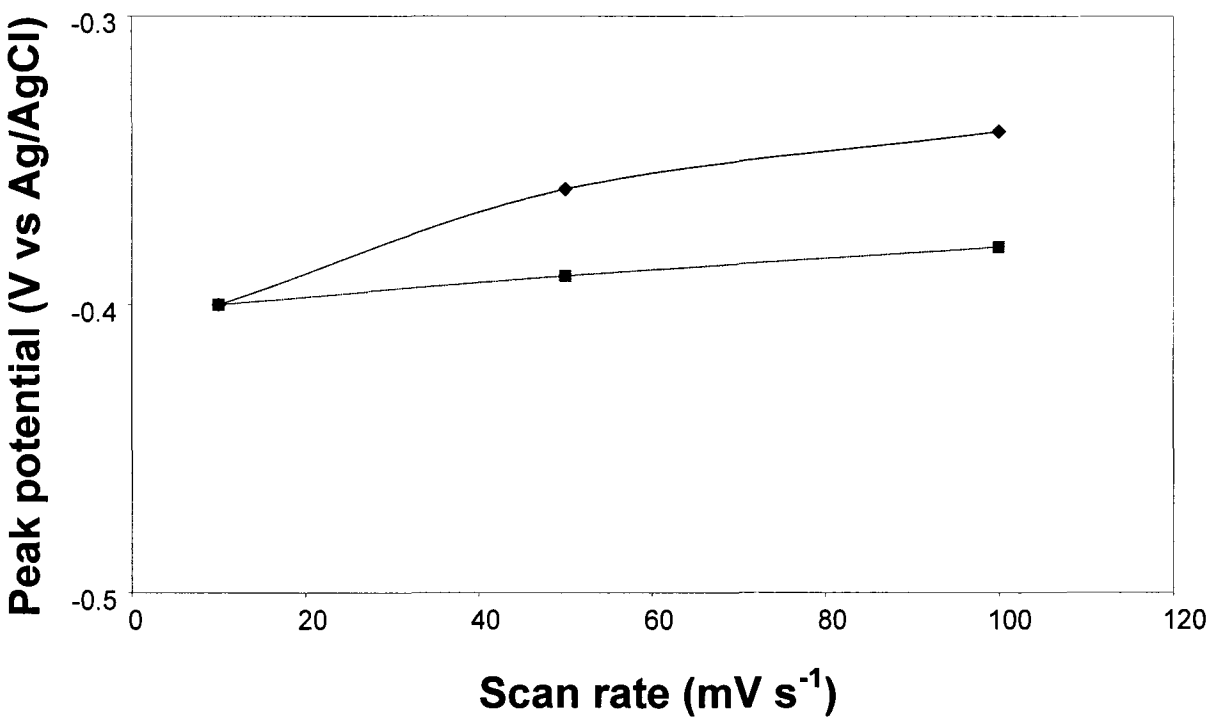

Figure 6.2 Plot of peak potentials vs scan rate for the cyclic voltammograms shown in Fig 6.1. Diamonds are for the anodic peak, squares are for the cathodic peak.

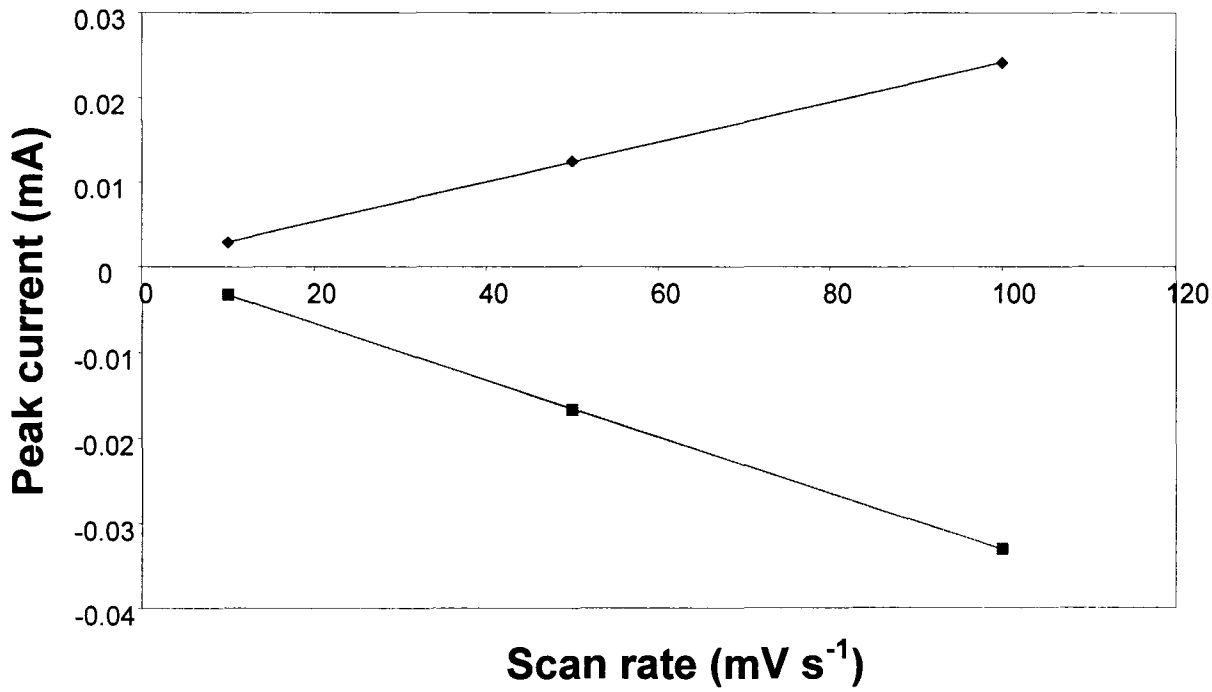

Figure 6.3 Plot of peak currents vs scan rate for the cyclic voltammograms shown in Fig 6.1. Diamonds are for the anodic peak, squares are for the cathodic peak.

both the anodic and cathodic peaks shift towards more positive potentials with increasing scan rate. The peak currents increased linearly with increasing scan rate up to 100 $mV \cdot s^{-1}$, which indicates the absence of charge-transport limitations.[9]

The first scan for the 10 $mV \cdot s^{-1}$ cycle shown in Fig 6.1 exhibits an anomalous sharp, cathodic reduction peak at ca. -0.55 V. This peak is thought to be due to the insertion of cations into the PPY/gel film.[15, 16] It has been proposed that the low mobility of counterions in the oxidized polymer necessitates cation insertion during the initial reduction.[15] The neutral reduced PPY/gel film then contains a high concentration of electrolyte and reoxidation of the film results in cation expulsion (at ca. -0.37 V) followed by anion insertion (at ca. 0.15 V). In other words, the electrochemical cycling of PPY/gel causes a non-equilibrium build up of electrolyte in the polymer film.[16] The various structures of the PPY/gel films in their neutral, reduced and oxidized states are shown below.

These conjectures are confirmed in section 6.3.3 by X-ray emission analysis.

The neutral PPY/gel film consists of n sulphonated silica sol gel units per polypyrrole unit, where n is expected to be ca. 1.2.[9] The negative charge associated with the sulphonate groups is balanced by the p-doping of the polypyrrole units. The composition of the neutral PPY/gel film can be represented as:

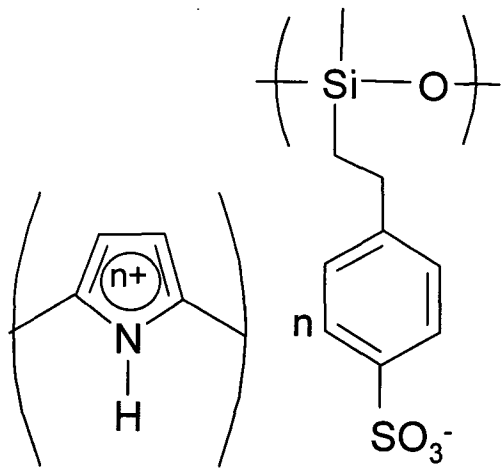

Scheme 6.9

Upon reduction of the PPY/gel film, the polypyrrole unit loses its positive charge and becomes neutral. In order to balance out the charge, cations are then incorporated into the PPY/gel film and are associated with the negative charges on the sulphonate groups of the gel. The composition of the reduced PPY/gel film can be represented as:

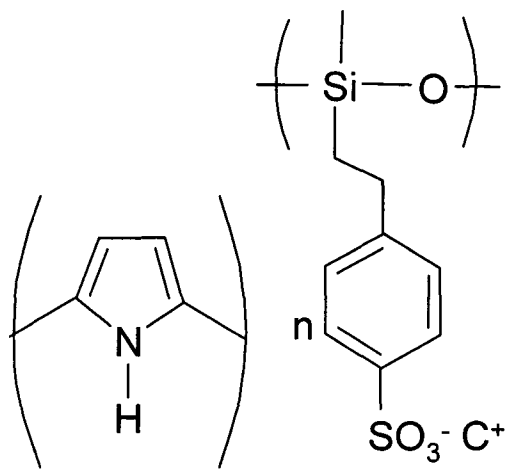

Scheme 6.10

Upon reoxidation, the PPY/gel film expels the cations as the polypyrrole unit becomes positively charged. Further oxidation leads to a build-up of excess positive charge on the polypyrrole. In order to balance this, anions are inserted into the film. The composition of the oxidized PPY/film, containing anions, can be represented as:

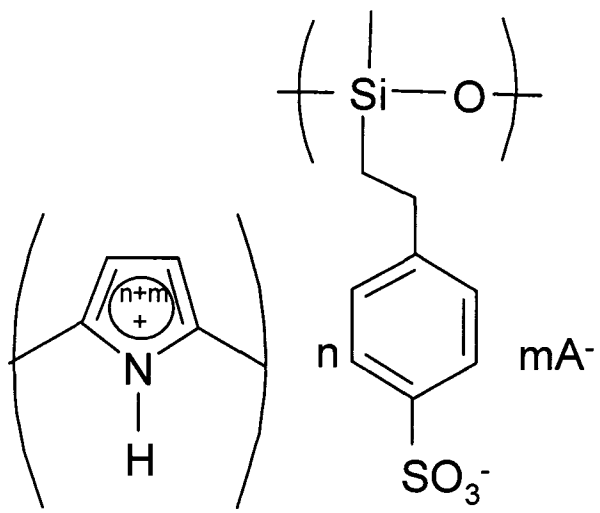

Scheme 6.11

6.3.2 Impedance Studies

Nyquist impedance plots for a PPY/gel coated electrode at selected potentials are shown in Figure 6.4. Several films were studied, using different batches of the same composition of sol-gel as the PPY/gel electrolyte. Results were reproducible so long as the electrode positioning in the cell was kept the same in all experiments. All plots shown in this section were obtained by changing the potential in the negative direction and were checked for reproducibility after each change in potential.

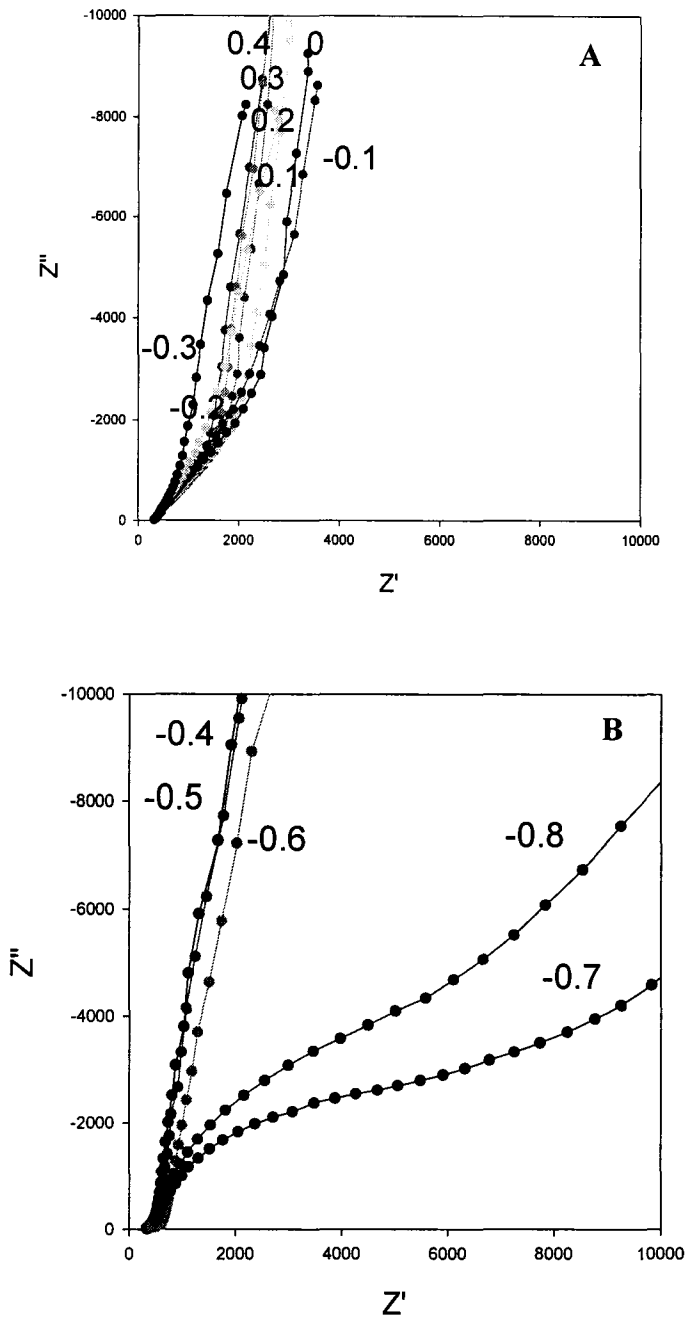

Figure 6.4 Complex plane impedance plots for a PPY/gel film on a Pt electrode in 0.2 M $NaClO_4$ (aq) in the frequency range of 6500 Hz to 0.1 Hz. Electrode potentials are indicated in Volts vs Ag/AgCl. (**A**) shows results for potentials between 0.4 V and -0.3 V and (**B**) shows the results for the more negative potentials.

The real axis high frequency intercept for all but the most negative potential data is independent of potential and coincides with the uncompensated resistance of the bulk electrolyte solution, R_s, as shown in Fig 6.5 (A). At potentials more negative than -0.5 V, the high frequency intercept becomes increasingly larger as the potential becomes more negative, as seen in Fig. 6.5 (B). Polypyrrole is known to have high electronic conductivity when even slightly oxidized. Because of the fast electron transport, it is reasonable to conclude that the electronic resistance of the polymer film was negligible at potentials above -0.6 V.[9]

Initially, the redox reaction induced by the ac potential wave at high frequency starts at the PPY/gel/solution interface. The 45° Warburg-type line observed in Fig. 6.4 (A) is a result of the redox reaction layer growing into the polymer film from the PPY/gel/solution interface as the frequency decreases.[9] When the redox reaction layer encompasses the whole PPY/gel film, the film remains in equilibrium with the changing potential and the polymer-coated electrode behaves as a capacitor,[9] which is seen in the almost vertical line observed in the spectra at low frequency.

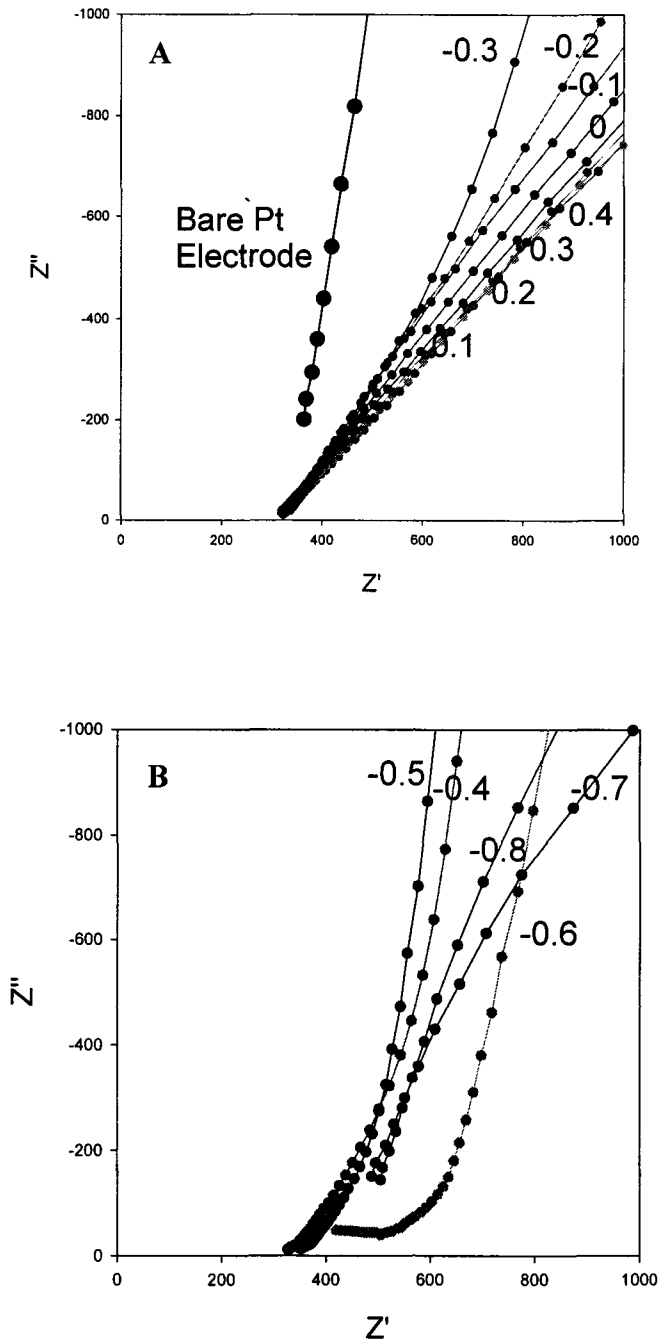

Figure 6.5 Expansion of the high frequency data in Fig 6.4. (**A**) shows results for potentials between 0.4 V and -0.3 V and (**B**) shows the results for the more negative potentials.

The ionic resistance R_{ion} of the PPY/gel film is given by[9,13]

$$R_{ion} = 3(R_{low}-R_s) \quad \text{Eq. 6.1}$$

where R_{low} is the real axis intercept (Z') of the nearly vertical low-frequency region of the Nyquist plot, as shown in Fig 6.6, and R_s is the solution resistance.

The ionic conductivity of the film, σ_{ion}, is calculated as follows

$$\sigma_{ion} = d/R_{ion} \cdot A \quad \text{Eq. 6.2}$$

where d is the film thickness and A is the geometric area of the electrode. It is known that a charge density of 0.48 $C \cdot cm^{-2}$ is required to deposit a 2 μm thick film of PPY/poly(styrenesulfonate).[9] The film thicknesses obtained in this work were taken to be 2 μm because the same charge density was applied while growing the films. The Pt electrode area was 0.0045 cm^2.

Figure 6.7 shows a plot of ionic conductivity vs. potential. Initially, the ionic conductivity of the PPY/gel decreased with decreasing potential as a decrease in the concentration of ionic charge carriers in the film occurs[9] due to anions being expelled from the film. At -0.1 V the ionic conductivity of the film starts to increase upon further decrease in potential. This is due to the insertion of cations into the PPY/gel film upon further reduction in accordance with expectations based on the cyclic voltammograms shown in Fig. 6.1.

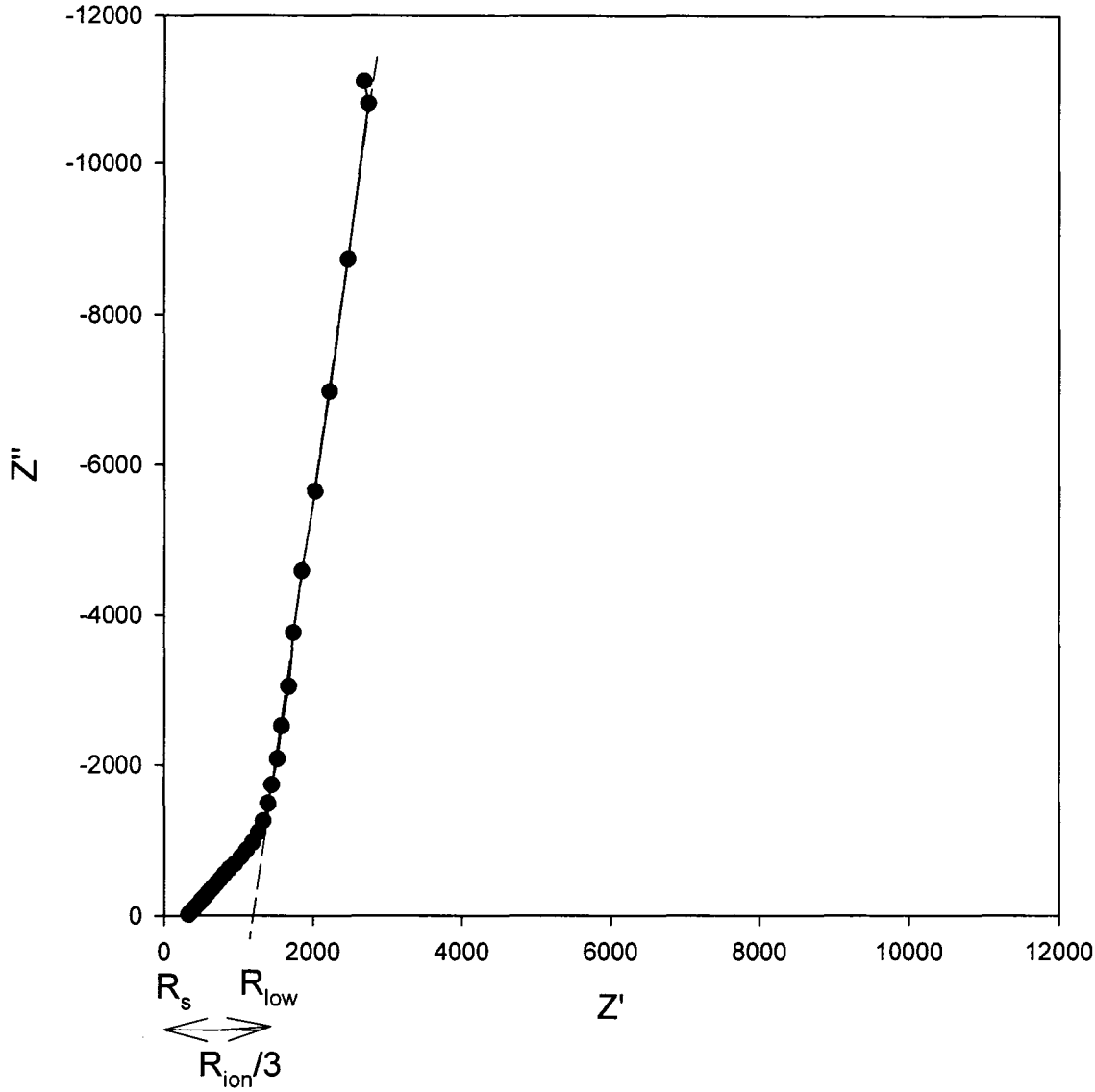

Figure 6.6 Complex plane impedance plot for a PPY/gel coated Pt electrode at 0.4 V vs Ag/AgCl in 0.2 M $NaClO_{4\,(aq)}$. R_s, R_{low} and R_{ion} are indicated on the plot.

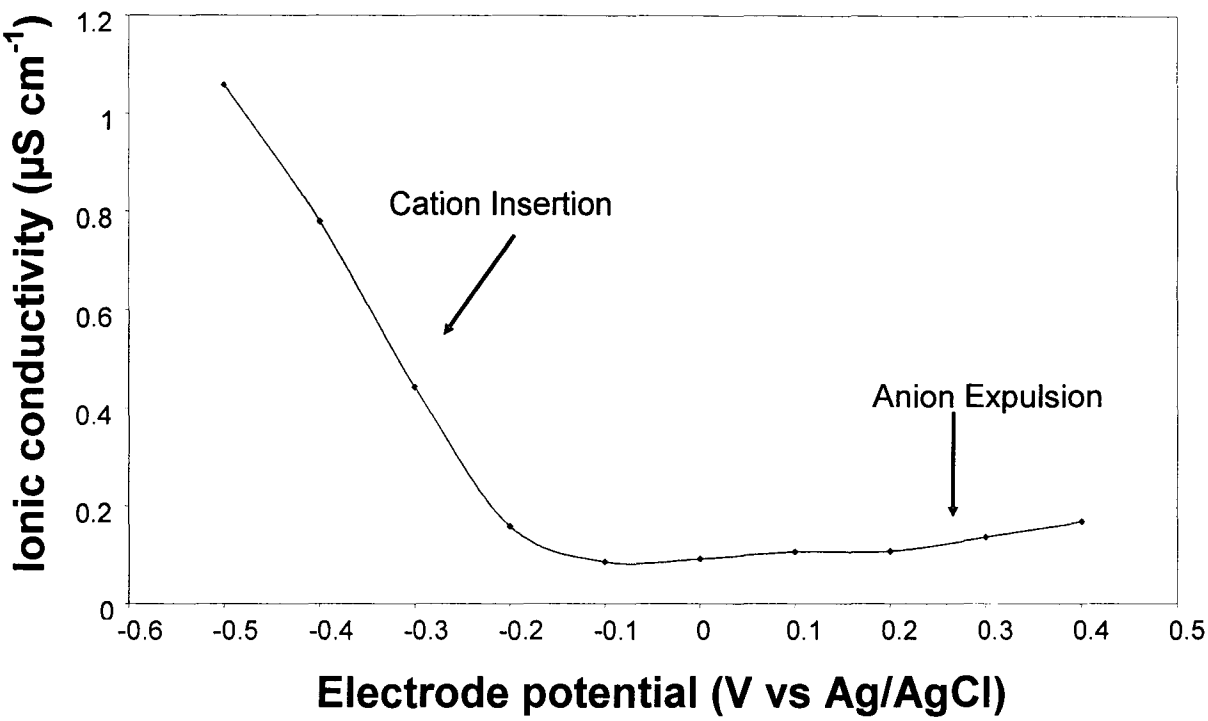

Figure 6.7 Plot of ionic conductivity vs potential from the impedance plots shown in Fig 6.1. Conductivities were measured in the order of decreasing potential.

Low frequency capacitances from the slopes of imaginary impedance (Z") vs. 1/frequency plots for data obtained from the almost vertical regions of the complex impedance plots are shown in Fig 6.8, where capacitance is C_F = 1/slope. Initially, there was an increase in capacitance observed when the potential of the working electrode was decreased from 0.4 V to 0.2 V. This was followed by a decrease in capacitance at potential 0.1 V. Further reduction produced a film with a capacitance of ca. 5.5 $F \cdot cm^{-2}$. The low frequency capacitance can also be obtained directly from the Nyquist plot (C_F = $1/j\omega Z$), which emphasizes the frequency dependence of charging processes at low frequency.[9]

At very low potentials, the impedance of the PPY/gel changed from the simple Warburg-type line observed at high potentials to a more complex response including a high frequency semicircle response in the complex plane representation. This indicates that an interfacial charge transfer process had become slow enough to be observed.[13] There was also a shift in the high frequency limiting real impedance as the electronic resistance, R_e, of the polymer became comparable with, and then greater than, the film's ionic resistance.[9, 13]

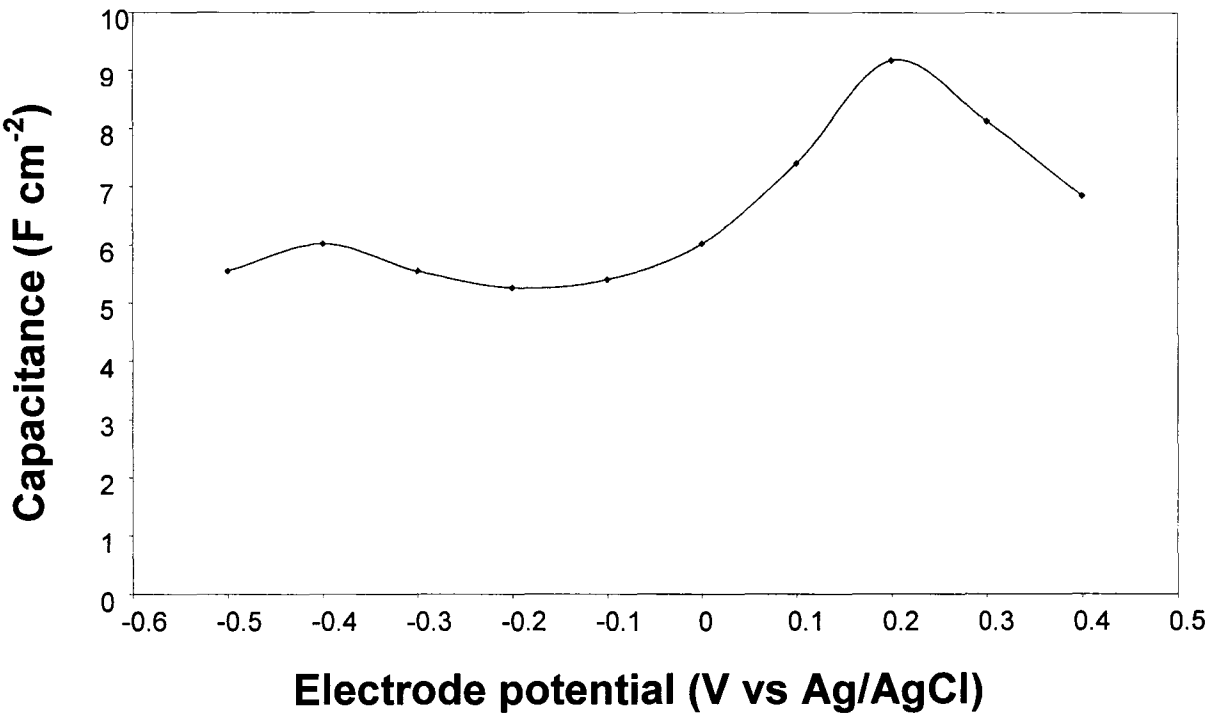

Figure 6.8 Plot of low-frequency capacitances from impedance spectroscopy vs electrode potential for PPY/gel films.

6.3.3 X-Ray Emission Analysis

X-ray emission (electron microprobe) analysis was performed on PPY/gel films to determine the ion contents of the oxidized and reduced states of the film. For this work, films were grown at constant current on 0.071 cm^2 glassy carbon disk electrodes (to reduce background noise) at 0.1 mA for 8 minutes. The cell potential during polymerization remained steady at 0.55 V. The films were dried in air for 2 days. Figure 6.9 shows the energy dispersive X-ray (EDX) spectrum for a film removed from the polymerization solution immediately after the polymerization current was turned off and rinsed well with deionized water. Si and S peaks show that the gel had been incorporated into the film. The small Cl peak is presumably from HCl that had not been fully removed from the gel. Figures 6.10 and 6.11 show the X-ray spectra of PPY/gel films that had been reduced (at –1.0 V) and reoxidized (at +0.1 V), respectively, in 0.05 M KCl (aq) for ca. 1 minute. These spectra clearly show that the electrolyte cation (K^+) is incorporated into the composite upon reduction and mostly expelled upon reoxidation.

The atomic ratio of S:Si obtained from the data in Fig 6.9 (by EDX analysis) was 1:2.8, a control gel without TMOS was therefore prepared to test the sensitivity of the microprobe. This control gel had a S:Si ratio of 1:1. The X-ray spectrum of the PPY/control, shown in Figure 6.12, gave a S:Si atomic ratio of 1.81:1 indicating that the microprobe is ca. 1.81 times more sensitive towards S than Si. This correction has been applied to the normal data to give a measured S:Si atomic ratio of 1:5.07.

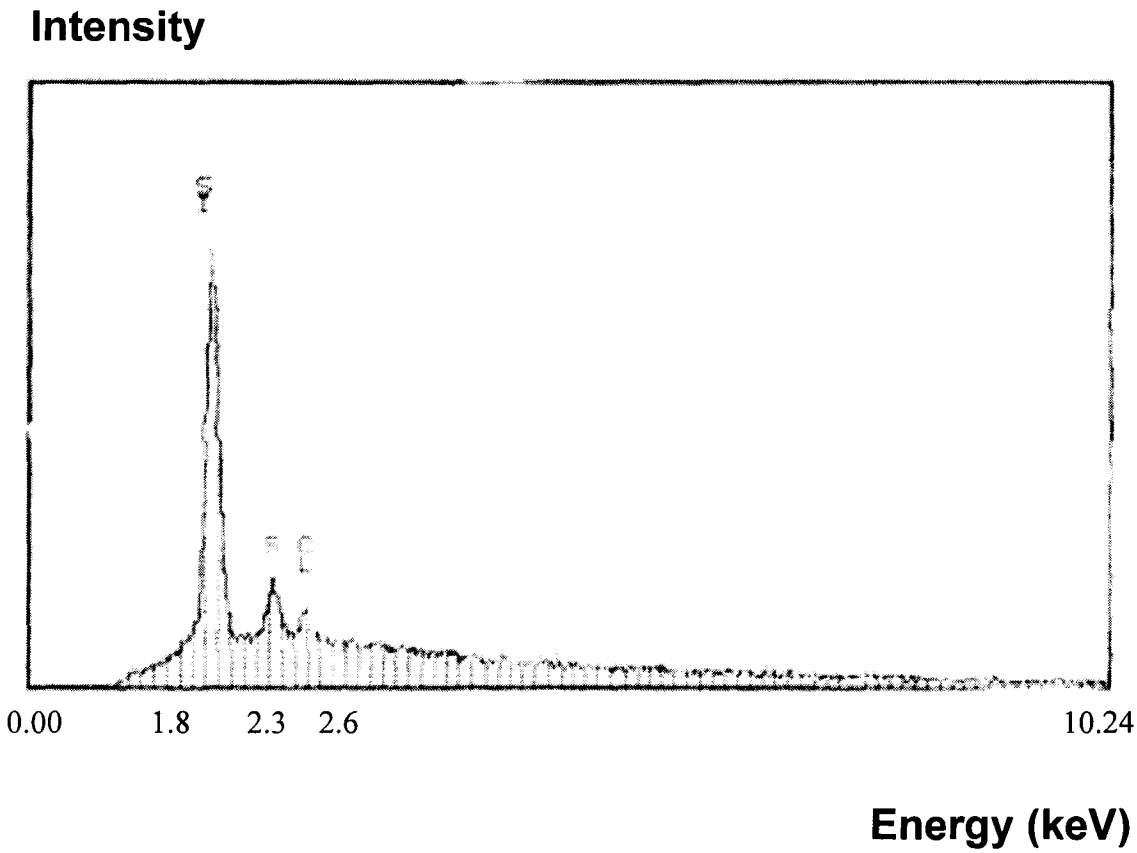

Figure 6.9 X-ray emission spectrum of a 2 μm PPY/gel film deposited onto a glassy carbon disk electrode.

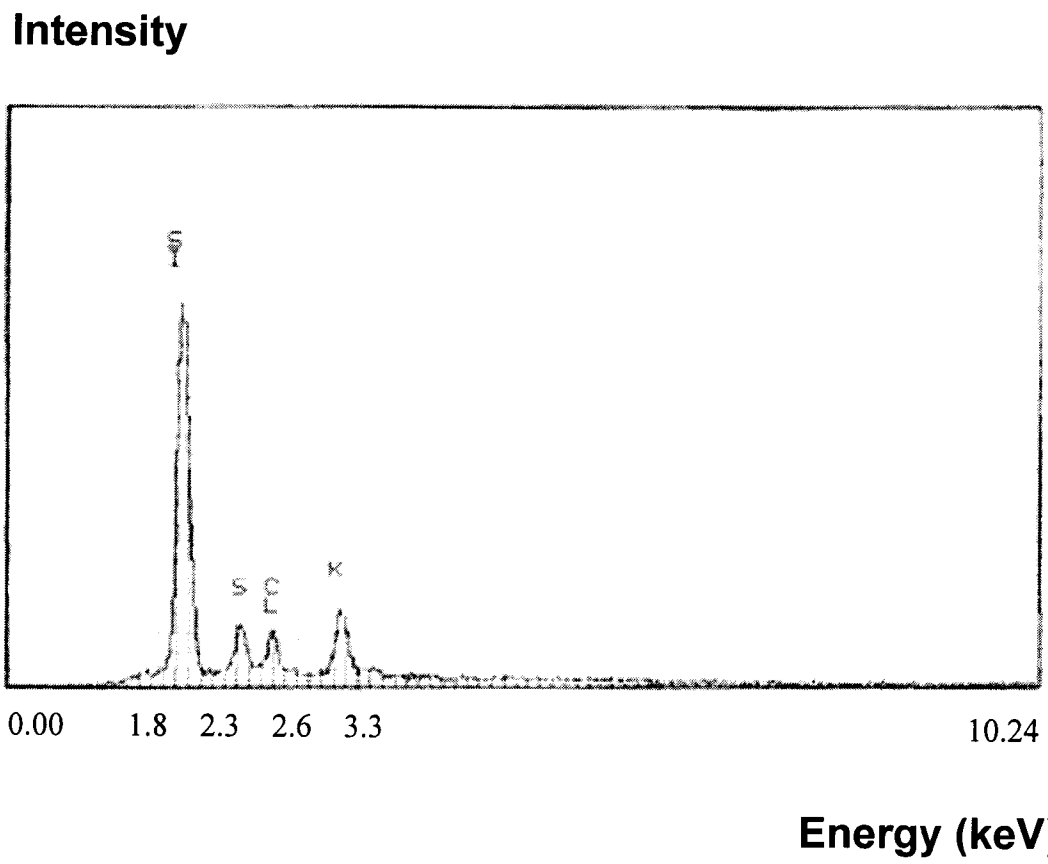

Figure 6.10 X-ray emission spectrum of a 2 μm PPY/gel film deposited onto a glassy carbon disk electrode, following reduction at –1.0 V in 0.05 M KCl $_{(aq)}$.

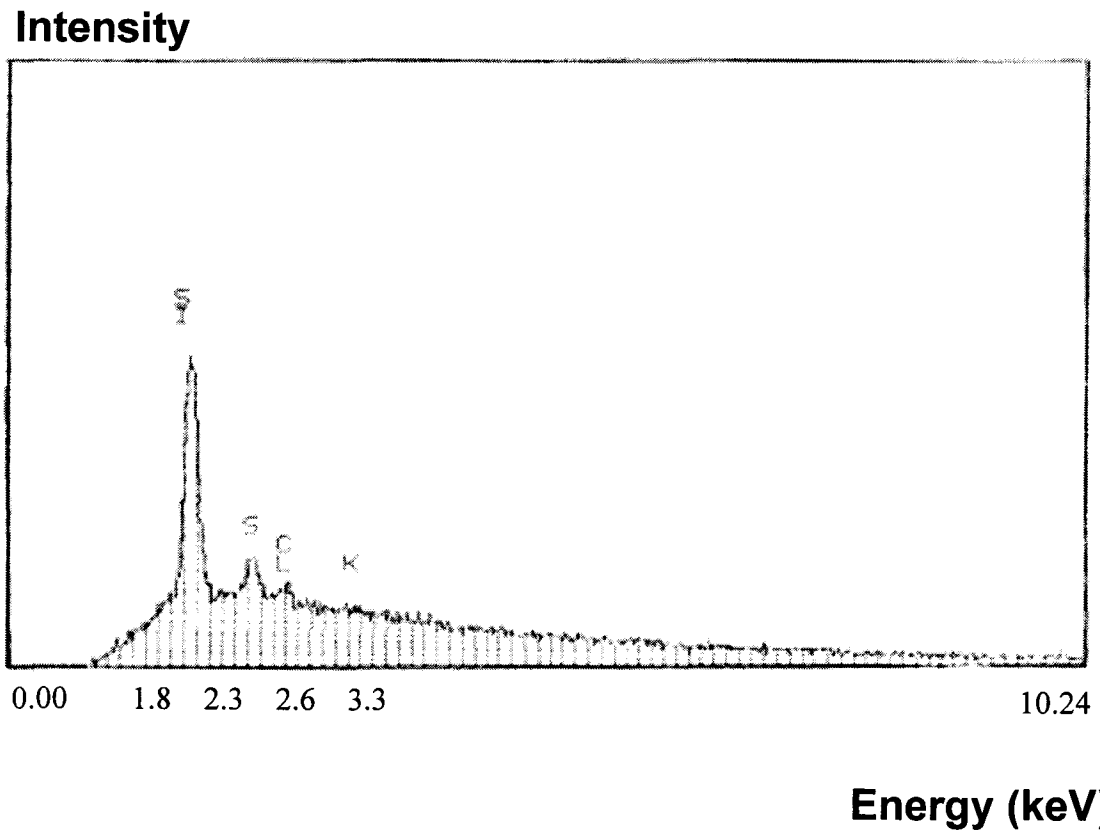

Figure 6.11 X-ray emission spectrum of a 2 μm PPY/gel film deposited on a glassy carbon disk electrode, following reoxidation at 0.1 V in 0.05 M $KCl_{(aq)}$.

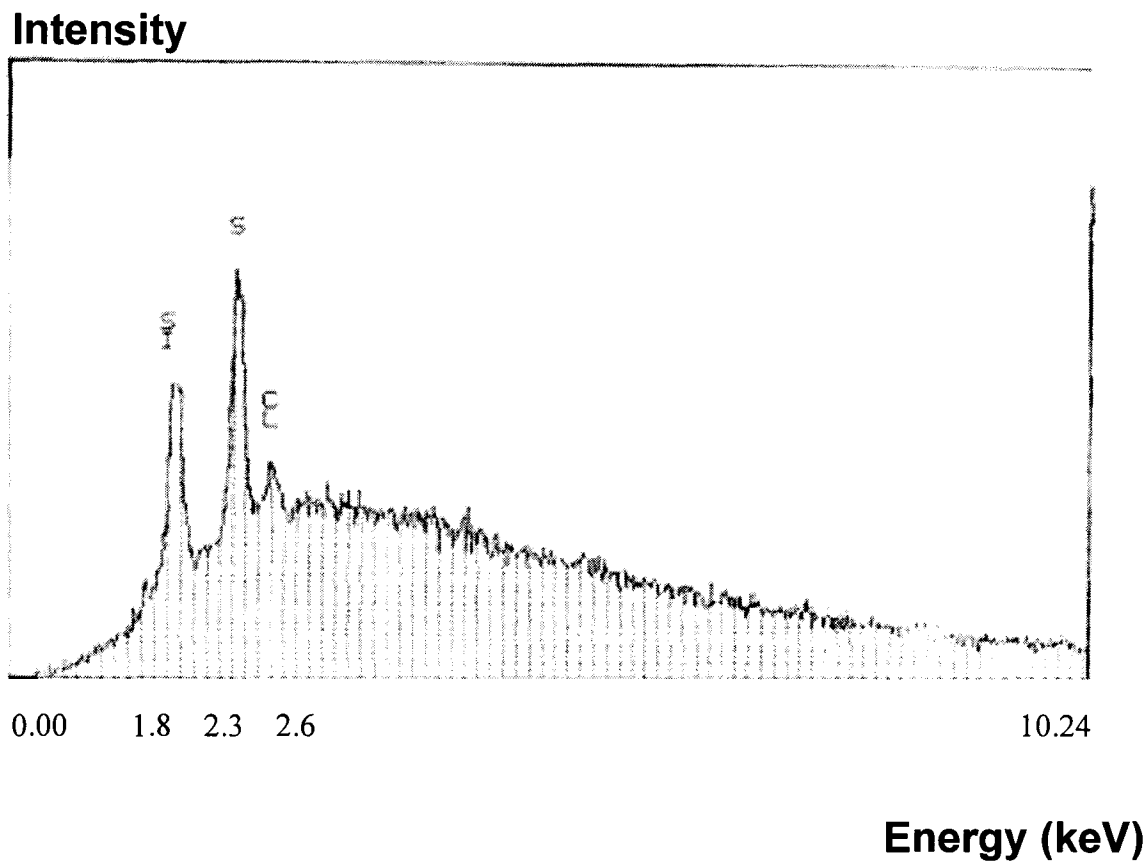

Figure 6.12 X-ray emission spectrum of a 2 μm PPY/control gel film deposited onto a glassy carbon disk electrode.

6.3.4 Discussion

Incorporating conducting polymers into sol-gel networks provides a means of fabricating an electronically conducting network without needing to add carbon to the electrode structure.[14] When designing these materials it is important to maintain a homogenous distribution of the conducting polymer so that good access to the gel silicon oxide phase is achieved.

Understanding the mass/charge transport processes in conducting polymer films is important for application purposes and is the subject of intensive research. The electrochemical switching of a conducting polymer film between the doped (conducting) and undoped (nonconducting) state involves electron and ion transport within the film.[9] Since ion transport is often the slower process, it limits the switching rate of devices based on conducting polymers.

Ion transport in polypyrrole can be controlled by the use of polymeric doping anions. In the case of polypyrrole, the polyanions become trapped within the polypyrrole matrix due to their large size and their entanglement with the polypyrrole chains. This also increases the stability and mechanical strength of the PPY film.[9] The electrochemistry of polypyyrole/polyanion composites generally involves cation transport.[9] Shimidzu et al. report that the transport of cations between the electrolyte solution and the composite is found to be as fast as for polypyrrole doped with chloride.[12] This has led to an increase in the interest of polymerizing pyrrole in polyanion electrolyte solutions.

For silica host sols, it is found that polymers form a continuous conducting network within a polymer/sol gel composite film and the overall porous morphology remains intact. This porous network allows contact with the gel electrolyte that penetrates into the pores, forming parallel ionic and electronic conducting paths.[6]

Chaubey et al have reported that the electro-entrapment of a polymer (polyaniline) into a sol-gel matrix provides environmental stability to films prepared from polymer/sol gel composites.[5]

SEM studies on electrochemically polymerized polypyrrole films in the literature have shown that the surface morphology of such films is greatly influenced by the dopant anion, composition of the electrolytic solution, composition of the sol-gel matrix, applied current density and electrode configuration.[5, 10]

Work on PPY/MoO_3 materials shows that the addition of a conducting polymer to a MoO_3 sol-gel enhanced the sol-gel conductivity,[14] while Oh et al report that there is a decrease in conductivity for PPY films doped with sulphonic acids (e.g. p-toluenesulphonic acid, naphthalenesulphonic acid, dodecylbenzenesulphonic acid, anthraquinone-2-sulphonic acid or polystyrenesulphonic acid) rather than HCl.[11]

It is clear from the cyclic voltammogram, impedance studies and X-ray emission analysis reported in this chapter that reduction and reoxidation of the PPY/gel involves uptake and expulsion of ions within the film. A fully oxidized film expels cations when the potential is decreased from 0.4 V to 0.1 V, at which point cations are inserted into the film upon further reduction. The ionic conductivity of the PPY/gel decreases with increasing potential because oxidation of the polypyrrole in the film causes a decrease in

the concentration of ionic charge carriers.[9] The ionic conductivity of the PPY/gel begins to increase again at -0.1 V as further oxidation involves the insertion of anions into the PPY/gel film. Duffit and Pickup[16] have reported similar results for polypyrrole in acetonitrile. However, this is not always the case for PPY/polyanions films. Previous work in this lab has shown that the reduction and reoxidation of PPY/poly(styrenesulfonate) films involve uptake and expulsion of cations only.[9,13] It is clear that the ion-transport properties of polypyrrole and polypyrrole/composites are largely dependant on the electrolyte and solvent.

6.4 Conclusions

PPY/gel films were prepared by a constant current deposition technique. X-ray emission analysis confirmed the incorporation of the gel into the film.

It is clear from the results presented here that electrolyte uptake by the PPY/gel films play a major role in determining its ion-transport properties. Reduction of the fully oxidized PPY/gel film in 0.05 M KCl (aq) is accompanied first by anion expulsion and then cation insertion, as shown in Figure 6.13. Ion transport in the electrolyte-loaded material appears to be dominated by direct contributions from the electrolyte. This is supported by cyclic voltammetry, impedance spectroscopy and X-Ray emission analyses.

The reasonable linearity of the two sections of the ionic conductivity vs. electrode potential plots (see Fig 6.7) suggests that the two processes (anion expulsion and cation insertion) are quite exclusive.

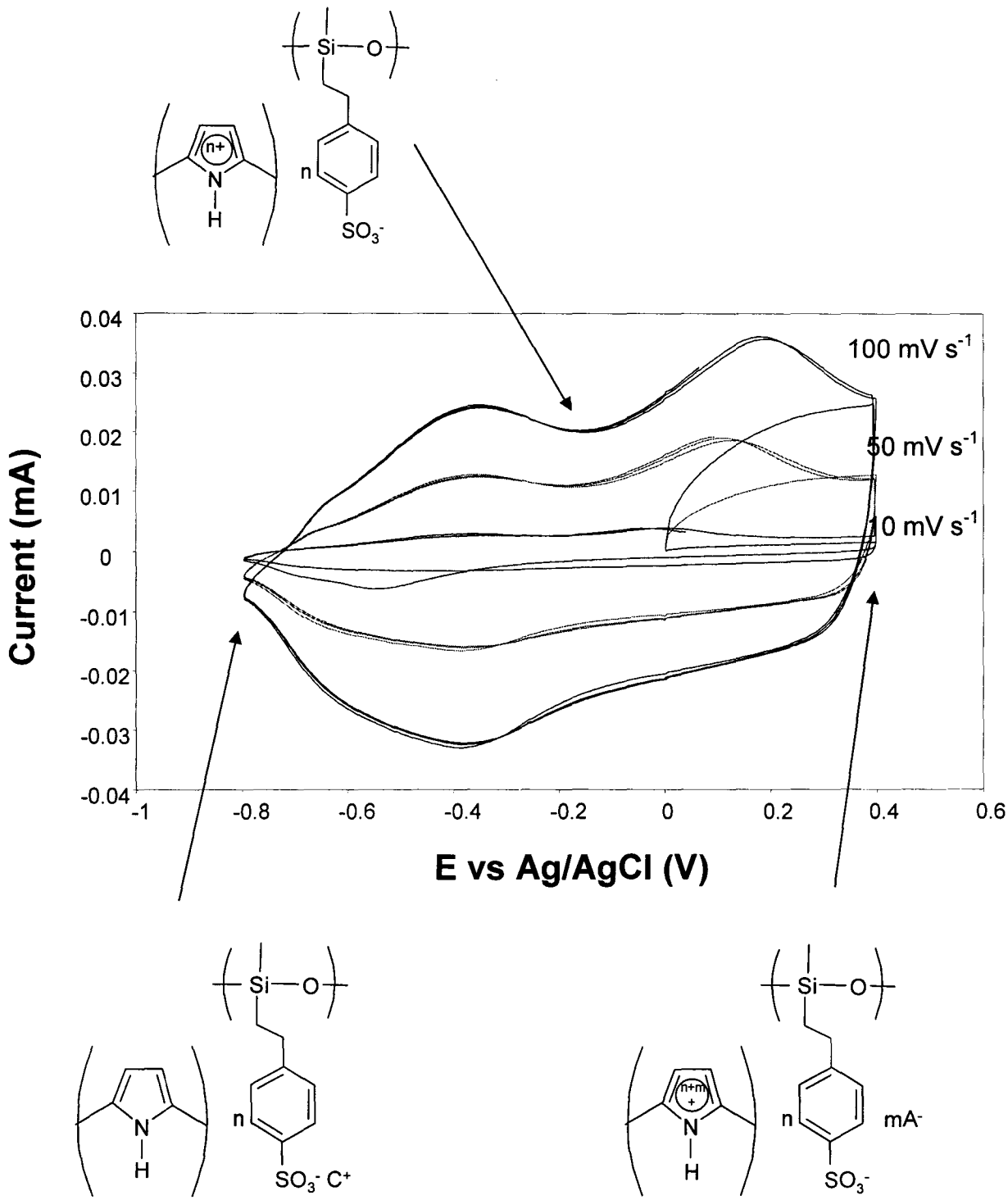

Figure 6.13 CVs of a PPY/gel coated Pt electrode in 0.2 M NaClO4 (aq) showing ion insertion and expulsion.

References

[1]Kanungo, M.; Collinson, M.M. *Langmuir*, **2005**, 21, 827

[2]Watton, S.P.; Taylor, C.M.; Kloster, G.M.; Bowman, S.C. Coordination Complexes in Sol-Gel Silica Materials in *Progress in Inorganic Chemistry* Vol. 51, ed. Kenneth D. Karlin, **2003**, 333-420

[3]Walcarius, A.; Delacote, C. *Chem. Mater.*, **2003**, 15, 4181

[4]Walcarius, A.; Delacote, C.; Sayen, S. *Electrochimica Acta*, **2004**, 49, 3775

[5]Chaubey, A.; Pande, K.K.; Malhotra, B.D. *Analytical Sciences*, **2003**, 19, 1477

[6]Neves, S.; Fonseca, C.P. *J. Braz. Chem. Soc.*, **2004**, 15, 395-399

[7]Ballarin, B.; Facchini, M.; Pozzo, L.D.; Martini, C. *Electrochemistry Communications*, **2003**, 5, 625

[8]McCaughey, B.; Costello, C.; Wang, D.; Hampsey, J.E.; Yang, Z.; Li, C.; Brinker, C.J.; Lu, Y. *Adv. Mater.*, **2003**, 15, 1266

[9]Ren, X.; Pickup, P.G. *The Journal of Physical Chemistry*, **1993**, 97, 5356

[10]Sadki, S.; Schottland, P.; Brodie, N.; Sabouraud, G. Chem. Soc. Rev., **2000**, 29, 283

[11]Oh, K.W.; Park, H.J.; Kim, S.H. *Journal of Applied Polymer Science*, **2004**, 91, 3659

[12]Shimidzu, T.; Ohtani, A.; Iyoda, T.; Honda, K. *J. Electroanal. Chem.*, **1987**, 224, 123-135

[13]Ren, X.; Pickup, P.G. *Journal of Electroanalytical Chemistry*, **1997**, 420, 251-257

[14]Rolison, D. R.; Dunn, B. *J. Mater. Chem.*, **2001**, 11, 963-980.

[15]Duffitt, G.L.; Pickup, P.G. J. Phys. Chem., **1991**, 95, 9634

[16]Duffitt, G.L.; Pickup, P.G. J. Chem. Soc. Faraday Trans., **1992**, 88, 1417

Chapter 7:

Modification of a Proton Exchange Membrane Fuel Cell Catalyst With a Sulphonated Silica Sol-Gel

7.1 Introduction to Fuel Cells

The increasing demands of, and declining reserves of, petroleum oil as well as the rising concerns about the environment and global warming have garnered attention to the possibility of making more efficient use of natural gas and hydrogen which are presently being underutilized. Fuel cells are widely viewed as a promising alternate source of low-cost and low-emission power generation as long as the energy consumption is sustainable and environmentally friendly.[1] Using fuel cells as electrical sources, hydrogen may be commonly used as fuel.

Fuel cells are electrochemical devices with continuous supplies of fuel and oxidant used to produce electricity.[1] This electrical energy is generated by the conversion of chemical energy generated at the anode (where oxidation occurs) and cathode (where reduction occurs) via redox reactions. The anode and cathode are separated by an electrolyte that keeps the cell from short circuiting and also allows ions to flow from one compartment to the other. Fuel cells are classified as "open systems" because the active masses undergoing the redox reaction are delivered from outside of the cell, either from the environment (e.g. air) or from a tank (e.g. hydrogen).[1] A schematic of a hydrogen proton exchange membrane fuel cell (PEMFC) is shown in Fig 7.1.

The basic reactions of a hydrogen fuel cell are[1]

Anode: $H_2 \rightarrow 2H^+ + 2e^-$ Eq. 7.1

Cathode: $O_2 + 2H^+ + 2e^- \rightarrow H_2O_2$ Eq. 7.2

$H_2O_2 + 2H^+ + 2e^- \rightarrow 2H_2O$ Eq. 7.3

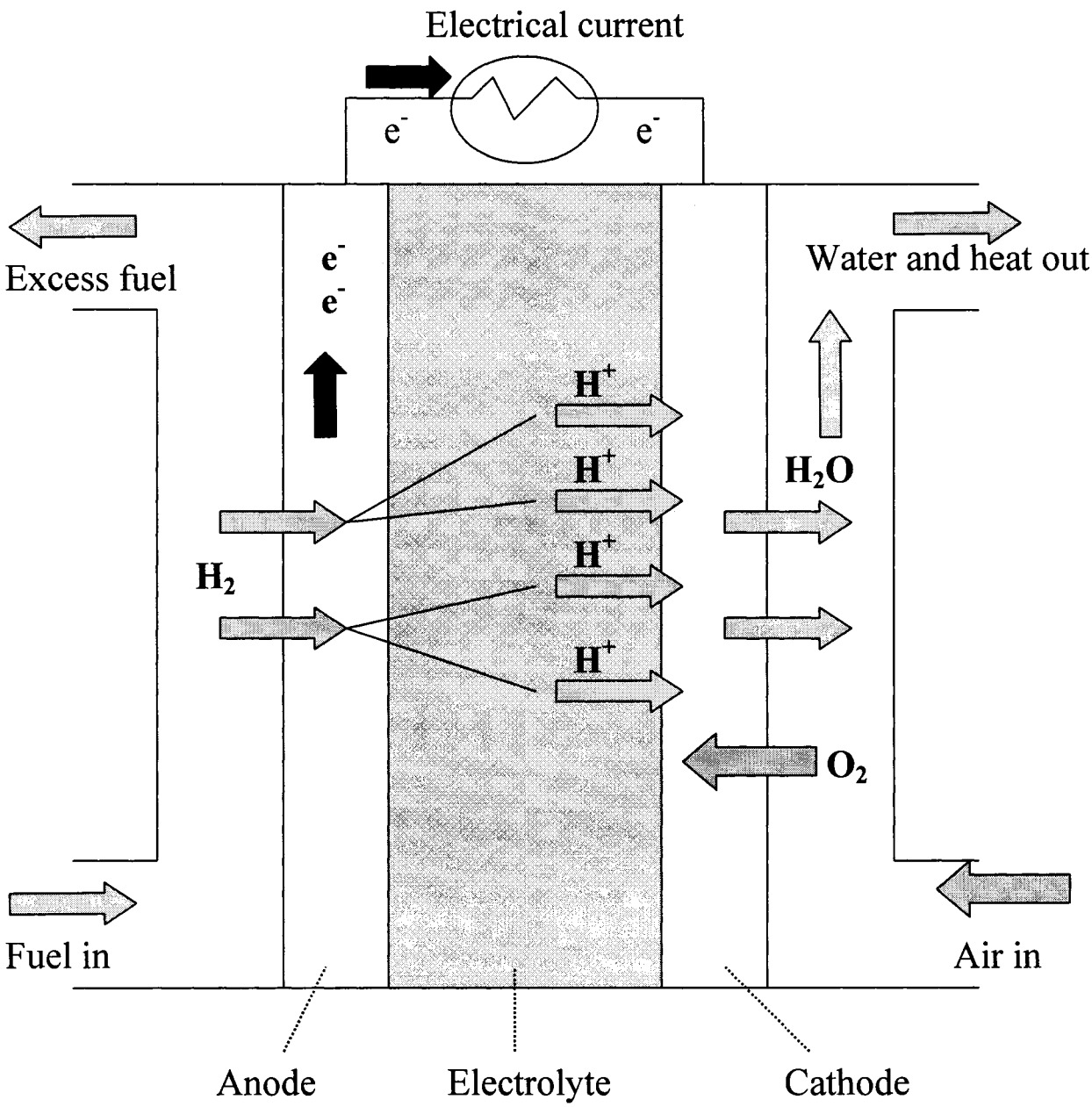

Figure 7.1 Diagram of a hydrogen proton exchange membrane fuel cell.

Overall: $O_2 + 4H^+ + 4e^- \rightarrow 2H_2O$ Eq. 7.4

Practical electrodes such as those found in fuel cells are composite structures containing an electrocatalyst and other components that optimize the performance of the cell.[2] These additional materials include conducting carbon black, polymeric binders and additives that improve proton conductivity.[1,2] Typically, these electrodes are highly porous with a complex surface extending throughout the electrode to provide larger surface areas for reactions.[1] Currently Nafion®, a perfluorosulphonic acid membrane developed by E.I. DuPont de Nemours & Co, is the best performing commercially available electrolyte for fuel cells.[3] Nafion, whose structure is shown in Fig 7.2, has good mechanical strength, chemical and thermal stability and is water insoluble.[3] Usually, Nafion is mixed with the catalyst[4] because of its proton-conducting nature. However, the high cost of Nafion, its high methanol permeability and its limited operational temperature impose physical limitations on its use for commercial fuel cells.[3] Platinum or platinum alloys are used as catalysts to speed the reactions on both electrodes in low-temperature fuel cells.[1]

Extensive research has been devoted to developing newer and cheaper materials for fuel cell usage with a major goal being to replace Nafion in the catalyst layer with another cheaper, highly ionic conductive binder and to reduce the catalyst loading in order to reduce manufacturing costs. To this end, Nishikawa et al. prepared gas diffusion electrodes for PEMFC using novel organic/inorganic hybrid electrolytes.[5] They report that the utilization of the Pt electrocatalyst was enhanced by using a nanohybrid material as the binding ionomer.

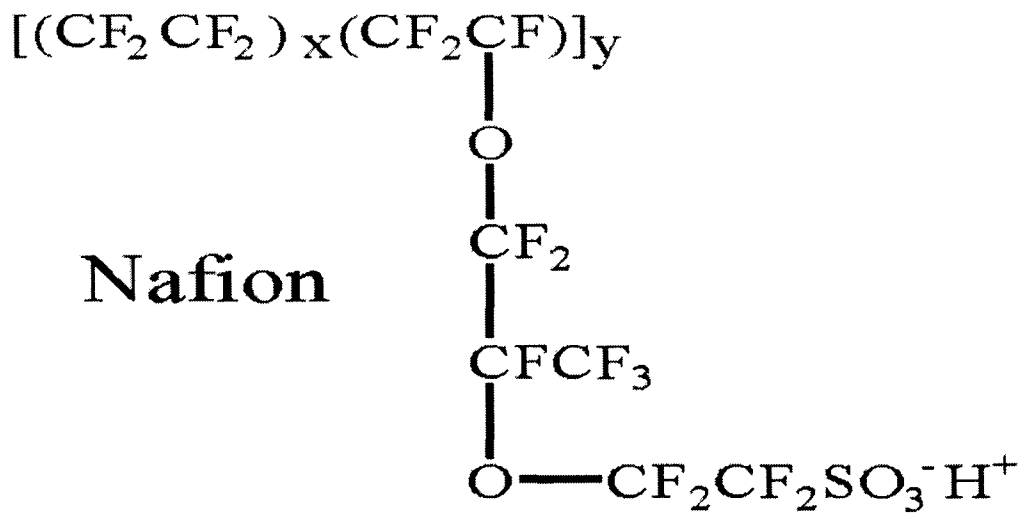

Figure 7.2 The structure of Nafion®. The values of x and y can be varied to create materials with varying equivalent weights (EW). 1100 EW is the most common.

Nafion is a registered trademark of E.I. DuPont de Nemours & Co.

Another problem associated with carbon supported electrodes in fuel cells is the self-agglomeration of the carbon particles within the electrode structures which limits the approach of fuel and oxidant to the catalyst active sites.[6] Anderson et al. reported that using a silica sol as a "nanoglue" to prepare composite catalysts circumvents this problem because the silica sol infuses into the carbon "bed" and breaks up the agglomerates which then freeze into place as the silica sol gels.[6] A diagram of a Pt/C-SiO_2 composite aerogel catalyst is shown in Fig 7.3.

In this work, sulphonated silica sol-gels were investigated to prepare highly proton conducting binders. When mixed with 20% Pt/C black, these materials display all of the necessary properties to make practical fuel cell electrodes.

The composite nature of such electrodes requires that the aerogel be durable in the face of grinding or pressing and that it exhibit some stability to heating. Studies done by Swider et al. on RuO_2-TiO_2 aerogels[7] and Richards et al. on MgO aerogels[8] show that both gels retained their large surface area when pressed. Rolison and Dunn propose that because the feature size of the solid phase in aerogels is on the order of 10 nm, it is reasonable to assume that such fine domains are not damaged during moderate mechanical treatments.[2]

The Ragone plot shown in Fig 7.4 compares power and energy capabilities between fuel cells, batteries and combustion engines. This plot clearly shows that fuel cells are considered to be high-energy systems but are not as powerful as combustion engines.[1] Therefore substantial improvements in fuel cell design and performance is needed before they can compete with internal combustion engines. Since fuel cells are

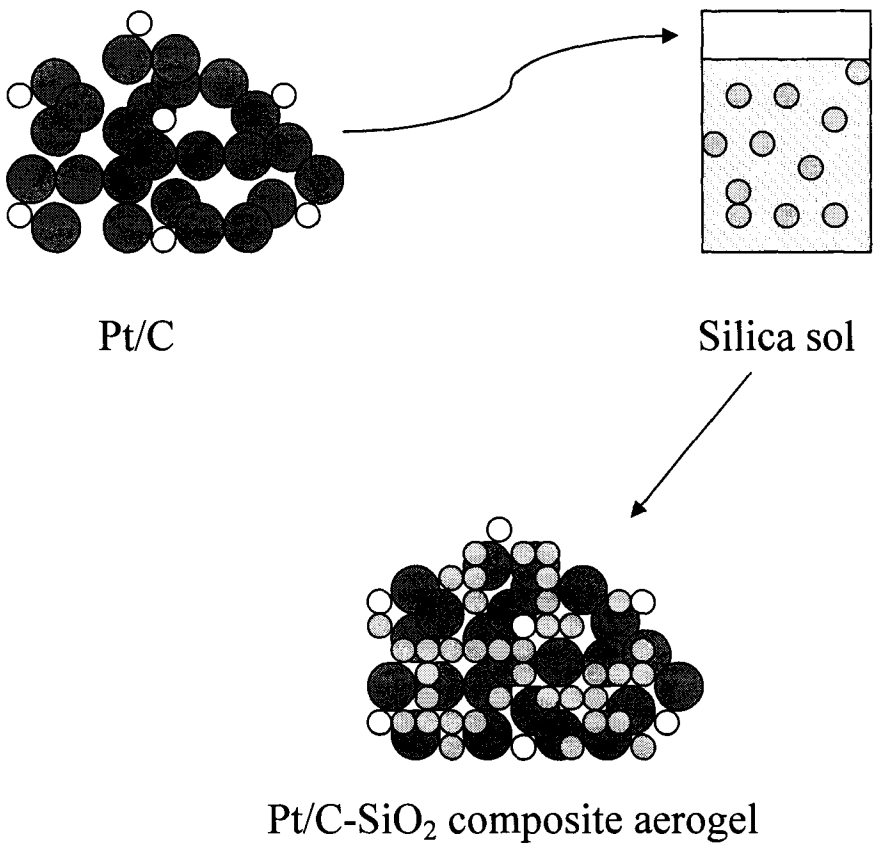

Figure 7.3 Diagram showing the synthesis of a composite gel comprising a Pt/C guest. In this protocol the wet composite gel is dried by supercritical extraction of CO_2 to produce an aerogel.

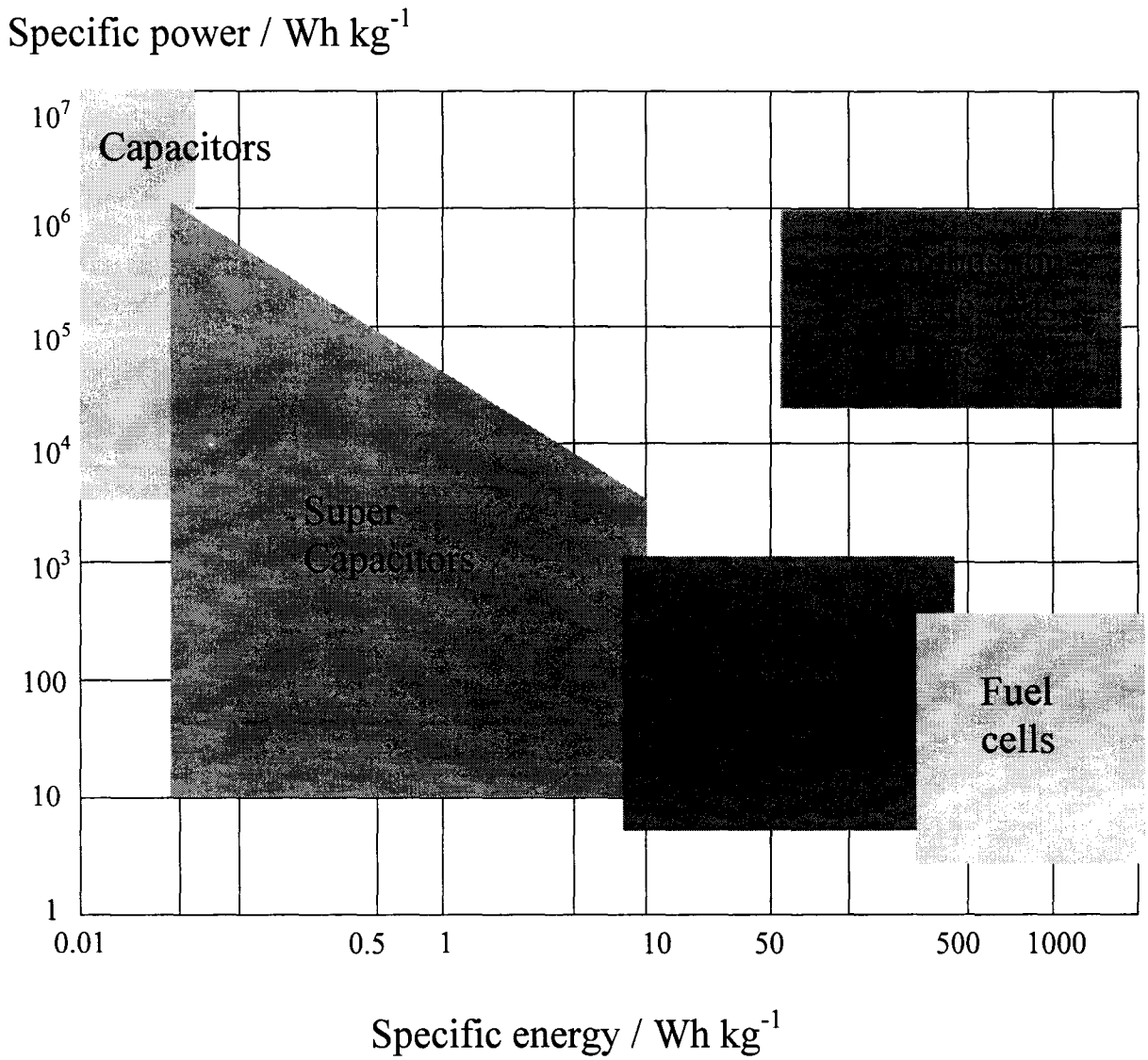

Figure 7.4 Simplified Ragone plot of the energy storage domains for various electrochemical energy conversion systems compared to an internal combustion engine. See Winter and Brodd[1] for original plot.

not subject to the Carnot cycle limitations,[1] they may operate with higher efficiencies than combustion engines.[1] Inert parts of the system, internal resistances within the electrodes and electrolyte and between other fuel cell components and limited utilization of the active catalysts and fuels still limit the practical energy conversion to well below the theoretical value.[1]

While fuel cells were originally intended to replace combustion power sources and engines, they are now also being developed to replace batteries to power appliances such as cellular telephones and notebook computers because the chemical energy stored in hydrogen and small organic compounds, such as methanol, is much greater than that found in common batteries.[1] Fuel cells are also appearing as stationary power sources for central and dispersed power stations.[1] As well, some companies, buildings and hospitals are switching to fuel cell power to avoid power outages experienced in utility supply lines.[1] In fact, fuel cells first established their usefulness in space applications with the Gemini and Apollo space programs[1] and an updated version of an alkaline fuel cell is still in use to provide electrical power for shuttle missions.

There is extensive research being conducted into fuel cells and much of the technology is reaching maturity.[1] Fuel cells offer very clean power generation, produce less greenhouse emissions, are more efficient in energy conversion than gasoline or utility thermal power plants and are quiet to operate.[1] However, the economics of fuel cells are still problematic and the commercial success of fuel cells will depend on reducing the manufacturing costs to a competitive level. In large part, the ability to do so will result on the ability to reduce the catalyst costs.

7.2 Experimental

7.2.1 Preparation of Nafion + Pt/C Paste Electrodes

Vulcan carbon, a highly disordered graphite-like carbon black commonly used in fuel cells and batteries[2] was chosen as the electrically conductive guest in preparing the electrode pastes. Nafion, a fluorinated polymer with SO_3^- terminated side-chains, was chosen as the ionically conductive substrate for comparison with the gel.

Pastes were prepared by stirring ca. 0.09 g of Nafion (5 wt % solution) with ca. 0.01 g of 20 % Pt on Vulcan C black. The thick paste was then spread evenly onto one side of a 5 cm^2 piece of Toray carbon fiber paper as the gas diffusion layer to provide a loading of 0.9 $mg \cdot cm^{-2}$ Nafion and 0.4 $mg \cdot cm^{-2}$ Pt. The electrode was allowed to dry in open air overnight. Following this, a membrane electrode assembly (MEA) was prepared by hot pressing (200 $kg \cdot cm^{-2}$ for 120 seconds at 130°C) a 1 cm^2 or 5 cm^2 4 mg Pt black$\cdot cm^{-2}$ anode and a similar sized Nafion + Pt/C cathode onto either side of a Nafion 115 membrane.

7.2.2 Preparation of Sulphonated Silica Sol-Gel + Pt/C Paste Electrodes

Sulphonated silica sol-gel (prepared with SiO_2:SO_3^- mole ratio of 9.3:1, see Section 3.2.1) + Pt/C paste electrodes with a sol (freshly prepared, still liquid) loading of 0.6 $mg \cdot cm^{-2}$ were prepared as described above for the Nafion electrodes, except that the sulphonated silica sol replaced the Nafion as the ionic conducting material. No pressing was used to prepare the MEA, as the effects of hot pressing the sol are unknown. Cold pressing did not adequately bond the paste to the Nafion 115 membrane. Rather, the

MEA was assembled inside the fuel cell using the mechanical pressing applied when the fuel cell was fully assembled.

7.2.3 Evaluating Fuel Cell Performance

Electrochemical experiments were performed using impedance spectroscopy and cyclic voltammetry. All experiments were collected using O_2 (g) at the working electrode, unless otherwise stated. The hydrogen electrode served as both the reference and the counter electrode. All gases were humidified at room temperature prior to entering the cell so as not to dry out the membrane. Gas flow rates were adjusted individually to provide maximum current density. The uncompensated resistance was determined from the high frequency intercept of a Nyquist plot. Before measurements were taken, the fuel cell was operated at a cell voltage of 0.5 V until a steady current was obtained.

The performance of a PEMFC is typically evaluated by obtaining a polarization curve where cell voltage is plotted against current density.[1,2] A higher cell potential at a given current density indicates better fuel cell performance. Figure 7.5 shows a typical polarization curve for a fuel cell. Also indicated on this figure are regions where kinetic, ohmic and mass transport losses occur. Impedance spectroscopy is also a very powerful tool in fuel cell studies because it has the ability to separate the individual contributions of the interfacial charge transfer resistance, mass transport resistances in the catalyst layer and backing diffusion layer, and ion and electron transport resistances.[4] Charge transfer

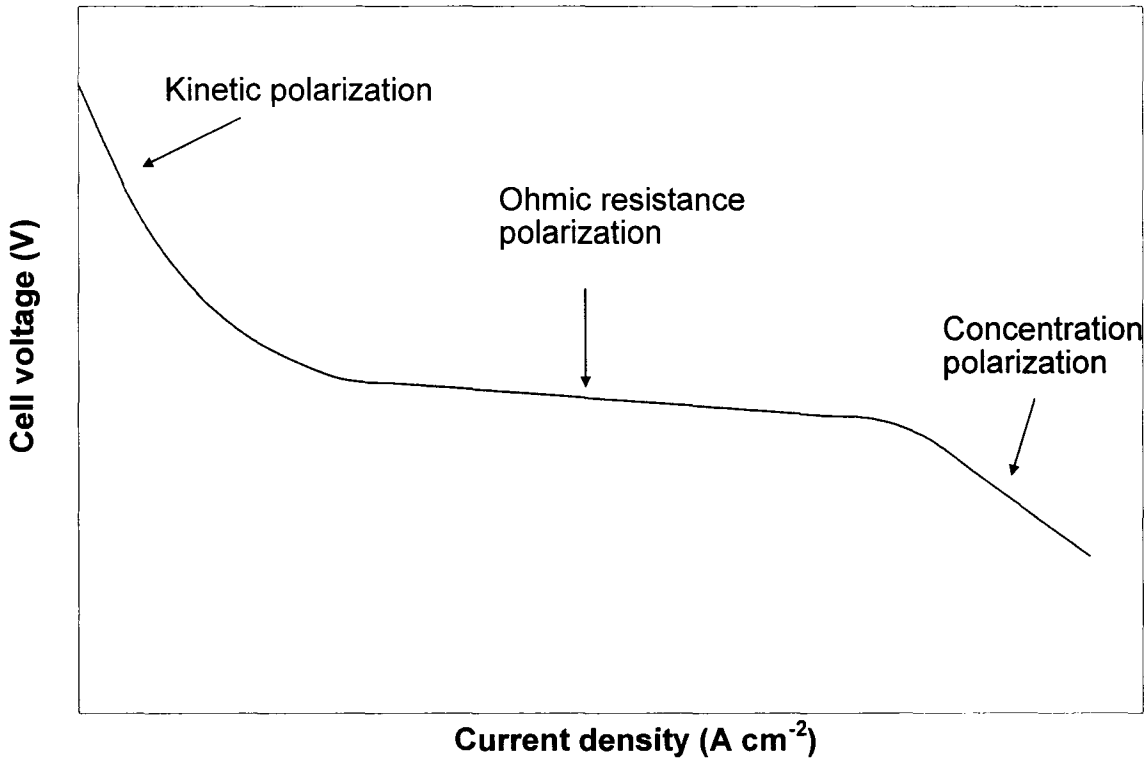

Figure 7.5 A schematic polarization curve for a fuel cell

resistance is reflected in the high frequency region of an impedance spectrum whereas mass transport resistance is found in the medium to low frequency range.[4]

7.3 Results and Discussion

7.3.1 Hydrogen - Oxygen Fuel Cell

Oxygen reduction at the cathode of a proton exchange membrane fuel cell (PEMFC) requires both electron and proton transport, as discussed in Section 7.1. The carbon support provides the necessary electron transport while Nafion (or the sulphonated silica sol) incorporated into the catalyst layer transports protons to the active Pt sites.[4] High performance for oxygen reduction is dependant on several factors: good accessibility of oxygen to the active sites of the cathode, fast interfacial electron transfer kinetics, fast electron transport through the hydrophobic carbon support, and ease of proton transport through the hydrophilic Nafion membrane.[4] Extensive research has been conducted to optimize the structure and composition of cathodes for good oxygen accessibility and facile proton transport in the catalyst layer. Studies focused on the effects of Nafion loading on the performance of cathodes performed by Li show that the optimum Nafion content for best cathode performance is approximately 0.9 $mg \cdot cm^{-2}$ (30 mass percent).[4] The ionic conductivity in the catalyst layer suffers and the performance of the PEMFC will be poor if the Nafion content is too low. However, too much Nafion will close the percolation path for electron transfer between catalyst particles resulting in poor electronic conduction, and will also hinder gas access to the reactive sites.[4] Due to the high cost associated with incorporating Nafion into the catalyst layer of a PEMFC,

this work reports on using a sulphonated silica sol proton conducting material in the catalyst layer.

Fig 7.6 show the cyclic voltammograms obtained under an inert nitrogen atmosphere for the as prepared Nation + Pt/C paste cathode and sol + Pt/C paste cathode at 20 $mV \cdot s^{-1}$ in the potential range of 0 V to 1.2 V for a home-made 1cm^2 cell. The curves are very similar to those of Pt catalysts supported on carbon and demonstrated that the Pt in the Nafion + Pt/C and Sol + Pt/C composites remained accessible to external reagents such as H^+/H_2O.[6] The area under the H adsorption peaks in the cyclic voltammograms can be used to determine the amount of active Pt surface sites.[6] As evident in Fig 7.6 the amount of active Pt surface sites is slightly larger for the Sol + Pt/C cathode than the Nafion + Pt/C cathode.

Figure 7.7 shows the Nyquist response for both the Nafion-based and sol-based cathodes in a commercial 5 cm^2 cell with oxygen fed to the cathode compartment. Within experimental error, the resistances for both cathodes were found to be the same. These resistances corresponded very well with values obtained historically with this cell. From these Nyquist plots the ionic resistances of the cathodes can be determined by subtracting the R_{high} intercept from the R_{low} value (see Section 1.7). Figure 7.8 shows capacitance plots for the same cathodes in a 1 cm^2 cell under inert nitrogen. Capacitance plots are included because they are often more informative than simple Nyquist plots since the limiting capacitance, obtained from the low-frequency plateau, is proportional to the electrochemically accessible surface area.[10] It is obvious from Fig 7.8 that the

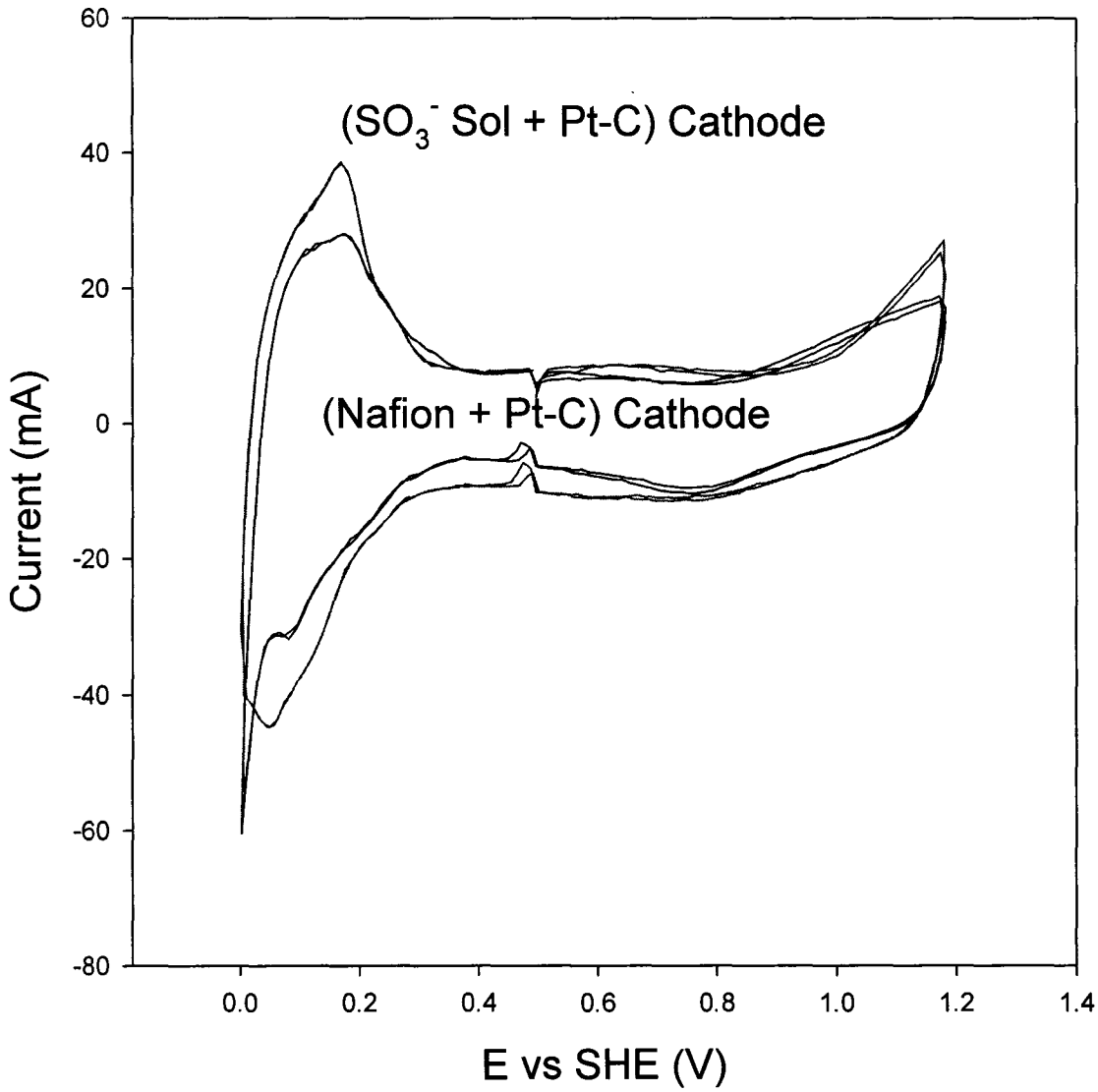

Figure 7.6 Cyclic voltammograms obtained for (Sol + Pt/C) and (Nafion + Pt/C) composite cathodes under an inert N_2 atmosphere.

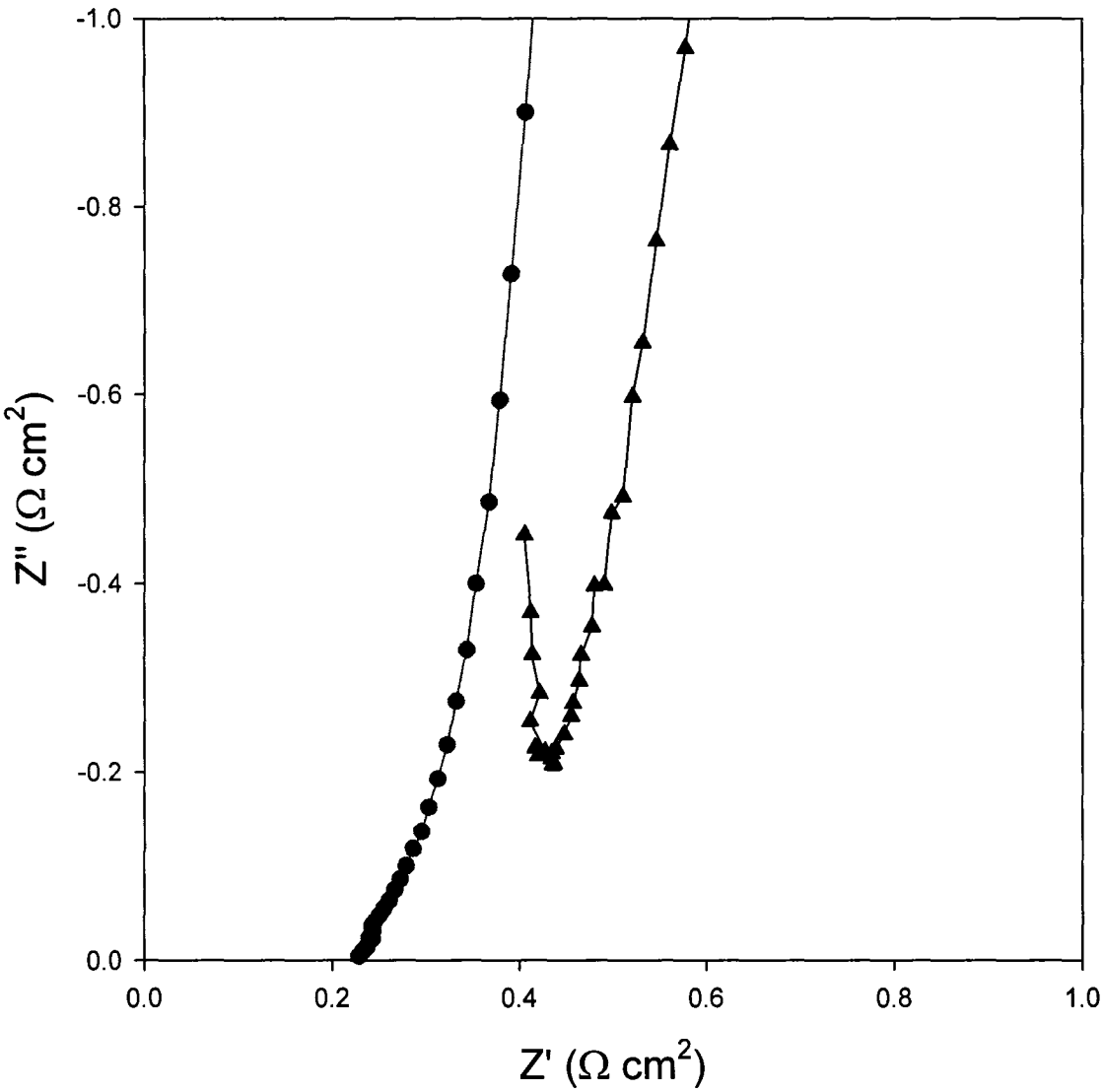

Figure 7.7 Nyquist plots comparing impedances displayed by SO_3^- sol + Pt/C (•) and Nafion + Pt/C (▲) composite cathodes.

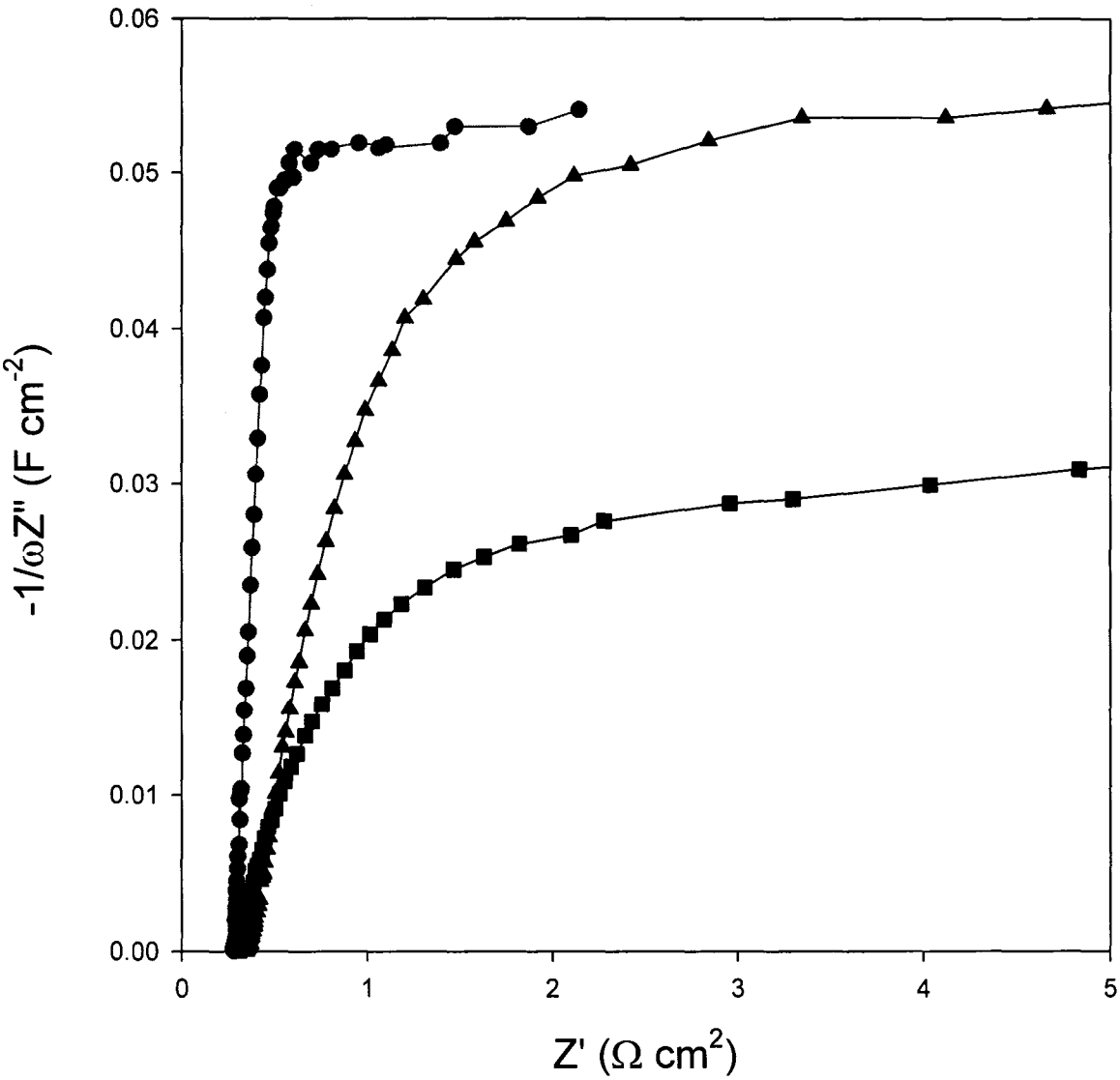

Figure 7.8 Capacitance plots for SO_3^- sol + Pt/C (•) and Nafion + Pt/C (▲) composite cathodes compared to a 4 mg Pt·cm^{-2} cathode that has no proton conductor (■).

capacitances for both composite cathodes were similar and were significantly larger than that of a 4 mg $Pt \cdot cm^{-2}$ cathode containing no proton conductor that was donated by Ballard Power Systems

Initially, the sulphonated silica sol-gel based electrodes showed very poor performance in the hydrogen-oxygen fuel cell and currents larger than ca. 10 mA were not achievable when the cell was run at a constant potential of 0.5 V. One possible reason may be poor water management in the sol-gel based cathode. Similar results were obtained by Easton et al when using a sulphonated poly (ether ether ketone) as the proton-conducting medium within the electrocatalytic layer of a fuel cell gas diffusion electrode.[10] Their results showed greatly enhanced fuel cell performance when polytetrafluoroethylene (PTFE) was incorporated into the catalyst layer. Therefore a similar approach was adopted in this work.

Pastes containing 10 wt % PTFE (relative to Pt/C) were prepared by thoroughly mixing 20% Pt/C with a 15 % PTFE suspension (in water; Aldrich) and spreading the paste onto the CFP. The electrodes were sintered by heating at 110°C, 280°C and 360°C, each for 30 minutes. After cooling to room temperature, the sulphonated silica sol was brush painted onto the electrode surface so the final sol content was 12% by dry mass. Membrane electrode assemblies (MEAs) were prepared as described previously. Treating the Sol + Pt/C composite with PTFE negatively affected the resistance of the cathode, as shown in Fig 7.9, but greatly increased the fuel cell performance as seen in Fig 7.10. While there was a marked improvement in fuel cell performance seen when incorporating PTFE into the catalyst, the cell performance was still not able to compete

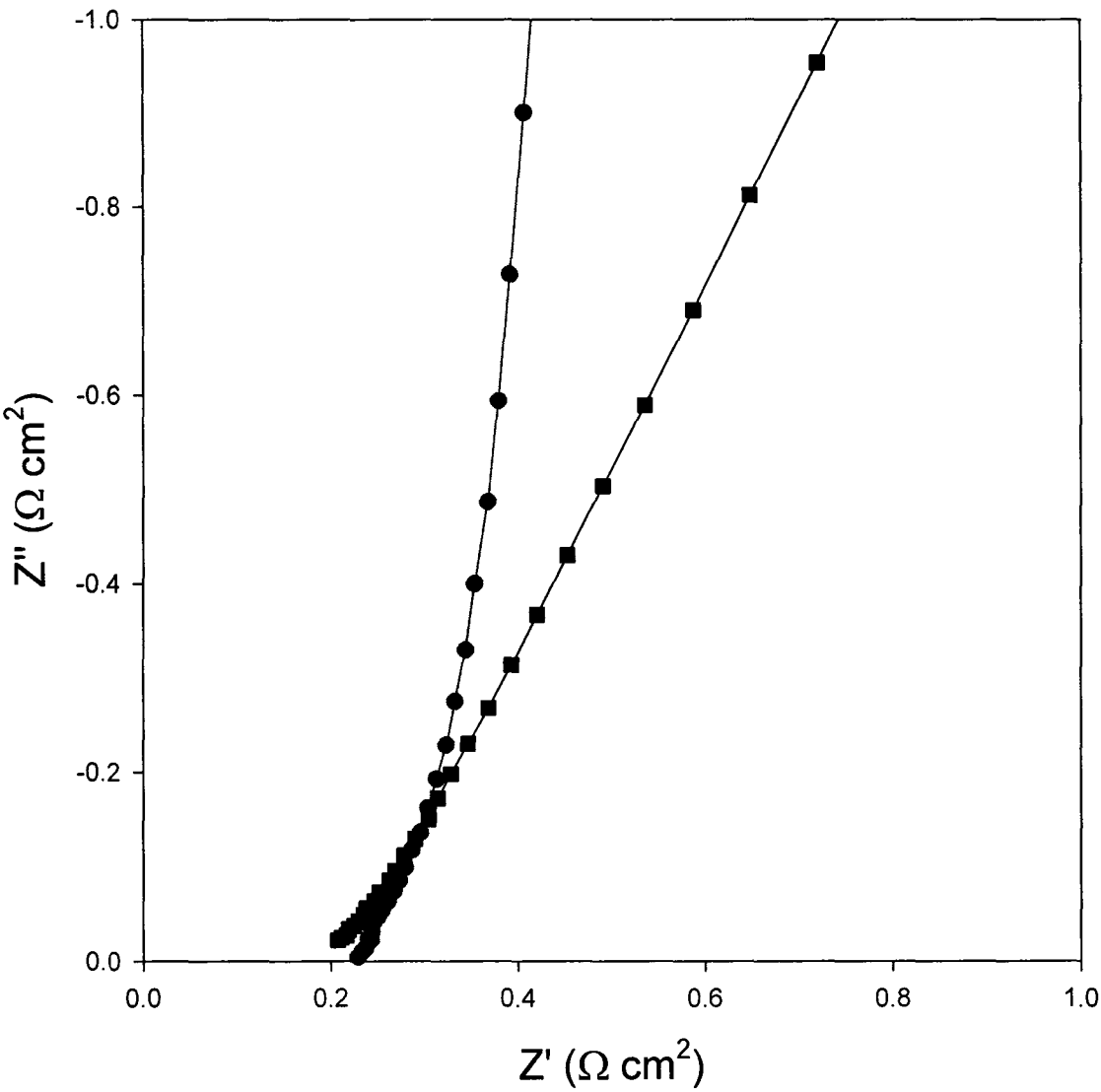

Figure 7.9 Nyquist plots showing the effect on resistance when PTFE (■) is incorporated into the SO_3^- sol + Pt/C (•) composite catalyst.

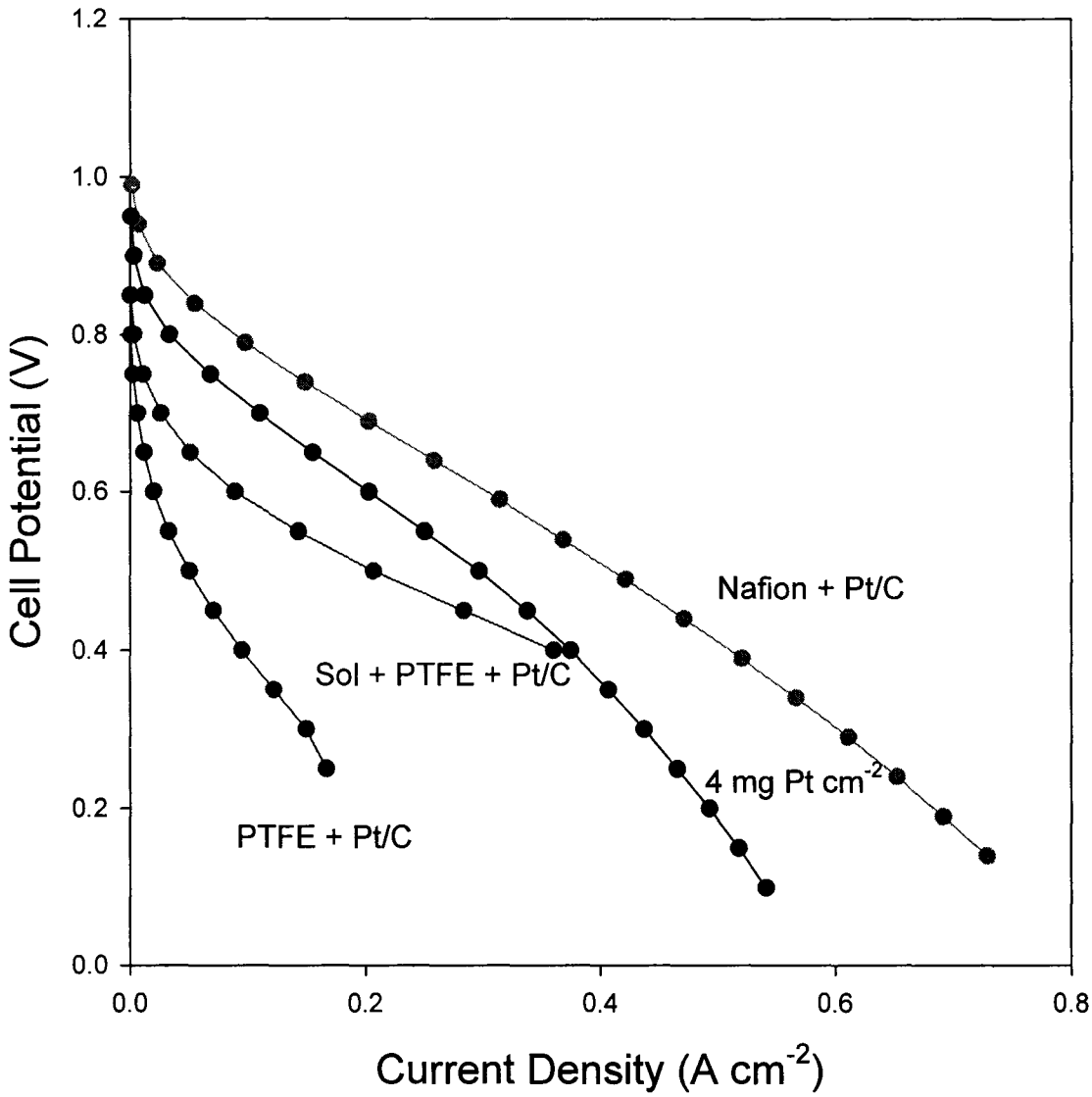

Figure 7.10 Fuel cell performances for a commercial 5 cm^2 cell with H_2 flowing to the anode and O_2 flowing to the cathode.

with the performance obtained using a Nafion + Pt/C cathode. Similar results were reported by Nishikawa et al. for a different Si + Pt/C composite catalyst.[5] However they were able to further improve their performance by adding uncatalyzed carbon black to the cathode catalyst layer.

Nafion-based gas diffusion electrodes (GDEs) appear to benefit from the hydrophobic PTFE backbone and hydrophilic sulphonic acid functional groups that aids in pore formation and water management.[10] Kreuer reports on the hydrophobic and hydrophilic duality of perflurosulphonic acids and how, in the presence of water, hydrophobic/hydrophilic nano-separation occurs.[11] Kreuer states that the sulphonic acid groups aggregate together to form a hydrophilic region where proton charge carriers can form upon hydration by dissociation of the acidic functional groups. The hydrophobic domains provide stability to the polymer and prevent it from dissolving in water. Because the sulphonated silica sol-gel lacks this backbone it is much less hydrophobic. This may lead to a lesser degree of hydrophobic/hydrophilic phase separation, which results in flooding of the sol-gel based electrode.

PTFE offers several other benefits to a GDE. Firstly, the presence of the PTFE helps to create a more porous structure in the catalyst layer, which greatly enhances both water management and mass transport in the layer.[10,11] Secondly, the presence of PTFE increases the oxygen permeability within the electrode since it is well known that oxygen is more permeable in PTFE than in water.[10] Therefore, a GDE that contains both the sulphonated silica sol and PTFE benefits from both the increased proton conductivity from the sol and increased oxygen solubility as well as a more porous structure from the

PTFE. This leads to a better performing GDE. The addition of PTFE may also promote better binding of the carbon particles within the catalyst layer, which reduces the electronic resistance.[10] Interfacial resistance may also be decreased in a fuel cell by adding PTFE to the GDE by enhancing the binding of the GDE to the Nafion membrane.[11]

7.3.2 Methanol Fuel Cell

While hydrogen-oxygen fuel cells are most capable of providing the needed power densities for most practical purposes, they still involve production, storage and distribution problems.[12] The ease of storage and distribution for liquid fuels, such as methanol, has made them attractive alternatives to hydrogen. The oxidation of methanol has been investigated since the 1960s[12] with methanol being among the most electroactive organic fuel.[13] To date Pt remains the most active single metal electrocatalyst for this reaction.[12, 14] However, intermediate species such as CO remain adsorbed on the surface of the Pt and inhibit the oxidation reaction.[12, 14] Therefore, extensive effort dedicated to the development of new electrocatalytic materials for the oxidation of methanol has been undertaken to circumvent the Pt poisoning issue.

Figure 7.11 shows a schematic of a direct methanol fuel cell (DMFC). A DMFC consists of two electrodes separated by an ionic conductor, such as an acid electrolyte membrane.[13] The oxidation of methanol occurs at the anode while the reduction of oxygen occurs at the cathode, as shown below:[1]

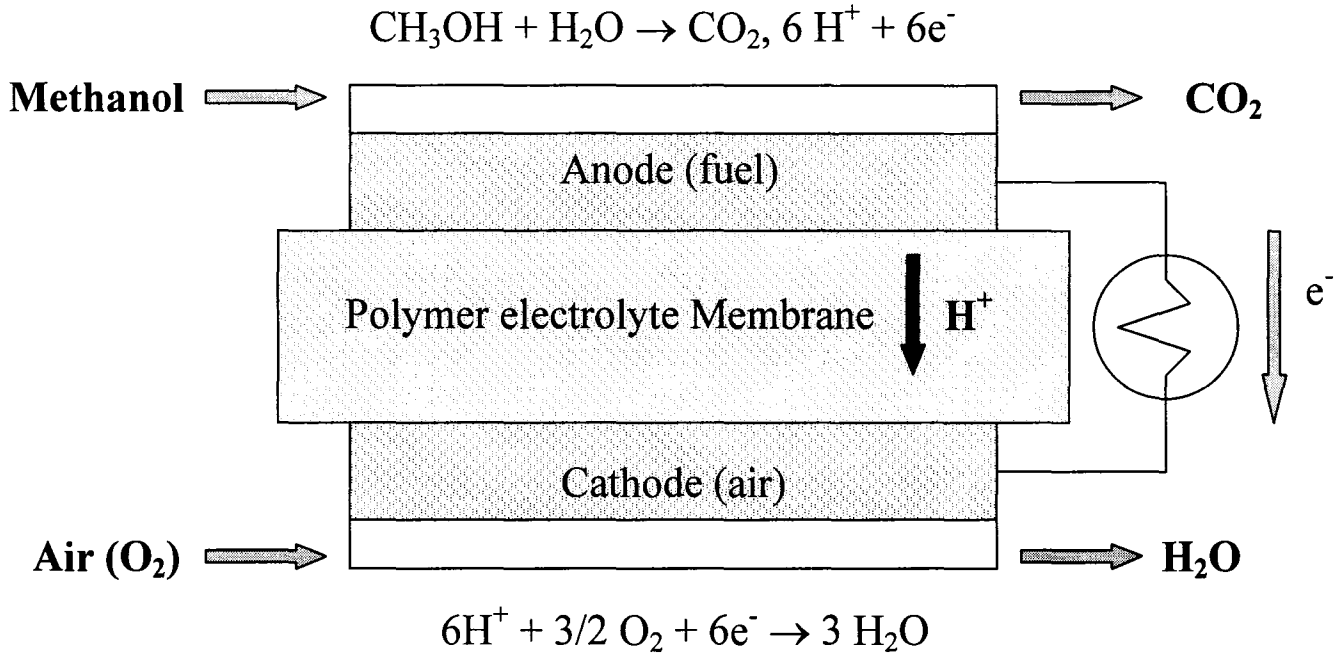

Figure 7.11 Schematic of a DMFC

Anode: $CH_3OH + H_2O \rightarrow 6H^+ + CO_2 + 6e^-$ Eq. 7.5

Cathode: $O_2 + 4H^+ + 4e^- \rightarrow 2\ H_2O$ Eq. 7.6

Overall: $CH_3OH + 3/2\ O_2 \rightarrow CO_2 + 2\ H_2O$ Eq. 7.7

For the complete combustion of methanol, 6 e^- per mole of methanol is theoretically achievable. However, the oxidation of methanol to CO_2 is rarely complete and the overall efficiency may be drastically decreased.[13] This may occur if the electrooxidation of methanol stops at the formaldehyde or formic acid stages, as shown below:[13]

Formaldehyde stage $CH_3OH \rightarrow HCHO + 2\ H^+(aq) + 2\ e^-$ Eq. 7.8

Formic acid stage $CH_3OH + H_2O \rightarrow HCOOH + 4\ H^+(aq) + 4\ e^-$ Eq. 7.9

The main objectives of DMFC investigations are to increase the reaction rates at both the methanol anode and oxygen cathode, to increase the reaction selectivity towards complete oxidation of methanol to CO_2, to find methanol-tolerant oxygen cathodes, and to decrease the effects of methanol crossover through the electrolyte membrane.[13]

One of the growing fields of DMFC research is to use sol-gel chemistry in preparing electrodes.[6, 9, 11, 12, 14] Si + Pt/C colloid gels prepared by nanoglueing platinum-colloid-modified Vulcan carbon to silica sol provide catalytic materials that are an order of magnitude more active for the oxidation of methanol per gram of Pt relative to the starting colloid-modified carbon black.[9]

In this work, the electrocatalytic activity towards the oxidation of methanol by sulphonated silica sol + C/Pt electrodes was briefly examined.

Electrochemical experiments were performed using impedance spectroscopy and cyclic voltammetry. All experiments were collected by pumping 1 M aqueous methanol to the working electrode at a fixed flow rate of 5 $mL \cdot min^{-1}$. A hydrogen cathode served as both the reference and the counter electrode. H_2 (g) was humidified at room temperature prior to entering the cell. The uncompensated resistance was determined from the high frequency intercept of a Nyquist plot. Before measurements were taken, the cell was operated at a cell voltage of 0.3 V until a steady current was obtained.

It is common practice in direct methanol fuel cell research to measure anode polarization by feeding the cathode side of the fuel cell with hydrogen and assuming that it behaves as a reversible hydrogen electrode.[15] Li has reported that the performance of a DMFC can be improved by optimizing the anode structure to promote mass transport.[15] The methanol oxidation polarization curve for a Sol + Pt/C anode is shown in Fig 7.12.

While the performance shown in Fig 7.12 for the Sol + Pt/C anode did not behave as well as that obtained for a 4 mg $Pt \cdot cm^{-2}$ anode, the results were still very promising because the Sol + Pt/C composite anode contained ten times less Pt.

7.3.3 Discussion

Sol-gel chemistry offers the possibility of preparing solid materials that exhibit ionic and electronic conductivity. These materials have found extensive application in the design of electrochromic devices, as supports for electrocatalysts and in the development of fuel cell electrodes.[16] Inclusion of carbon powder into the bulk of silica-based sol-gels increases the electronic conductivity of the composite.[16]

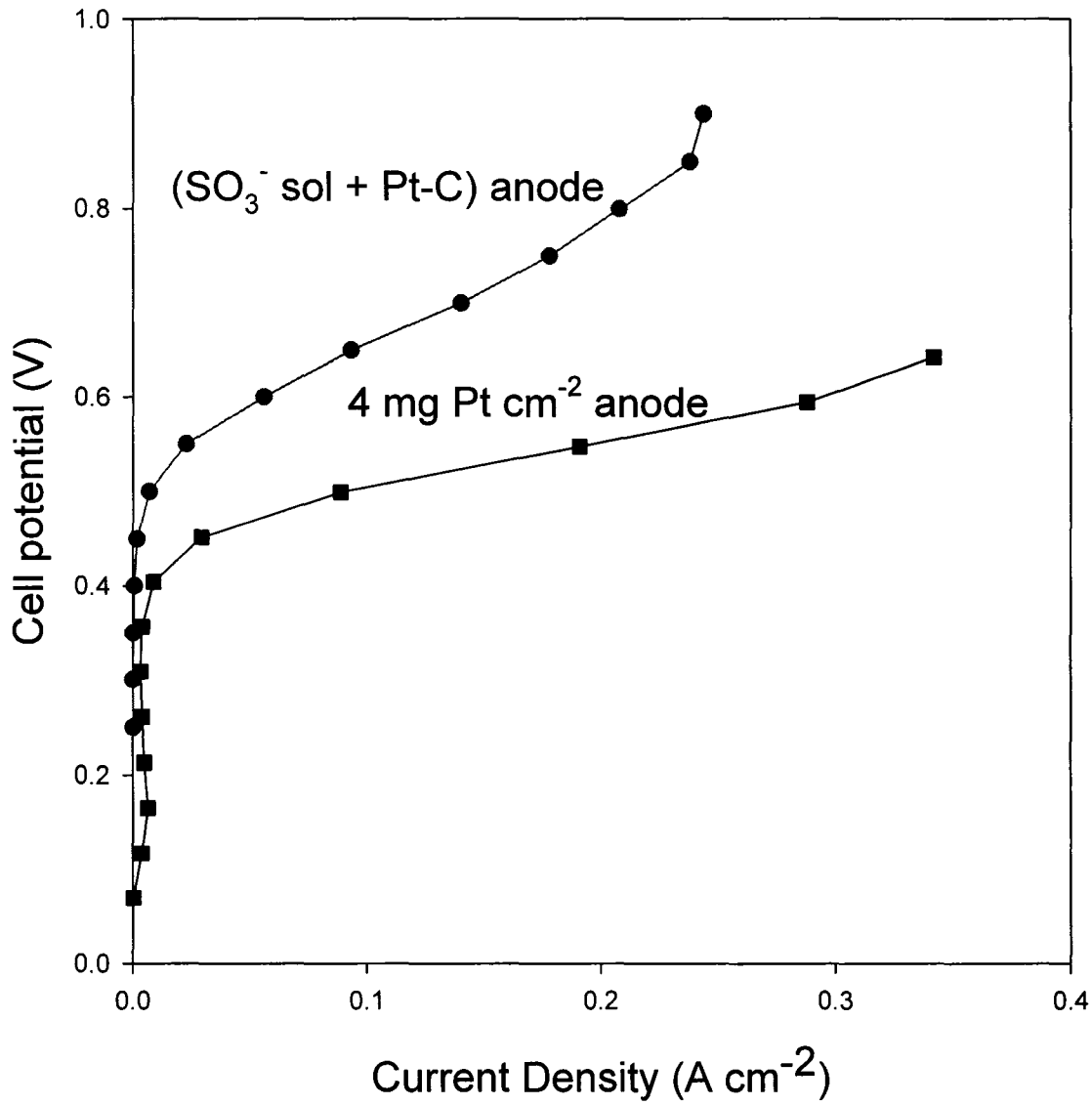

Figure 7.12 Anode performance for a DMFC for a SO_3^- sol + Pt/C composite anode compared to a 4 mg Pt·cm^{-2} anode.

4 mg Pt·cm^{-2} anode data (■) reproduced from Li[12]

While the use of novel nanohybrid materials as ionomers in fuel cell catalyst layers was shown to increase Pt utilization in the literature, reports state that the limiting current density at the cathode was lower than that prepared with conventional Nafion[5] as was indeed the case for the Sol + Pt/C composite cathodes. In fact, cathodes prepared from the sulphonate silica Sol + Pt/C composites did not perform very well at all in a commercial hydrogen fuel cell due to water management issues. The hydrophobicity of the catalyst was therefore increased by incorporating PTFE into the catalyst layer, which greatly increased the fuel cell performance. Furthermore, as evident from Fig 7.10, the sulphonated silica sol plays an important role in the catalyst as the performance of a PTFE + Pt/C composite cathode is increased by the addition of the sol to it.

It has been suggested that direct methanol fuel cells may benefit from the use of polymers based on sulphonated polyetherketones as alternative membrane materials because they may help to reduce the high water drag and high methanol cross-over problems often displayed in these fuel cells.[11] Despite the challenges to developing DMFC, there is great hope for them because methanol is a liquid fuel with a high energy content and DMFCs eliminate the need for bulky, heavy and complex fuel processors.[13]

Based on this, the sulphonated silica sol-gel was used to prepare composite catalyst materials for use in a DMFC.

7.4 Conclusions

Proton conducting SO_3^- sol + Pt/C composites were prepared using the sol-gel process. These nanocomposites were used as catalytic materials in both hydrogen and

direct methanol fuel cells. For the hydrogen fuel cell, it was necessary to incorporate PTFE into the catalytic layer to control water management. Although catalysts prepared with the SO_3^- sol + Pt/C displayed a larger active Pt area and higher ionic conductivity than Nafion + Pt/C catalysts, the fuel cell performance was not as great. Larger current densities were obtained using the SO_3^- sol + Pt/C catalyst when switched to a direct methanol fuel cell. The DMFC performance was not as great as that obtained for a commercial 4 mg $Pt \cdot cm^{-2}$ anode.

The results presented in this chapter are preliminary ones that demonstrate that the sulphonated silica sol-gel is effective as a proton transporting material in both O_2 cathodes and methanol anodes. Optimization is needed to improve the fuel cell performance in order to approach that of Nafion-based electrodes.

Catalysts based on the dispersion of metals on aerogel supports have been well studied and aerogels have long been investigated as heterogeneous catalysts because they offer more active sites per gram for gas/solid interactions than do most other solid materials.[2] Not only is the internal surface area of an aerogel much greater than its external surface, but the continuous mesoporous network of an aerogel facilitates the flux of reactant molecules that access the catalytically active areas internal to the sol-gel network.[2, 6] Thus aerogels provide ready mass transport of reactants to an increased area of catalytic surface.[2] Other benefits of the sol-gel method for preparing catalysts include liquid-phase syntheses that give rise to homogeneous products, the ability to adapt the physical properties of aerogels and moderate temperatures of sol-gel chemistry allows the preparation of amorphous catalysts.[2, 17] This type of catalytic architecture differs from

standard impregnated catalysts in several important ways. First, the sol-gel oxide particle size is comparable to the metallic catalyst particle size. Secondly, the 3-dimensional, continuous and mesoporous solid network provides easy molecular transport while minimizing agglomeration or the networked oxide nanoparticles. And lastly, the bifunctional catalyst is a multiparticulate arrangement in which multiple oxide-to-metal contacts minimize the transport distances over which surface diffusion must occur for the relevant species to come together and react.[18]

References

[1]Winter, M.; Brodd, R. J. *Chem. Rev.*, **2004**, 104, 4245

[2]Rolison, D. R.; Dunn, B. *J. Mater. Chem.*, **2001**, 11, 963

[3]E. B. Easton, Ph.D. Thesis, Memorial University of Newfoundland, Newfoundland (2003)

[4]Li, G.; Pickup, P.G. *Journal of the Electrochemical Society*, **2003**, 150, C745

[5] Nishikawa, O.; Doyama, K.; Miyatake, K.; Uchida, H.; Watanabe, M. *Electrochimica Acta*, **2005**, 50, 2719

[6]Anderson, M. L.; Stroud, R. M.; Rolison, D. R. *Nano Letters*, **2002**, 2, 235

[7]Swider, K.E.; Hagans, P.L.; Merzbacher, C.I.; Rolison, D.R. *Chem. Mater.* **1997**, 9, 1248

[8]Richards, R.; Li, W.; Decker, S.; Davidson, C.; Koper, O.; Zaikovski, V.; Volodin, A.; Rieker, T.; Klabunde, K.J. *J. Am. Chem. Soc.* **2000**, 122, 4921

[9]G. Li, Ph.D Thesis, Memorial University of Newfoundland, Newfoundland (2006)

[10]Easton, E.B.; Astill, T.D.; Holdcroft, S. *Journal of the Electrochemical Society*, **2005**, 152, A752

[11] Kreuer, K.D. *Journal of Membrane Science*, **2001**, 185, 29

[12]Villullas, H. M.; Mattos-Costa, F. I.; Bulhoes, L. O. S. *J. Phys. Chem. B.* **2004**, 108, 12898

[13]Lamy, C.; Leger, J-M.; Srinivasan, S. Modern Aspects of Electrochemistry, No. 34, ed. John O'M. Bockris et al. Kluwer Academic/Plenum Publishers, New York, 2001.

[14] Villullas, H.M.; Mattos-Costa, F.I.; Nascente, P.A.P.; Bulhoes, L.O.S. *Electrochimica Acta*, **2004**, 49, 3909

[15] Li, G.; Pickup, P.G. *Electrochimica Acta*, **2004**, 49, 4119

[16]Alber, K. S.; Cox, J. A. *Mikrochim. Acta*, **1997**, 127, 131

[17]Lev, O.; Bharathi, W.S.; Glezer, V.; Modestov, A.; Gun, J.; Rabinovich, L.; Sampath, S. *Chem. Mater.*, **1997**, 9, 2352

[18]Rolison, D. R. *Science*, **2003**, 299, 1698

[19]Mehta, V.; Cooper, J. S. *Journal of Power Sources*, **2003**, 114, 32

Chapter 8:

Summary and Future Work

In this thesis, the ion exchange and ion transport properties of sulphonated silica ormosil hydrogels has been a major theme. The sol-gel process was successful in preparing silica materials containing sulphonate groups by incorporating 2-(4-chlorosulfonylphenyl) ethyl-trichlorosilane into a tetramethyl orthosilicate sol-gel network. Working electrodes were prepared by impregnating carbon fiber paper with sol and allowing the sol to age inside the electrode porous structure. The method of incorporating electroactive probes into the cyclic voltammetry, chronoamperometry and chronocoulometry investigations of the hydrogels has shown to be effective in studying these properties. It was demonstrated that the quantity of the probe present inside the sol-gel network can readily be determined and that partition and apparent diffusion coefficients can be experimentally determined. It was shown in this work how the different synthetic and experimental parameters influenced the ion exchange and transport properties of these materials. The ormosil hydrogels studied in this work exhibited excellent ion exchange and ion transport properties, which were very stable in electrochemical studies. Redox probes (of different sizes and charges) also enabled the investigation into the permselective behaviour of these solid materials.

Future work in the area of characterization of sol-gel materials should include the synthesis of other metal oxide or mixed metal oxide solids, such as RuOx or Ti-RuOx. These materials could be investigated as other ionic conducting solids or as super capacitors. Further characterization with different redox probes of even larger size or charge differences could be beneficial.

Electrochemical impedance spectroscopy was shown to be an effective method for determining the ionic conductivities of solid sol-gel materials. It has been shown in this work that the incorporation of the sulphonate functionality into a silica sol-gel greatly increased the ionic conductivity of the solids.

Further work in this area should include other metal oxide or mixed metal oxide sol-gels for comparison with silica-based materials.

Two examples of nanocomposites were prepared and studied to demonstrate the ease of tailoring the sol-gel process to specific applications. In one example, nanocomposites of polypyrrole and sulphonated silica sol-gel (PPY/gel) were prepared in order to incorporate the electronic conductivity of the conducting polymer into the ionic conducting network of the sol-gel. These films contained redox characteristics that aided in the rapid electron transfer at an electrode surface. In the second example, nanocomposites of sulphonated silica sol-gel and Pt/C were prepared as highly proton conducting binders for fuel cell catalysts. Preliminary experiments using this catalyst for hydrogen and direct methanol fuel cells showed promise for future use of these catalysts. Further optimization will be needed to improve the fuel cell performance to levels approaching those of Nafion-based Pt/C catalysts.

Further work with the (PPY/gel) nanocomposites should include a study of hysteresis for the ionic conductivity measurements. Conducting polymers almost always show higher conductivities when measured in the order of increasing potential, but the work shown in this thesis involved only the measurement in the order of decreasing potential. Nanocomposites prepared with conducting polymers other than polypyrrole

(for example, polyaniline) should also be investigated for comparison with the work reported here.

The method of treating a Pt/C catalyst with sulphonated silica sol has been shown to increase the active Pt area of these catalysts, relative to Nafion treated Pt/C, while reducing the amount of Pt compared to commercial 4 mg $Pt \cdot cm^{-2}$ fuel cell electrodes. It was also shown that the capacitance and ionic conductivity for the sulphonated silica sol-Pt/C composite electrodes were significantly larger than those obtained for Nafion treated Pt/C electrodes. Significant improvement in hydrogen fuel cell performance has been achieved when the sol-treated Pt/C catalyst was also treated with polytetrafluoroethylene due to improved water management control from the hydrophobic backbone of the PTFE. Hydrogen fuel cell performance was shown to be poor compared to Nafion treated catalysts.

Significant improvements were shown when the sulphonated silica sol-Pt/C electrode was used in a direct methanol fuel cell. The electrocatalytic activity towards the oxidation of methanol by these nanocomposites was briefly examined and shown to be slightly inferior to commercial 4 mg $Pt \cdot cm^{-2}$ fuel cell electrodes, but contained ten times less Pt.

Further work should include the optimization of composite composition (amounts of sulphonated silica sol, Pt/C, and PTFE in the composite as well as the amount of sulphonated silane in the sol). Procedural optimization should also include optimization of the membrane electrode assembly fabrication (membrane, pressing, how to deposit the composite onto the gas diffusion electrode, etc.) and optimization of fuel flow rates.

Future work could also include preparing nanocomposites of other metal oxide or mixed metal oxide sol-gels and/or catalysts other than Pt/C.